Electroweak Symmetry Breaking and Higgs Physics[*]

Michael Spira[1] and Peter M. Zerwas[2]

[1] *CERN, Theory Division, CH-1211 Geneva 23, Switzerland*
[2] *Deutsches Elektronen-Synchrotron DESY, D-22603 Hamburg, Germany*

Abstract

An introduction to electroweak symmetry breaking and Higgs physics is presented for the Standard Model and its supersymmetric extensions. A brief overview will also be given on strong interactions of the electroweak gauge bosons in alternative scenarios. In addition to the theoretical basis, the present experimental status of Higgs physics and implications for future experiments at the LHC and e^+e^- linear colliders are discussed.

---

[*]Lectures at 36. Internationale Universitätswochen für Kern- und Teilchenphysik, Schladming 1997.

1 Introduction

1. Revealing the physical mechanism that is responsible for the breaking of electroweak symmetries is one of the key problems in particle physics. If the fundamental particles – leptons, quarks and gauge bosons – remain weakly interacting up to very high energies, the sector in which the electroweak symmetry is broken must contain one or more fundamental scalar Higgs bosons with light masses of the order of the symmetry-breaking scale $v \sim 246$ GeV. The masses of the fundamental particles are generated through the interaction with the scalar background Higgs field, which is non-zero in the ground state [1]. Alternatively, the symmetry breaking could be generated dynamically by new strong forces characterized by an interaction scale $\Lambda \sim 1$ TeV [2]. If global symmetries of the strong interactions are broken spontaneously, the associated Goldstone bosons can be absorbed by the gauge fields, generating the masses of the gauge particles. The masses of leptons and quarks can be generated through interactions with the fermion condensate.

2. A simple mechanism for the breaking of the electroweak symmetry is incorporated in the Standard Model (SM) [3]. To accommodate all observed phenomena, a complex isodoublet scalar field is introduced through self-interactions; this acquires a non-vanishing vacuum expectation value, breaking spontaneously the electroweak symmetry $SU(2)_I \times U(1)_Y$ down to the electromagnetic $U(1)_{EM}$ symmetry. The interactions of the gauge bosons and fermions with the background field generate the masses of these particles. One scalar field component is not absorbed in this process, manifesting itself as the physical Higgs particle H.

The mass of the Higgs boson is the only unknown parameter in the symmetry-breaking sector of the Standard Model, while all couplings are fixed by the masses of the particles, a consequence of the Higgs mechanism *per se*. However, the mass of the Higgs boson is constrained in two ways. Since the quartic self-coupling of the Higgs field grows indefinitely with rising energy, an upper limit on the Higgs mass can be derived from demanding the SM particles to remain weakly interacting up to a scale Λ [4]. On the other hand, stringent lower bounds on the Higgs mass follow from requiring the electroweak vacuum to be stable [5]. If the Standard Model is valid up to scales near the Planck scale, the SM Higgs mass is restricted to a narrow window between 130 and 190 GeV. For Higgs masses either above or below this window, new physical phenomena are expected to occur at a scale Λ between ~ 1 TeV and the Planck scale. For Higgs masses near 700 GeV, the scale of new strong interactions would be as low as ~ 1 TeV [4, 6].

The electroweak observables are affected by the Higgs mass through radiative corrections [7]. Despite the weak logarithmic dependence, the high-precision electroweak data indicate a preference for light Higgs masses close to ~ 100 GeV [8]. At the 95% CL, the data require a value of the Higgs mass within the canonical range of the Standard Model. By searching directly for the SM Higgs particle, the LEP experiments have set a lower limit of $M_H \gtrsim 84$ to 88 GeV on the Higgs mass [9]. If the Higgs boson will not be found at LEP2 with a mass of less than about 100 GeV [10], the search will continue at the Tevatron, which may reach masses up to ~ 120 GeV [11]. The proton collider LHC can

sweep the entire canonical Higgs mass range of the Standard Model [12]. The properties of the Higgs particle can be analysed very accurately at e^+e^- linear colliders [13], thus establishing the Higgs mechanism experimentally.

3. If the Standard Model is embedded in a Grand Unified Theory (GUT) at high energies, the natural scale of electroweak symmetry breaking would be expected close to the unification scale M_{GUT}. Supersymmetry [14] provides a solution of this hierarchy problem. The quadratically divergent contributions to the radiative corrections of the scalar Higgs boson mass are cancelled by the destructive interference between bosonic and fermionic loops in sypersymmetric theories [15]. The Minimal Supersymmetric extension of the Standard Model (MSSM) can be derived as an effective theory from supersymmetric grand unified theories. A strong indication for the realization of this physical picture in nature is the excellent agreement between the value of the electroweak mixing angle $\sin^2 \theta_W$ predicted by the unification of the gauge couplings, and the experimentally measured value. If the gauge couplings are unified in the minimal supersymmetric theory at a scale $M_{GUT} = \mathcal{O}(10^{16}$ GeV$)$, the electroweak mixing angle is predicted to be $\sin^2 \theta_W = 0.2336 \pm 0.0017$ [16] for a mass spectrum of the supersymmetric particles of order M_Z to 1 TeV. This theoretical prediction is matched very well by the experimental result $\sin^2 \theta_W^{exp} = 0.2316 \pm 0.0003$ [8]; the difference between the two numbers is less than 2 per mille.

In the MSSM, the Higgs sector is built up by two Higgs doublets [17]. The doubling is necessary to generate masses for up- and down-type fermions in a supersymmetric theory and to render the theory anomaly-free. The Higgs particle spectrum consists of a quintet of states: two CP-even scalar neutral (h, H), one CP-odd pseudoscalar neutral (A), and a pair of charged $(H^\pm)$ Higgs bosons [18]. The masses of the heavy Higgs bosons, $H, A, H^\pm$, are expected to be of order v, but they may extend up to the TeV range. By contrast, since the quartic Higgs self-couplings are determined by the gauge couplings, the mass of the lightest Higgs boson h is constrained very stringently. At tree level, the mass has been predicted to be smaller than the Z mass [18]. Radiative corrections, increasing as the fourth power of the top mass, shift the upper limit to a value between ~ 100 GeV and ~ 130 GeV, depending on the parameter tgβ, the ratio of the vacuum expectation values of the two neutral scalar Higgs fields.

A general lower bound of 73 GeV has been experimentally established for the Higgs particle h at LEP [9]. Continuing this search, the entire h mass range can be covered for tg$\beta \lesssim 2$, a value compatible with the unification of the b and τ masses at high energies. The search for h masses in excess of ~ 100 GeV and the search for the heavy Higgs bosons will continue at the Tevatron, the LHC and e^+e^- linear colliders. In these machines the mass range can be covered up to ~ 1 TeV [11–13].

4. Elastic-scattering amplitudes of massive vector bosons grow indefinitely with energy if they are calculated as a perturbative expansion in the coupling of a non-Abelian gauge theory. As a result, they violate the unitarity beyond a critical energy scale of ~ 1.2 TeV. This problem can be solved by introducing a light Higgs boson. In alternative scenarios,

the W bosons may become strongly interacting at TeV energies, thus damping the rise of the elastic-scattering amplitudes. Naturally, the strong forces between the W bosons may be traced back to new fundamental interactions characterized by a scale of order 1 TeV [2]. If the underlying theory is globally chiral-invariant, this symmetry may be broken spontaneously. The Goldstone bosons associated with the spontaneous breaking of the symmetry can be absorbed by gauge bosons to generate their masses and to build up the longitudinal degrees of freedom of the wave functions.

Since the longitudinally polarized W bosons are associated with the Goldstone modes of chiral symmetry breaking, the scattering amplitudes of the W_L bosons can be predicted for high energies by a systematic expansion in the energy. The leading term is parameter-free, a consequence of the chiral symmetry-breaking mechanism *per se*, which is independent of the particular structure of the dynamical theory. The higher-order terms in the chiral expansion however are defined by the detailed structure of the underlying theory. With rising energy the chiral expansion is expected to diverge and new resonances may be generated in WW scattering at mass scales between 1 and 3 TeV. This picture is analogous to pion dynamics in QCD, where the threshold amplitudes can be predicted in a chiral expansion, while at higher energies vector and scalar resonances are formed in $\pi\pi$ scattering.

Such a scenario can be studied in WW scattering experiments, where the W bosons are radiated, as quasi-real particles [19], off high-energy quarks in the proton beams of the LHC [12], [20–22] or off electrons and positrons in TeV linear colliders [13, 23, 24].

5. This report is divided into three parts. A basic introduction and a summary of the main theoretical and experimental results will be presented in the next section on the Higgs sector of the Standard Model. Also the search for the Higgs particle at future e^+e^- and hadron colliders will be described. In the same way, the Higgs spectrum of supersymmetric theories will be discussed in the following section. Finally, the main features of strong W interactions and their analysis in WW scattering experiments will be presented in the last section.

Only the basic elements of electroweak symmetry breaking and Higgs mechanism can be reviewed in this report. Other aspects may be traced back from Ref. [25] and recent reports collected in Ref. [26].

2   The Higgs Sector of the Standard Model

2.1   The Higgs Mechanism

At high energies, the amplitude for the elastic scattering of massive W bosons, $WW \rightarrow WW$, grows indefinitely with energy for longitudinally polarized particles, Fig. 1a. This is
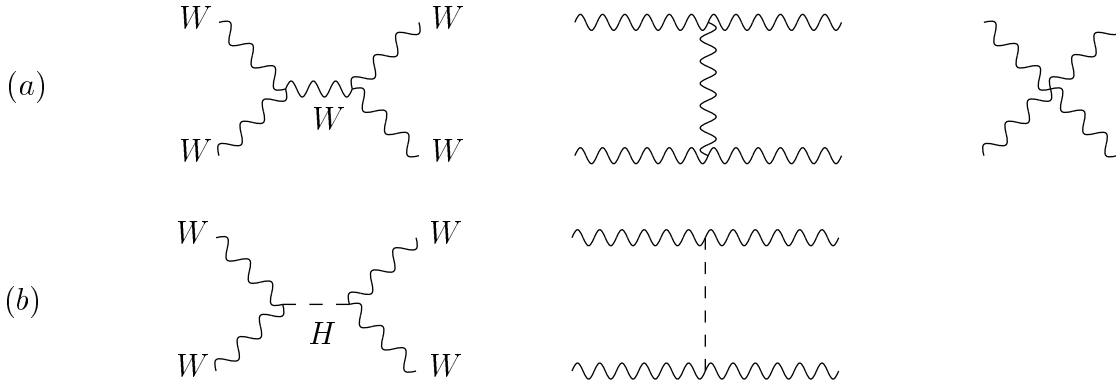
Figure 1: *Generic diagrams of elastic WW scattering: (a) pure gauge-boson dynamics, and (b) Higgs-boson exchange.*

a consequence of the linear rise of the longitudinal W_L wave function, $\epsilon_L = (p, 0, 0, E)/M_W$, with the energy of the particle. Even though the term of the scattering amplitude rising as the fourth power in the energy is cancelled by virtue of the non-Abelian gauge symmetry, the amplitude remains quadratically divergent in the energy. On the other hand, unitarity requires elastic-scattering amplitudes of partial waves J to be bounded by $\Re e A_J \leq 1/2$. Applied to the asymptotic S-wave amplitude $A_0 = G_F s/8\pi\sqrt{2}$ of the isospin-zero channel $2W_L^+ W_L^- + Z_L Z_L$, the bound [27]

$$s \leq 4\pi\sqrt{2}/G_F \sim (1.2 \text{ TeV})^2 \tag{1}$$

on the c.m. energy $\sqrt{s}$ can be derived for the validity of a theory of weakly coupled massive gauge bosons.

However, the quadratic rise in the energy can be damped by exchanging a new scalar particle, Fig. 1b. To achieve the cancellation, the size of the coupling must be given by the product of the gauge coupling with the gauge boson mass. For high energies, the amplitude $A_0' = -G_F s/8\pi\sqrt{2}$ cancels exactly the quadratic divergence of the pure gauge-boson amplitude A_0. Thus, unitarity can be restored by introducing a weakly coupled *Higgs particle*.

In the same way, the linear divergence of the amplitude $A(f\bar{f} \to W_L W_L) \sim g m_f \sqrt{s}$ for the annihilation of a fermion–antifermion pair to a pair of longitudinally polarized gauge bosons, can be damped by adding the Higgs exchange to the gauge-boson exchange. In this case the Higgs particle must couple proportionally to the mass m_f of the fermion f.

These observations can be summarized in a theorem: *A theory of massive gauge bosons and fermions that are weakly coupled up to very high energies, requires, by unitarity, the existence of a Higgs particle; the Higgs particle is a scalar 0^+ particle that couples to other particles proportionally to the masses of the particles.*

The assumption that the couplings of the fundamental particles are weak up to very high energies is qualitatively supported by the perturbative renormalization of the electroweak mixing angle $\sin^2 \theta_W$ from the symmetry value 3/8 at the GUT scale down to

4

~ 0.2, which is close to the experimentally observed value at low energies.

These ideas can be cast into an elegant mathematical form by interpreting the electroweak interactions as a gauge theory with spontaneous symmetry breaking in the scalar sector. Such a theory consists of fermion fields, gauge fields and a scalar field coupled by the standard gauge interactions and Yukawa interactions to the other fields. Moreover, a self-interaction

$$V = \frac{\lambda}{2} \left[|\phi|^2 - \frac{v^2}{2} \right]^2 \tag{2}$$

is introduced in the scalar sector, which leads to a non-zero ground-state value $v/\sqrt{2}$ of the scalar field. By fixing the phase of the vacuum amplitude to zero, the gauge symmetry is spontaneously broken in the scalar sector. Interactions of the gauge fields with the scalar background field, Fig. 2a, and Yukawa interactions of the fermion fields with the background field, Fig. 2b, shift the masses of these fields from zero to non-zero values:

$$(a) \qquad \frac{1}{q^2} \;\rightarrow\; \frac{1}{q^2} + \sum_j \frac{1}{q^2} \left[\left(\frac{gv}{\sqrt{2}} \right)^2 \frac{1}{q^2} \right]^j \;=\; \frac{1}{q^2 - M^2} \;\;:\;\; M^2 = g^2 \frac{v^2}{2}$$

$$(b) \qquad \frac{1}{\slashed{q}} \;\rightarrow\; \frac{1}{\slashed{q}} + \sum_j \frac{1}{\slashed{q}} \left[\frac{g_f v}{\sqrt{2}} \frac{1}{\slashed{q}} \right]^j \;=\; \frac{1}{\slashed{q} - m_f} \;\;:\;\; m_f = g_f \frac{v}{\sqrt{2}}$$

$$\tag{3}$$

Thus, in theories with gauge and Yukawa interactions, in which the scalar field acquires a non-zero ground-state value, the couplings are naturally proportional to the masses. This ensures the unitarity of the theory as discussed before. These theories are renormalizable (as a result of the gauge invariance, which is only disguised in the unitary formulation adopted so far), and thus they are well-defined and mathematically consistent.
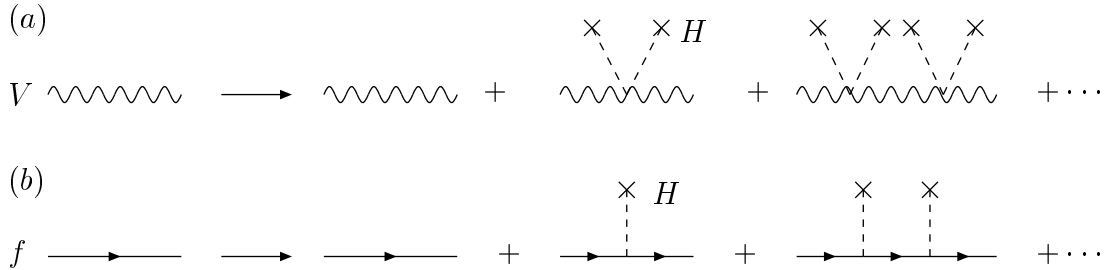

Figure 2: *Generating (a) gauge boson and (b) fermion masses through interactions with the scalar background field.*

2.2   The Higgs Mechanism in the Standard Model

Besides the Yang–Mills and the fermion parts, the electroweak $SU_2 \times U_1$ Lagrangian includes a scalar isodoublet field ϕ, coupled to itself in the potential V, cf. eq. (2), to the

gauge fields through the covariant derivative $iD = i\partial - g\vec{I}\vec{W} - g'YB$, and to the up and down fermion fields u, d through Yukawa interactions:

$$\mathcal{L}_0 = |D\phi|^2 - \frac{\lambda}{2}\left[|\phi|^2 - \frac{v^2}{2}\right]^2 - g_d\bar{d}_L\phi d_R - g_u\bar{u}_L\phi_c u_R + \text{hc} . \tag{4}$$

In the unitary gauge, the isodoublet ϕ is replaced by the physical Higgs field H, $\phi \to [0, (v+H)/\sqrt{2}]$, which describes the fluctuation of the $I_3 = -1/2$ component of the isodoublet field about the ground-state value $v/\sqrt{2}$. The scale v of the electroweak symmetry breaking is fixed by the W mass, which in turn can be reexpressed by the Fermi coupling, $v = 1/\sqrt{\sqrt{2}G_F} \approx 246$ GeV. The quartic coupling λ and the Yukawa couplings g_f can be reexpressed in terms of the physical Higgs mass M_H and the fermion masses m_f:

$$\begin{aligned} M_H^2 &= \lambda v^2 \\ m_f &= g_f v/\sqrt{2} \end{aligned} \tag{5}$$

respectively.

Since the couplings of the Higgs particle to gauge particles, to fermions and to itself are given by the gauge couplings and the masses of the particles, the only unknown parameter in the Higgs sector (apart from the CKM mixing matrix) is the Higgs mass. When this mass is fixed, all properties of the Higgs particle can be predicted, i.e. the lifetime and decay branching ratios, as well as the production mechanisms and the corresponding cross sections.

2.2.1   The SM Higgs Mass

Even though the mass of the Higgs boson cannot be predicted in the Standard Model, stringent upper and lower bounds can nevertheless be derived from internal consistency conditions and extrapolations of the model to high energies.

The Higgs boson has been introduced as a fundamental particle to render 2–2 scattering amplitudes involving longitudinally polarized W bosons compatible with unitarity. Based on the general principle of time-energy uncertainty, particles must decouple from a physical system if their mass grows indefinitely. The mass of the Higgs particle must therefore be bounded to restore unitarity in the perturbative regime. From the asymptotic expansion of the elastic $W_L W_L$ S-wave scattering amplitude including W and Higgs exchanges, $A(W_L W_L \to W_L W_L) \to -G_F M_H^2/4\sqrt{2}\pi$, it follows [27] that

$$M_H^2 \leq 2\sqrt{2}\pi/G_F \sim (850 \text{ GeV})^2 . \tag{6}$$

Within the canonical formulation of the Standard Model, consistency conditions therefore require a Higgs mass below 1 TeV.

Quite restrictive bounds on the value of the SM Higgs mass follow from hypotheses on the energy scale Λ up to which the Standard Model can be extended before new physical
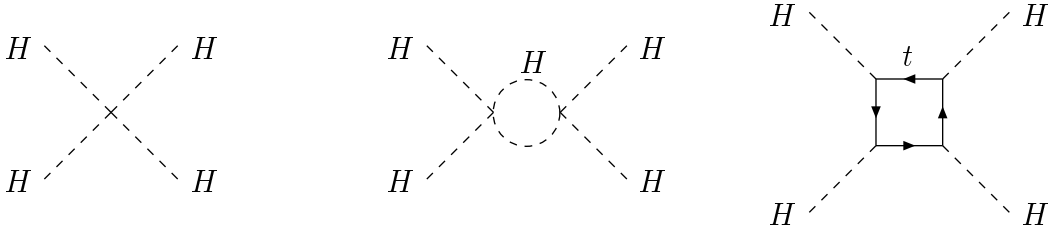
Figure 3: *Diagrams generating the evolution of the Higgs self-interaction λ.*

phenomena emerge, which would be associated with new strong interactions between the fundamental particles. The key to these bounds is the evolution of the quartic coupling λ with the energy (i.e. the field strength) due to quantum fluctuations [4]. The basic contributions are depicted in Fig. 3. The Higgs loop itself gives rise to an indefinite increase of the coupling while the fermionic top-quark loop, with increasing top mass, drives the coupling to smaller values, finally even to values below zero. The variation of the quartic Higgs coupling λ and the top-Higgs Yukawa coupling g_t with energy, parametrized by $t = \log \mu^2/v^2$, may be written as [4]

$$
\begin{aligned}
\frac{d\lambda}{dt} &= \frac{3}{8\pi^2}\left[\lambda^2 + \lambda g_t^2 - g_t^4\right] \quad : \quad \lambda(v^2) = M_H^2/v^2 \\
\frac{dg_t}{dt} &= \frac{1}{32\pi^2}\left[\frac{9}{2}g_t^3 - 8g_t g_s^2\right] \quad : \quad g_t(v^2) = \sqrt{2}\, m_f/v \; .
\end{aligned}
\tag{7}
$$

Only the leading contributions from Higgs, top and QCD loops are taken into account.

For moderate top masses, the quartic coupling λ rises indefinitely, $\partial\lambda/\partial t \sim +\lambda^2$, and the coupling becomes strong shortly before reaching the Landau pole:

$$
\lambda(\mu^2) = \frac{\lambda(v^2)}{1 - \frac{3\lambda(v^2)}{8\pi^2}\log\frac{\mu^2}{v^2}} \; .
\tag{8}
$$

Reexpressing the initial value of λ by the Higgs mass, the condition $\lambda(\Lambda) < \infty$, can be translated to an <u>upper bound</u> on the Higgs mass:

$$
M_H^2 \leq \frac{8\pi^2 v^2}{3\log\frac{\Lambda^2}{v^2}} \; .
\tag{9}
$$

This mass bound is related logarithmically to the energy Λ up to which the Standard Model is assumed to be valid. The maximal value of M_H for the minimal cut-off $\Lambda \sim 1$ TeV is given by ~ 750 GeV. This bound is close to the estimate of ~ 700 GeV in lattice calculations for $\Lambda \sim 1$ TeV, which allow proper control of non-perturbative effects near the boundary [6].
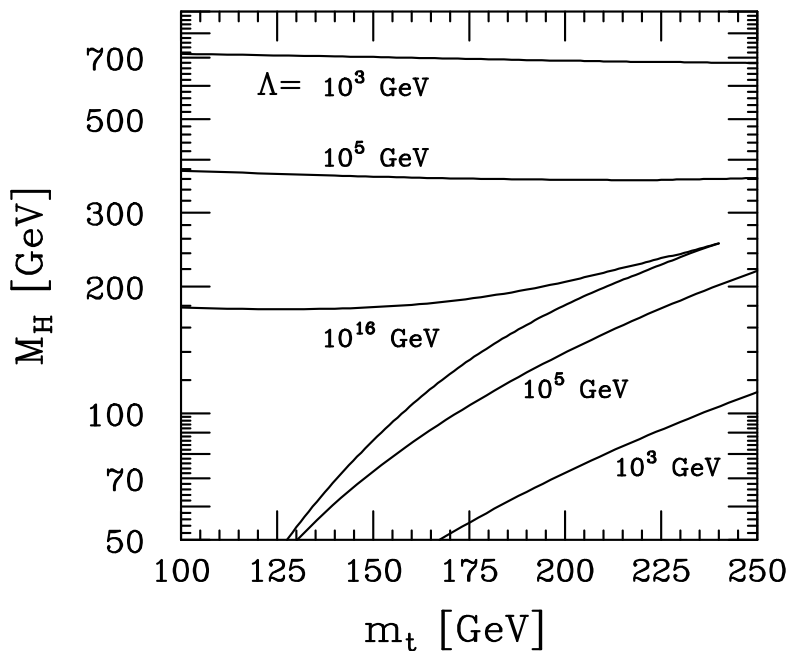
Figure 4: *Bounds on the mass of the Higgs boson in the SM. Here Λ denotes the energy scale at which the Higgs-boson system of the SM would become strongly interacting (upper bound); the lower bound follows from the requirement of vacuum stability. (Refs. [4, 5].)*

A <u>lower bound</u> on the Higgs mass can be derived from the requirement of vacuum stability [4, 5]. Since top-loop corrections reduce λ for increasing top-Yukawa coupling, λ becomes negative if the top mass becomes too large. In such a case, the self-energy potential would become deep negative and the ground state would no longer be stable. To avoid the instability, the Higgs mass must exceed a minimal value for a given top mass. This lower bound depends on the cut-off value Λ.

For any given Λ the allowed values of (M_t, M_H) pairs are shown in Fig. 4. For a central top mass $M_t = 175$ GeV, the allowed Higgs mass values are collected in Table 1 for two specific cut-off values Λ. If the Standard Model is assumed to be valid up to the scale of grand unification, the Higgs mass is restricted to a narrow window between

Λ	M_H
1 TeV	55 GeV $\lesssim M_H \lesssim$ 700 GeV
10^{19} GeV	130 GeV $\lesssim M_H \lesssim$ 190 GeV

Table 1: *Higgs mass bounds for two values of the cut-off Λ.*

8

130 and 190 GeV. The observation of a Higgs mass above or below this window would demand a new physics scale below the GUT scale.

2.2.2 Decays of the Higgs Particle

The profile of the Higgs particle is uniquely determined if the Higgs mass is fixed. The strength of the Yukawa couplings of the Higgs boson to fermions is set by the fermion masses m_j, and the coupling to the electroweak gauge bosons $V = W, Z$ by their masses M_V:

$$\begin{aligned} g_{ffH} &= \left[\sqrt{2} G_F \right]^{1/2} m_f \\ g_{VVH} &= 2 \left[\sqrt{2} G_F \right]^{1/2} M_V^2 \ . \end{aligned} \tag{10}$$

The total decay width and lifetime, as well as the branching ratios for specific decay channels, are determined by these parameters. The measurement of the decay characteristics can therefore by exploited to establish, experimentally, that Higgs couplings grow with the masses of the particles, a direct consequence of the Higgs mechanism *sui generis*.

For Higgs particles in the intermediate mass range $\mathcal{O}(M_Z) \leq M_H \leq 2M_Z$, the main decay modes are decays into $b\bar{b}$ pairs and WW, ZZ pairs, one of the gauge bosons being virtual below the respective threshold. Above the WW, ZZ pair thresholds, the Higgs particles decay almost exclusively into these two channels, with a small admixture of top decays near the $t\bar{t}$ threshold. Below 140 GeV, the decays $H \rightarrow \tau^+\tau^-, c\bar{c}$ and gg are also important besides the dominating $b\bar{b}$ channel; $\gamma\gamma$ decays, though suppressed in rate, nevertheless provide a clear 2-body signature for the formation of Higgs particles in this mass range.

(a) Higgs decays to fermions

The partial width of Higgs decays to lepton and quark pairs is given by [28]

$$\Gamma(H \rightarrow f\bar{f}) = \mathcal{N}_c \frac{G_F}{4\sqrt{2}\pi} m_f^2(M_H^2) M_H \ , \tag{11}$$

$\mathcal{N}_c = 1$ or 3 being the colour factor. Near threshold the partial width is suppressed by an additional factor β_f^3, where β_f is the fermion velocity. Asymptotically, the fermionic width grows only linearly with the Higgs mass. The bulk of QCD radiative corrections can be mapped into the scale dependence of the quark mass, evaluated at the Higgs mass. For $M_H \sim 100$ GeV the relevant parameters are $m_b(M_H^2) \simeq 3$ GeV and $m_c(M_H^2) \simeq 0.6$ GeV. The reduction of the effective c-quark mass overcompensates the colour factor in the ratio between charm and τ decays of Higgs bosons. The residual QCD corrections, $\sim 5.7 \times (\alpha_s/\pi)$, modify the widths only slightly.

9

(b) Higgs decays to WW and ZZ boson pairs

Above the WW and ZZ decay thresholds, the partial widths for these channels may be written as [29]

$$\Gamma(H \to VV) = \delta_V \frac{G_F}{16\sqrt{2}\pi} M_H^3 (1 - 4x + 12x^2)\beta_V \ , \qquad (12)$$

where $x = M_V^2/M_H^2$ and $\delta_V = 2$ and 1 for $V = W$ and Z, respectively. For large Higgs masses, the vector bosons are longitudinally polarized. Since the wave functions of these states are linear in the energy, the widths grow as the third power of the Higgs mass. Below the threshold for two real bosons, the Higgs particle can decay into VV^* pairs, one of the vector bosons being virtual. The partial width is given in this case [30] by

$$\Gamma(H \to VV^*) = \frac{3G_F^2 M_V^4}{16\pi^3} \ M_H R(x) \ \delta_V' \ , \qquad (13)$$

where $\delta_W' = 1$, $\delta_Z' = 7/12 - 10\sin^2\theta_W/9 + 40\sin^4\theta_W/27$ and

$$R(x) = \frac{3(1 - 8x + 20x^2)}{(4x - 1)^{1/2}} \arccos\left(\frac{3x - 1}{2x^{3/2}}\right) - \frac{1 - x}{2x}(2 - 13x + 47x^2) - \frac{3}{2}(1 - 6x + 4x^2)\log x \ .$$

The ZZ^* channel becomes relevant for Higgs masses beyond ~ 140 GeV. Above the threshold, the 4-lepton channel $H \to ZZ \to 4\ell^\pm$ provides a very clear signal for Higgs bosons.

(c) Higgs decays to gg and $\gamma\gamma$ pairs

In the Standard Model, gluonic Higgs decays are mediated by top- and bottom-quark loops, photonic decays in addition by W loops. Since these decay modes are significant only far below the top and W thresholds, they are described by the approximate expressions [31, 32]

$$\Gamma(H \to gg) \ = \ \frac{G_F \alpha_s^2(M_H^2)}{36\sqrt{2}\pi^3} M_H^3 \left[1 + \left(\frac{95}{4} - \frac{7N_F}{6}\right)\frac{\alpha_s}{\pi}\right] \qquad (14)$$

$$\Gamma(H \to \gamma\gamma) \ = \ \frac{G_F \alpha^2}{128\sqrt{2}\pi^3} M_H^3 \left|\frac{4}{3}\mathcal{N}_C e_t^2 - 7\right|^2 \ , \qquad (15)$$

which are valid in the limit $M_H^2 \ll 4M_W^2, 4M_t^2$. The QCD radiative corrections, which include the ggg and $gq\bar{q}$ final states in (14), are very important; they increase the partial width by about 65%. Even though photonic Higgs decays are very rare, they nevertheless offer a simple and attractive signature for Higgs particles by leading to just two stable particles in the final state.

Digression: Loop-mediated Higgs couplings can easily be calculated in the limit in which the Higgs mass is small compared to the loop mass, by exploiting a low-energy theorem [31–34] for the external Higgs amplitude $\mathcal{A}(XH)$:

$$\lim_{p_H \to 0} \mathcal{A}(XH) = \frac{1}{v} \frac{\partial \mathcal{A}(X)}{\partial \log m} \; . \tag{16}$$

The theorem can be derived by observing that the insertion of an external zero-energy Higgs line into a fermionic propagator, for instance, is equivalent to the substitution

$$\frac{1}{\not{p} - m} \to \frac{1}{\not{p} - m} \frac{m}{v} \frac{1}{\not{p} - m} = \frac{1}{v} \frac{\partial}{\partial \log m} \frac{1}{\not{p} - m} \; .$$

The amplitudes for processes including an external Higgs line can therefore be obtained from the amplitude without the external Higgs line by taking the logarithmic derivative. If applied to the gluon propagator at $Q^2 = 0$, $\Pi_{gg} \sim \frac{\alpha_s}{12\pi} GG \log m$, the Hgg amplitude can easily be derived as $\mathcal{A}(Hgg) = GG \frac{\alpha_s}{12\pi} \frac{1}{v}$. If higher orders are included, the parameter m must be interpreted as bare mass.

(d) Summary

By adding up all possible decay channels, we obtain the total width shown in Fig. 5a. Up to masses of 140 GeV, the Higgs particle is very narrow, $\Gamma(H) \leq 10$ MeV. After opening up the real and virtual gauge-boson channels, the state rapidly becomes wider, reaching a width of ~ 1 GeV at the ZZ threshold. The width cannot be measured directly in the intermediate mass region at the LHC or e^+e^- colliders; however, it could be measured directly at muon colliders [35]. Above a mass of ~ 250 GeV, the state becomes wide enough to be resolved experimentally in general.

The branching ratios of the main decay modes are displayed in Fig. 5b. A large variety of channels will be accessible for Higgs masses below 140 GeV. The dominant mode is $b\bar{b}$ decays, yet $c\bar{c}, \tau^+\tau^-$ and gg decays still occur at a level of several per cent. At $M_H = 120$ GeV for instance, the branching ratios are 68% for $b\bar{b}$, 3.1% for $c\bar{c}$, 6.9% for $\tau^+\tau^-$ and 7% for gg. $\gamma\gamma$ decays occur at a level of 1 per mille. Above this mass value, the Higgs boson decay into W's becomes dominant, overwhelming all other channels if the decay mode into two real W's is kinematically possible. For Higgs masses far above the thresholds, ZZ and WW decays occur at a ratio of 1:2, slightly modified only just above the $t\bar{t}$ threshold. Since the width grows as the third power of the mass, the Higgs particle becomes very wide, $\Gamma(H) \sim \frac{1}{2} M_H^3$ [TeV]. In fact, for $M_H \sim 1$ TeV, the width reaches $\sim \frac{1}{2}$ TeV.

2.3   Electroweak Precision Data: Estimate of the Higgs Mass

Indirect evidence for a light Higgs boson can be derived from the high-precision measurements of electroweak observables at LEP and elsewhere. Indeed, the fact that the
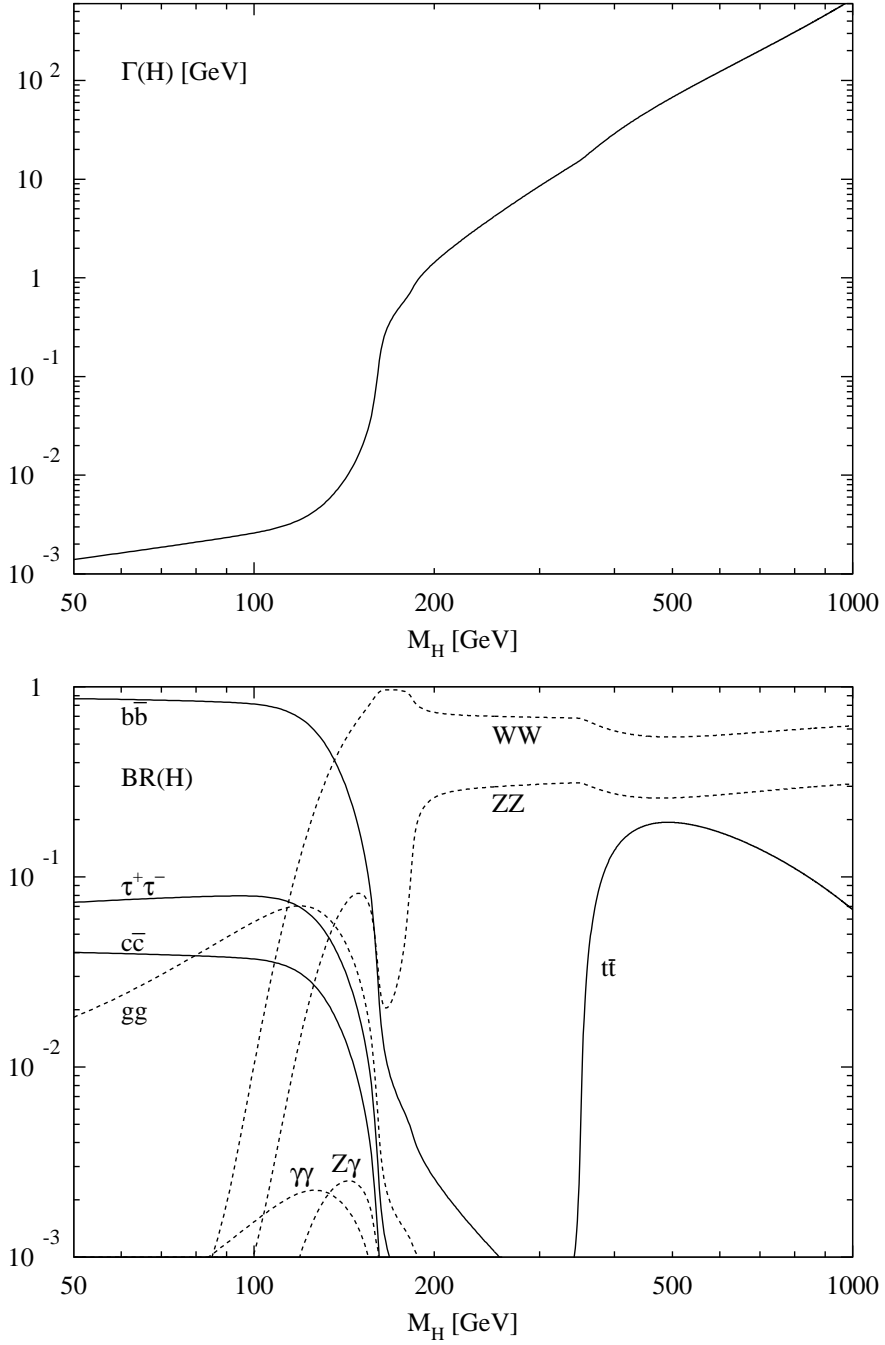
Figure 5: *(a) Total decay width (in GeV) of the SM Higgs boson as a function of its mass.
(b) Branching ratios of the dominant decay modes of the SM Higgs particle. All relevant
higher-order corrections are taken into account.*

12

Standard Model is renormalizable only after including the top and Higgs particles in the loop corrections, indicates that the electroweak observables are sensitive to the masses of these particles.

The Fermi coupling can be rewritten in terms of the weak coupling and the W mass; at lowest order, $G_F/\sqrt{2} = g^2/8M_W^2$. After substituting the electromagnetic coupling, the electroweak mixing angle and the Z mass for the weak coupling, and the W mass, this relation can be rewritten as

$$\frac{G_F}{\sqrt{2}} = \frac{2\pi\alpha}{\sin^2 2\theta_W M_Z^2}[1 + \Delta r_\alpha + \Delta r_t + \Delta r_H] \; . \tag{17}$$

The Δ terms take account of the radiative corrections: Δr_α describes the shift in the electromagnetic coupling if evaluated at the scale M_Z^2 instead of zero-momentum; Δr_t denotes the top (and bottom) quark contributions to the W and Z masses, which are quadratic in the top mass. Finally, Δr_H accounts for the virtual Higgs contributions to the masses; this term depends only logarithmically [7] on the Higgs mass at leading order:

$$\Delta r_H = \frac{G_F M_W^2}{8\sqrt{2}\pi^2} \frac{11}{3} \left[\log \frac{M_H^2}{M_W^2} - \frac{5}{6} \right] \qquad (M_H^2 \gg M_W^2) \; . \tag{18}$$

The screening effect reflects the role of the Higgs field as a regulator that renders the electroweak theory renormalizable.

Although the sensitivity on the Higgs mass is only logarithmic, the increasing precision in the measurement of the electroweak observables allows us to derive interesting estimates and constraints on the Higgs mass [8]:

$$\begin{aligned} M_H &= 115^{+116}_{-66} \text{ GeV} \\ &< 420 \text{ GeV} \quad (95\% \text{ CL}) \; . \end{aligned} \tag{19}$$

It may be concluded from these numbers that the canonical formulation of the Standard Model, which includes the existence of a Higgs boson with a mass below ~ 700 GeV, is compatible with the electroweak data. However, alternative mechanisms cannot be ruled out.

2.4 Higgs Production Channels at e^+e^- Colliders

The first process that was used to search directly for Higgs bosons over a large mass range, was the Bjorken process, $Z \to Z^*H, Z^* \to f\bar{f}$ [36]. By exploring this production channel, Higgs bosons with masses less than 65.4 GeV were excluded by the LEP1 experiments. The search now continues by reversing the role of the real and virtual Z bosons in the e^+e^- continuum at LEP2.

The main production mechanisms for Higgs bosons in e^+e^- collisions are

$$\text{Higgs-strahlung} \;\; : \;\; e^+e^- \to Z^* \to ZH \tag{20}$$

$$WW \text{ fusion} \;\; : \;\; e^+e^- \to \bar{\nu}_e\nu_e(WW) \to \bar{\nu}_e\nu_e H \tag{21}$$

13

In Higgs-strahlung [32, 36, 37] the Higgs boson is emitted from the Z-boson line, while WW fusion is a formation process of Higgs bosons in the collision of two quasi-real W bosons radiated off the electron and positron beams [38].

As evident from the subsequent analyses, LEP2 can cover the SM Higgs mass range up to about 100 GeV [10]. The high-energy e^+e^- linear colliders can cover the entire Higgs mass range in the second phase of the machines in which they will reach a total energy of about 2 TeV [13].

(a) Higgs-strahlung

The cross section for Higgs-strahlung can be written in a compact form as

$$\sigma(e^+e^- \to ZH) = \frac{G_F^2 M_Z^4}{96\pi s} \left[v_e^2 + a_e^2\right] \lambda^{1/2} \frac{\lambda + 12M_Z^2/s}{\left[1 - M_Z^2/s\right]^2} , \tag{22}$$

where $v_e = -1 + 4\sin^2\theta_W$ and $a_e = -1$ are the vector and axial-vector Z charges of the electron and $\lambda = [1 - (M_H + M_Z)^2/s][1 - (M_H - M_Z)^2/s]$ is the usual two-particle phase-space function. The cross section is of the size $\sigma \sim \alpha_W^2/s$, i.e. of second order in the weak coupling, and it scales in the squared energy.
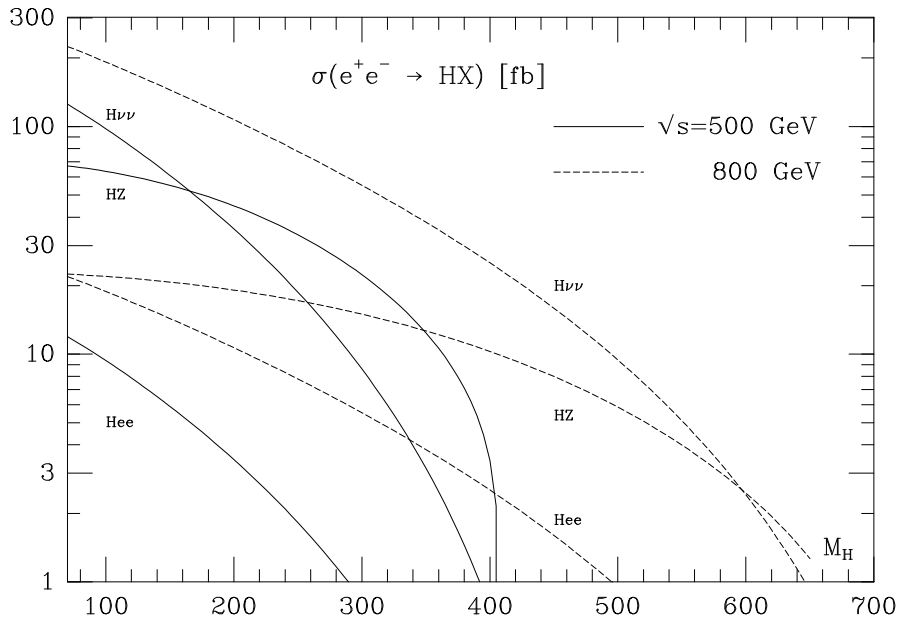
Figure 6: *The cross section for the production of SM Higgs bosons in Higgs-strahlung $e^+e^- \to ZH$ and WW/ZZ fusion $e^+e^- \to \bar{\nu}_e\nu_e/e^+e^-H$; solid curves: $\sqrt{s} = 500$ GeV, dashed curves: $\sqrt{s} = 800$ GeV.*

Since the cross section vanishes for asymptotic energies, the Higgs-strahlung process is most useful for searching Higgs bosons in the range where the collider energy is of the

14

same order as the Higgs mass, $\sqrt{s} \gtrsim \mathcal{O}(M_H)$. The size of the cross section is illustrated in Fig. 6 for the energy $\sqrt{s} = 500$ GeV of e^+e^- linear colliders as a function of the Higgs mass. Since the recoiling Z mass in the two-body reaction $e^+e^- \to ZH$ is mono-energetic, the mass of the Higgs boson can be reconstructed from the energy of the Z boson, $M_H^2 = s - 2\sqrt{s}E_Z + M_Z^2$, without any need to analyse the decay products of the Higgs boson. For leptonic Z decays, missing-mass techniques provide a very clear signal, as demonstrated in Fig. 7.
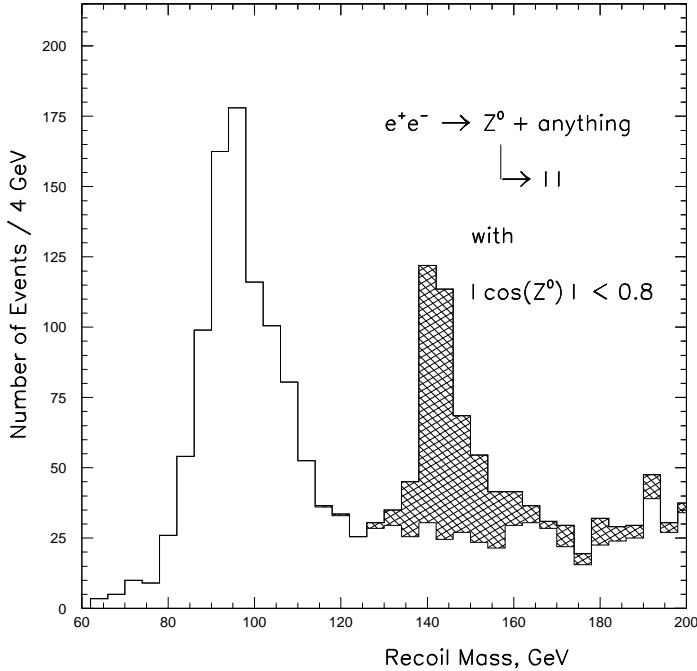

Figure 7: *Dilepton recoil mass analysis of Higgs-strahlung $e^+e^- \to ZH \to \ell^+\ell^- +$ anything in the intermediate Higgs mass range for $M_H = 140$ GeV. The c.m. energy is $\sqrt{s} = 360$ GeV and the integrated luminosity $\int \mathcal{L} = 50 fb^{-1}$. Ref. [39].*

(b) WW fusion

Also the cross section for the fusion process (21) can be cast implicitly into a compact form:

$$\sigma(e^+e^- \to \bar{\nu}_e\nu_e H) = \frac{G_F^3 M_W^4}{4\sqrt{2}\pi^3} \int_{\kappa_H}^1 \int_x^1 \frac{dx\,dy}{[1 + (y-x)/\kappa_W]^2} f(x,y) \tag{23}$$

$$f(x,y) = \left(\frac{2x}{y^3} - \frac{1+3x}{y^2} + \frac{2+x}{y} - 1\right)\left[\frac{z}{1+z} - \log(1+z)\right] + \frac{x}{y^3}\frac{z^2(1-y)}{1+z} ,$$

with $\kappa_H = M_H^2/s$, $\kappa_W = M_W^2/s$ and $z = y(x - \kappa_H)/(\kappa_W x)$.

15

Since the fusion process is a t-channel exchange process, the size is set by the W Compton wavelength, suppressed however with respect to Higgs-strahlung by the third power of the electroweak coupling, $\sigma \sim \alpha_W^3/M_W^2$. As a result, W fusion becomes the leading production process for Higgs particles at high energies. At asymptotic energies the cross section simplifies to

$$\sigma(e^+ e^- \to \bar{\nu}_e \nu_e H) \to \frac{G_F^3 M_W^4}{4\sqrt{2}\pi^3} \left[\log \frac{s}{M_H^2} - 2 \right] \;. \tag{24}$$

In this limit, W fusion to Higgs bosons can be interpreted as a two-step process: the W bosons are radiated as quasi-real particles from electrons and positrons, $e \to \nu W$, with the Higgs bosons formed subsequently in the colliding W beams.

The size of the fusion cross section is compared with Higgs-strahlung in Fig. 6. At $\sqrt{s} = 500$ GeV the two cross sections are of the same order, yet the fusion process becomes increasingly important with rising energy.

(c) $\gamma\gamma$ fusion

The production of Higgs bosons in $\gamma\gamma$ collisions [40] can be exploited to determine important properties of these particles, in particular the two-photon decay width. The $H\gamma\gamma$ coupling is mediated by loops of charged particles. If the mass of the loop particle is generated through the Higgs mechanism, the decoupling of the heavy particles is lifted and the $\gamma\gamma$ width reflects the spectrum of these states with masses possibly far above the Higgs mass.

The two-photon width is related to the production cross section for polarized γ beams by

$$\sigma(\gamma\gamma \to H) = \frac{16\pi^2 \Gamma(H \to \gamma\gamma)}{M_H} \times BW \;, \tag{25}$$

where BW denotes the Breit–Wigner resonance factor in terms of the $\gamma\gamma$ energy squared. For narrow Higgs bosons the observed cross section is found by folding the parton cross section with the invariant $\gamma\gamma$ energy flux $\tau d\mathcal{L}^{\gamma\gamma}/d\tau$ for $J_z^{\gamma\gamma} = 0$ at $\tau = M_H^2/s_{ee}$.

The event rate for the production of Higgs bosons in $\gamma\gamma$ collisions of Weizsäcker–Williams photons is too small to play a role in practice. However, the rate is sufficiently large if the photon spectra are generated by Compton back-scattering of laser light, Fig. 8. The $\gamma\gamma$ invariant energy in such a Compton collider [41] is nearly of the same size as the parent $e^+ e^-$ energy and the luminosity is expected to be only slightly smaller than the luminosity in $e^+ e^-$ collisions. In the Higgs mass range between 100 and 150 GeV, the final state consists primarily of $b\bar{b}$ pairs. The large $\gamma\gamma$ continuum background is suppressed in the $J_z^{\gamma\gamma} = 0$ polarization state. For Higgs masses above 150 GeV, WW final states become dominant, supplemented in the ratio 1:2 by ZZ final states above the ZZ decay threshold. While the continuum WW background in $\gamma\gamma$ collisions is very large, the ZZ background appears under control for masses up to order 300 GeV [42].
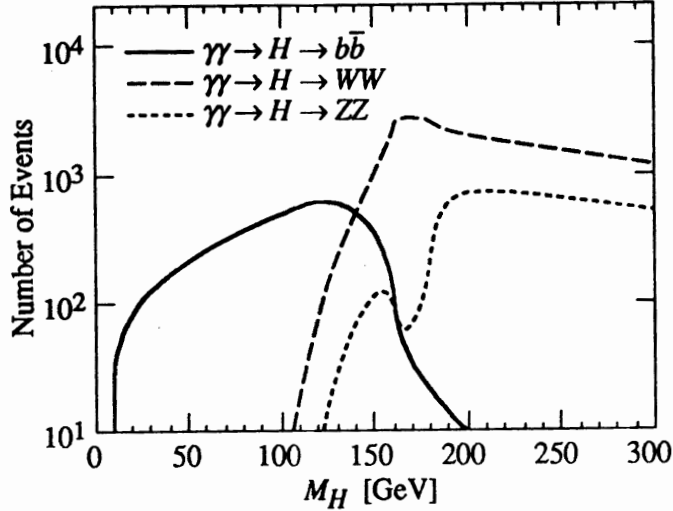
16

Figure 8: *Production rate of Standard Model Higgs bosons for three exclusive final states relevant for the intermediate- and heavy-mass regions in $\gamma\gamma$ collisions. A value of $4 \times 10^{-2} fb^{-1}/GeV$ is assumed for $d\mathcal{L}^{\gamma\gamma}/dW_{\gamma\gamma}$. Ref. [40].*

2.5   Higgs Production at Hadron Colliders

Several processes can be exploited to produce Higgs particles in hadron colliders [34, 43]:

$$\text{gluon fusion} \qquad\qquad : \quad gg \to H$$

$$WW, ZZ \text{ fusion} \qquad\qquad : \quad W^+W^-, ZZ \to H$$

$$\text{Higgs-strahlung off } W, Z \qquad : \quad q\bar{q} \to W, Z \to W, Z + H$$

$$\text{Higgs bremsstrahlung off top} \quad : \quad q\bar{q}, gg \to t\bar{t} + H$$

While gluon fusion plays a dominant role throughout the entire Higgs mass range of the Standard Model, the WW/ZZ fusion process becomes increasingly important with rising Higgs mass. The last two radiation processes are relevant only for light Higgs masses.

The production cross sections at hadron colliders, at the LHC in particular, are quite sizeable so that a large sample of SM Higgs particles can be produced in this machine. Experimental difficulties arise from the huge number of background events that come along with the Higgs signal events. This problem will be tackled by either triggering on leptonic decays of W, Z and t in the radiation processes or by exploiting the resonance character of the Higgs decays $H \to \gamma\gamma$ and $H \to ZZ \to 4\ell^{\pm}$. In this way, the Tevatron is expected to search for Higgs particles in the mass range above that of LEP2 up to about 110 to 120 GeV [11]. The LHC is expected to cover the entire canonical Higgs mass range $M_H \lesssim 700$ GeV of the Standard Model [12].

17

(a) Gluon fusion

The gluon-fusion mechanism [31, 34, 44]

$$pp \to gg \to H$$

provides the dominant production mechanism of Higgs bosons at the LHC in the entire relevant Higgs mass range up to about 1 TeV. The gluon coupling to the Higgs boson in the SM is mediated by triangular loops of top and bottom quarks, cf. Fig. 9. Since the Yukawa coupling of the Higgs particle to heavy quarks grows with the quark mass, thus balancing the decrease of the amplitude, the form factor approaches a non-zero value for large loop-quark masses. [If the masses of heavy quarks beyond the third generation were generated solely by the Higgs mechanism, these particles would add the same amount to the form factor as the top quark in the asymptotic heavy-quark limit.]
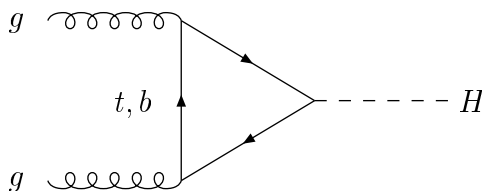

Figure 9: *Diagram contributing to the formation of Higgs bosons in gluon-gluon collisions at lowest order.*

The partonic cross section, Fig. 9, can be expressed by the gluonic width of the Higgs boson at lowest order [34]:

$$\hat{\sigma}_{LO}(gg \to H) = \sigma_0 M_H^2 \delta(\hat{s} - M_H^2) \tag{26}$$

$$\sigma_0 = \frac{\pi^2}{8M_H^2} \Gamma_{LO}(H \to gg) = \frac{G_F \alpha_s^2}{288\sqrt{2}\pi} \left| \sum_Q A_Q^H(\tau_Q) \right|^2 ,$$

where the scaling variable is defined as $\tau_Q = 4M_Q^2/M_H^2$ and $\hat{s}$ denotes the partonic c.m. energy squared. The form factor can easily be evaluated:

$$A_Q^H(\tau_Q) = \frac{3}{2}\tau_Q \left[1 + (1 - \tau_Q)f(\tau_Q)\right] \tag{27}$$

$$f(\tau_Q) = \begin{cases} \arcsin^2 \dfrac{1}{\sqrt{\tau_Q}} & \tau_Q \geq 1 \\[2mm] -\dfrac{1}{4}\left[\log\dfrac{1+\sqrt{1-\tau_Q}}{1-\sqrt{1-\tau_Q}} - i\pi\right]^2 & \tau_Q < 1 \end{cases}$$

18

For small loop masses the form factor vanishes, $A_Q^H(\tau_Q) \sim -3/8\tau_Q[\log(\tau_Q/4) + i\pi]^2$, while for large loop masses it approaches a non-zero value, $A_Q^H(\tau_Q) \to 1$.

In the narrow-width approximation, the hadronic cross section can be cast into the form

$$\sigma_{LO}(pp \to H) = \sigma_0 \tau_H \frac{d\mathcal{L}^{gg}}{d\tau_H} \ , \tag{28}$$

with $d\mathcal{L}^{gg}/d\tau_H$ denoting the gg luminosity of the pp collider, evaluated for the Drell–Yan variable $\tau_H = M_H^2/s$, where s is the total hadronic energy squared.
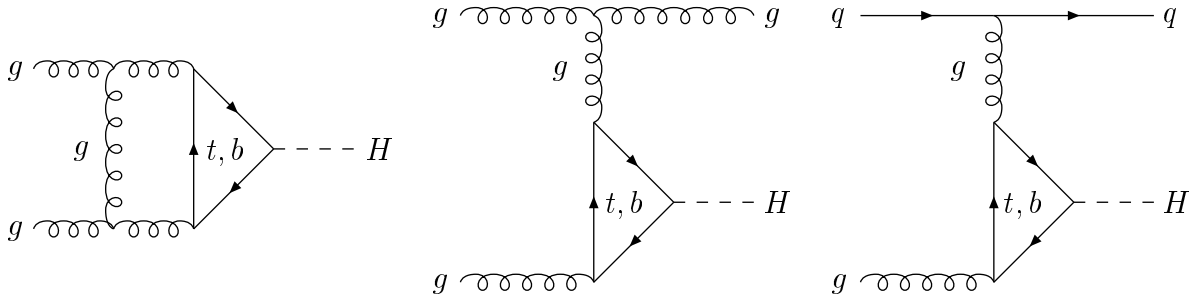

Figure 10: *Typical diagrams contributing to the virtual/real QCD corrections to* $gg \to H$.

The QCD corrections to the gluon fusion process [34] are very important. They stabilize the theoretical predictions for the cross section when the renormalization and factorization scales are varied. Moreover, they are large and positive, thus increasing the production cross section for Higgs bosons. The QCD corrections consist of virtual corrections to the basic process $gg \to H$, and of real corrections due to the associated production of the Higgs boson with massless partons, $gg \to Hg$ and $gq \to Hq$, $q\bar{q} \to Hg$. These subprocesses contribute to Higgs production at $\mathcal{O}(\alpha_s^3)$. The virtual corrections rescale the lowest-order fusion cross section with a coefficient that depends only on the ratios of the Higgs and quark masses. Gluon radiation leads to two-parton final states with invariant energy $\hat{s} \geq M_H^2$ in the gg, gq and $q\bar{q}$ channels.

The final result for the hadronic cross section can be split into five parts:

$$\sigma(pp \to H + X) = \sigma_0 \left[1 + C\frac{\alpha_s}{\pi}\right] \tau_H \frac{d\mathcal{L}^{gg}}{d\tau_H} + \Delta\sigma_{gg} + \Delta\sigma_{gq} + \Delta\sigma_{q\bar{q}} \ . \tag{29}$$

The calculation of the corrections has been performed in the $\overline{MS}$ scheme. The mass M_Q is identified with the pole quark mass and the renormalization scale in α_s and the factorization scale of the parton densities can be fixed at the Higgs mass. [The general scale dependence is also known.]

The coefficient $C(\tau_Q)$ denotes the finite part of the virtual two-loop corrections. It splits into the infrared part π^2 and the finite piece, which depends on the quark mass:

$$C(\tau_Q) = \pi^2 + c(\tau_Q) \ . \tag{30}$$

19

The finite parts of the hard contributions from gluon radiation in gg scattering, gq scattering and $q\bar{q}$ annihilation, may be written as

$$\Delta\sigma_{gg} = \int_{\tau_H}^{1} d\tau \frac{d\mathcal{L}^{gg}}{d\tau} \times \frac{\alpha_s}{\pi}\sigma_0 \Big\{ -zP_{gg}(z)\log z + d_{gg}(z,\tau_Q)$$
$$+12\left[\left(\frac{\log(1-z)}{1-z}\right)_+ - z[2-z(1-z)]\log(1-z)\right]\Big\}$$

$$\Delta\sigma_{gq} = \int_{\tau_H}^{1} d\tau \sum_{q,\bar{q}} \frac{d\mathcal{L}^{gq}}{d\tau} \times \frac{\alpha_s}{\pi}\sigma_0 \left\{ -\frac{z}{2}P_{gq}(z)\log\frac{z}{(1-z)^2} + d_{gq}(z,\tau_Q)\right\}$$

$$\Delta\sigma_{q\bar{q}} = \int_{\tau_H}^{1} d\tau \sum_{q} \frac{d\mathcal{L}^{q\bar{q}}}{d\tau} \times \frac{\alpha_s}{\pi}\sigma_0 \; d_{q\bar{q}}(z,\tau_Q) \tag{31}$$

with $z = \tau_H/\tau = M_H^2/\hat{s}$; P_{gg} and P_{gq} are the standard Altarelli–Parisi splitting functions. The coefficient functions $c(\tau_Q)$ and $d(z,\tau_Q)$ can be reduced analytically to one-dimensional integrals, which must, in general, be evaluated numerically. However, they can be calculated analytically in the heavy-quark limit [34, 45]:

$$c(\tau_Q) \rightarrow \frac{11}{2} \qquad\qquad d_{gg}(z,\tau_Q) \rightarrow -\frac{11}{2}(1-z)^3$$
$$d_{gq}(z,\tau_Q) \rightarrow \frac{2}{3}z^2 - (1-z)^2 \qquad\qquad d_{q\bar{q}}(z,\tau_Q) \rightarrow \frac{32}{27}(1-z)^3 \tag{32}$$

Thus, for light Higgs bosons the production cross section is available in complete analytic form, including the complicated QCD radiative corrections.

The size of the radiative corrections can be parametrized by defining the K factor as $K = \sigma_{NLO}/\sigma_{LO}$, in which all quantities are evaluated in the numerator and denominator in next-to-leading and leading order, respectively. The results of this calculation are shown in Fig. 11. The virtual corrections K_{virt} and the real corrections K_{gg} for the gg collisions are apparently of the same size, and both are large and positive; the corrections for $q\bar{q}$ collisions and the gq inelastic Compton contributions are less important. After including these higher-order QCD corrections, the dependence of the cross section on the renormalization and factorization scales is significantly reduced from a level of $\mathcal{O}(100\%)$ down to a level of about 20%.

The theoretical prediction for the production cross section of Higgs particles is presented in Fig. 12 for the LHC as a function of the Higgs mass. The cross section decreases with increasing Higgs mass. This is, to a large extent, a consequence of the sharply falling gg luminosity for large invariant masses. The bump in the cross section is induced by the $t\bar{t}$ threshold in the top triangle. The overall theoretical accuracy of this calculation is expected to be at a level of 20 to 30%.

(b) Vector-boson fusion

The second important channel for Higgs production at the LHC is vector-boson fusion,
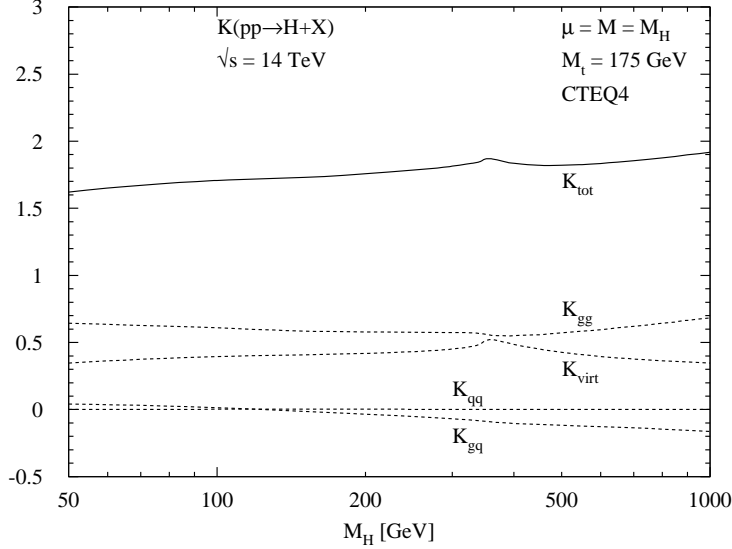
Figure 11: *K factors of the QCD-corrected gluon-fusion cross section $\sigma(pp \to H{+}X)$ at the LHC with c.m. energy $\sqrt{s} = 14$ TeV. The dashed lines show the individual contributions of the four terms of the QCD corrections defined in eq. (29). The renormalization and factorization scales have been identified with the Higgs mass, and CTEQ4 parton densities have been adopted.*

$W^+W^- \to H$ [20, 43]. For large Higgs masses this mechanism becomes competitive to gluon fusion; for intermediate masses the cross section is smaller by about an order of magnitude.

For large Higgs masses, the two electroweak bosons W, Z that form the Higgs boson are predominantly longitudinally polarized. At high energies, the equivalent particle spectra of the longitudinal W, Z bosons in quark beams are given by

$$f_L^W(x) \;\; = \;\; \frac{G_F M_W^2}{2\sqrt{2}\pi^2} \frac{1-x}{x} \tag{33}$$

$$f_L^Z(x) \;\; = \;\; \frac{G_F M_Z^2}{2\sqrt{2}\pi^2} \left[(I_3^q - 2e_q \sin^2\theta_W)^2 + (I_3^q)^2 \right] \frac{1-x}{x} \; ,$$

where x is the fraction of energy transferred from the quark to the W, Z boson in the splitting process $q \to q{+}W/Z$. From these particle spectra, the WW and ZZ luminosities can easily be derived:

$$\frac{d\mathcal{L}^{WW}}{d\tau_W} \;\; = \;\; \frac{G_F^2 M_W^4}{8\pi^4} \left[2 - \frac{2}{\tau_W} - \frac{1+\tau_W}{\tau_W} \log \tau_W \right] \tag{34}$$

$$\frac{d\mathcal{L}^{ZZ}}{d\tau_Z} \;\; = \;\; \frac{G_F^2 M_Z^4}{8\pi^4} \left[(I_3^q - 2e_q \sin^2\theta_W)^2 + (I_3^q)^2 \right] \left[(I_3^{q'} - 2e_{q'} \sin^2\theta_W)^2 + (I_3^{q'})^2 \right]$$

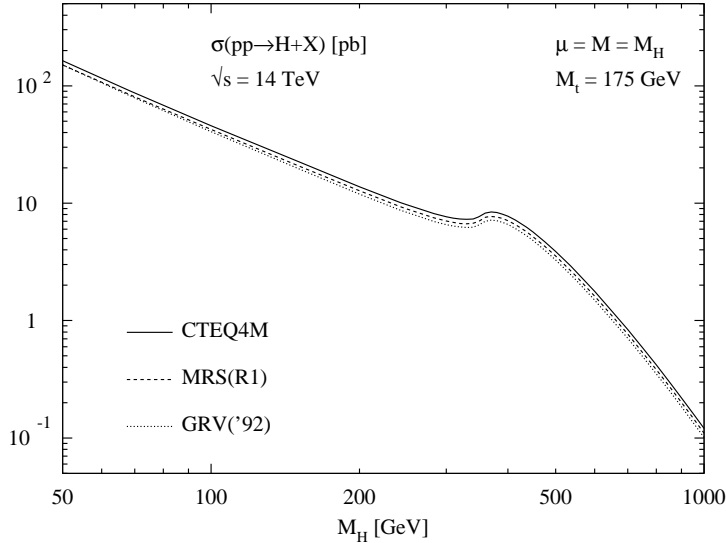$$\cdot \left[2 - \frac{2}{\tau_Z} - \frac{1+\tau_Z}{\tau_Z} \log \tau_Z \right]$$

21

Figure 12: *The cross section for the production of Higgs bosons; three different sets of parton densities are shown [CTEQ4M, MRS(R1) and GRV('92)].*

with the Drell–Yan variable defined as $\tau_V = M_{VV}^2/s$. Denoting the parton cross section for $WW, ZZ \to H$ by $\hat{\sigma}_0$ with

$$\hat{\sigma}_0(VV \to H) = \sigma_0 \delta\left(1 - M_H^2/\hat{s}\right) \tag{35}$$
$$\sigma_0 = \sqrt{2}\,\pi G_F\,,$$

the cross section for Higgs production in quark–quark collisions is given by

$$\hat{\sigma}(qq \to qqH) = \frac{d\mathcal{L}^{VV}}{d\tau_V}\sigma_0\,. \tag{36}$$

The hadronic cross section is finally obtained by summing the parton cross section (36) over the flux of all possible pairs of quark–quark and antiquark combinations

$$\sigma(qq' \to VV \to H) = \int_{M_H^2/s}^1 d\tau \sum_{qq'} \frac{d\mathcal{L}^{qq'}}{d\tau}\hat{\sigma}(qq' \to qq'H; \hat{s} = \tau s)\,. \tag{37}$$

Since to lowest order the proton remnants are colour singlets in the WW, ZZ fusion processes, no colour will be exchanged between the two quark lines from which the two vector bosons are radiated. As a result, the leading QCD corrections to these processes are already accounted for by the corrections to the quark parton densities.

The WW/ZZ fusion cross section for Higgs bosons at the LHC is shown in Fig. 13. The process is apparently most important in the upper range of Higgs masses, where the cross section approaches values close to gluon fusion.

22

(c) Higgs-strahlung off vector bosons

Higgs-strahlung $q\bar{q} \to V^* \to VH$ ($V = W, Z$) is a very important mechanism (Fig. 13) for the search of light Higgs bosons at the hadron colliders Tevatron and LHC. Though the cross section is smaller than for gluon fusion, leptonic decays of the electroweak vector bosons are extremely useful to filter Higgs signal events out of the huge background. Since the dynamical mechanism is the same as for e^+e^- colliders, except for the folding with the quark–antiquark densities, intermediate steps of the calculation need not be noted, and merely the final values of the cross sections for the Tevatron and the LHC are recorded in Fig. 13.

(d) Higgs bremsstrahlung off top quarks

Also the process $gg, q\bar{q} \to t\bar{t}H$ is relevant only for small Higgs masses, Fig. 13. The analytical expression for the parton cross section, even at lowest order, is quite involved, so that just the final results for the LHC cross section are shown in Fig. 13.

Higgs bremsstrahlung off top quarks is also an interesting process for measurements of the fundamental Htt Yukawa coupling. The cross section $\sigma(pp \to t\bar{t}H)$ is directly proportional to the square of this fundamental coupling.

Summary. An overview of the production cross sections for Higgs particles at the LHC is presented in Fig. 13. Three classes of channels can be distinguished. The gluon fusion of Higgs particles is a universal process, dominant over the entire SM Higgs mass range. Higgs-strahlung off electroweak W, Z bosons or top quarks is prominent for light Higgs bosons. The WW/ZZ fusion channel, by contrast, becomes increasingly important in the upper part of the SM Higgs mass range.

The signatures for the search for Higgs particles are dictated by the decay branching ratios. In the lower part of the intermediate mass range, resonance reconstruction in $\gamma\gamma$ final states and $b\bar{b}$ jets can be exploited. In the upper part of the intermediate mass range, decays to ZZ^* and WW^* are important, with the two electroweak bosons decaying leptonically. In the mass range above the on-shell ZZ decay threshold, the charged-lepton decays $H \to ZZ \to 4\ell^{\pm}$ provide gold-plated signatures. Only at the upper end of the classical SM Higgs mass range, decays to neutrinos and jets, generated in W and Z decays, complete the search techniques.

2.6 The Profile of the SM Higgs Particle

To establish the Higgs mechanism experimentally, the nature of this particle must be explored by measuring all its characteristics, the mass and lifetime, the external quantum numbers spin-parity, the couplings to gauge bosons and fermions, and last but not least, the Higgs self-couplings. While part of this program can be realized at the LHC, the complete profile of the particle can be reconstructed across the entire mass range in e^+e^- colliders.
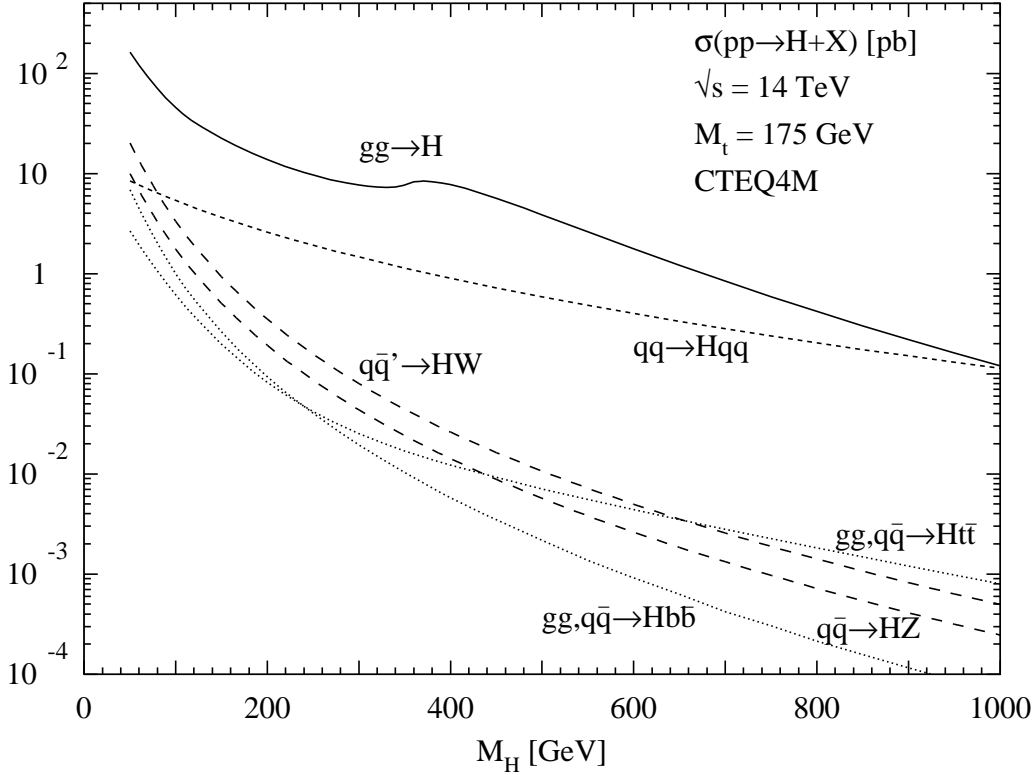
Figure 13: *Higgs production cross sections at the LHC for the various production mechanisms as a function of the Higgs mass. The full QCD-corrected results for the gluon fusion $gg \rightarrow H$, vector-boson fusion $qq \rightarrow VVqq \rightarrow Hqq$, vector-boson bremsstrahlung $q\bar{q} \rightarrow V^* \rightarrow HV$ and associated production $gg, q\bar{q} \rightarrow Ht\bar{t}, Hb\bar{b}$ are shown. [The QCD corrections to the last processes are unknown.]*

(a) Mass

The mass of the Higgs particle can be measured by collecting the decay products of the particle at hadron and e^+e^- colliders. Moreover, in e^+e^- collisions Higgs-strahlung can be exploited to reconstruct the mass very precisely from the Z recoil energy in the two-body process $e^+e^- \rightarrow ZH$. An overall accuracy of about $\delta M_H \sim 100$ MeV can be expected.

(b) Width/lifetime

The width of the state, i.e. the lifetime of the particle, can be directly measured above the ZZ decay threshold where the width grows rapidly. In the lower part of the intermediate mass range the width can be measured indirectly, by combining the branching ratio for $H \rightarrow \gamma\gamma$, accessible at the LHC, with the measurement of the partial $\gamma\gamma$ width, accessible through $\gamma\gamma$ production at a Compton collider: $\Gamma_{tot} = \Gamma_{\gamma\gamma}/BR_{\gamma\gamma}$. In the upper part of the intermediate mass range, the combination of the branching ratios for $H \rightarrow WW, ZZ$

decays with the production cross sections for WW fusion and Higgs-strahlung, which can be expressed both through the partial Higgs decay widths to WW and ZZ pairs, will allow us to extract the width of the Higgs particle. Thus, the total width of the Higgs particle can be determined throughout the entire mass range when the experimental results from the LHC, e^+e^- and $\gamma\gamma$ colliders can be combined. The direct measurement of the width in the intermediate mass range will be possible at muon colliders in which Higgs bosons can be generated as s-channel resonances: $\mu^+\mu^- \to H \to f\bar{f}, VV$. The energy resolution of the muon beams is expected to be so high that the Breit–Wigner excitation curve can be reconstructed [35].

(c) Spin-parity

The angular distribution of the Z/H bosons in the Higgs-strahlung process is sensitive to the spin and parity of the Higgs particle [13]. Since the production amplitude is given by $\mathcal{A}(0^+) \sim \vec{\epsilon}_{Z^*} \cdot \vec{\epsilon}_Z$, the Z boson is produced in a state of longitudinal polarization at high energies – in accordance with the equivalence theorem. As a result, the angular distribution

$$\frac{d\sigma}{d\cos\theta} \sim \sin^2\theta + \frac{8M_Z^2}{\lambda s} \tag{38}$$

approaches the spin-zero $\sin^2\theta$ law asymptotically. This may be contrasted with the distribution $\sim 1 + \cos^2\theta$ for negative parity states, which follows from the transverse polarization amplitude $\mathcal{A}(0^-) \sim \vec{\epsilon}_{Z^*} \times \vec{\epsilon}_Z \cdot \vec{k}_Z$. It is also characteristically different from the distribution of the background process $e^+e^- \to ZZ$, which, as a result of t/u-channel e exchange, is strongly peaked in the forward/backward direction, Fig. 14.

In a similar way, the zero-spin of the Higgs particle can be determined from the isotropic distribution of the decay products. Moreover, the parity can be measured by observing the spin correlations of the decay products. According to the equivalence theorem, the azimuthal angles of the decay planes in $H \to ZZ \to (\mu^+\mu^-)(\mu^+\mu^-)$ are asymptotically uncorrelated, $d\Gamma^+/d\phi_* \to 0$, for a 0^+ particle; this is to be contrasted with $d\Gamma^-/d\phi_* \to 1 - \frac{1}{4}\cos 2\phi_*$ for the distribution of the azimuthal angle between the planes for the decay of a 0^- particle. The difference between the angular distributions is a consequence of the different polarization states of the vector bosons in the two cases. While they approach states of longitudinal polarization for scalar Higgs decays, they are transversely polarized for pseudoscalar particle decays.

(d) Higgs couplings

Since the fundamental particles acquires a mass through the interaction with the Higgs field, the strength of the Higgs couplings to fermions and gauge bosons is set by the masses of these particles. It will therefore be a very important experimental task to measure these couplings, which are uniquely predicted by the very nature of the Higgs mechanism.
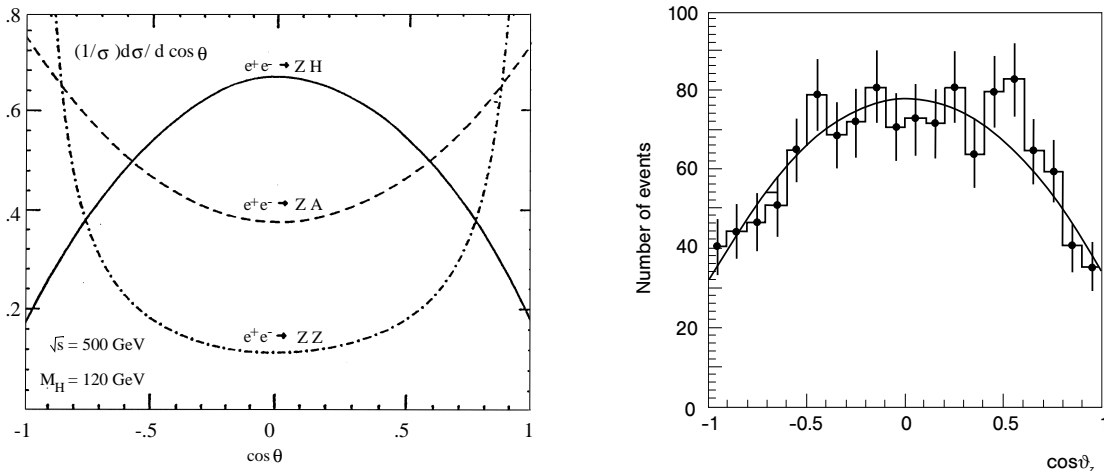
Figure 14: *Left: Angular distribution of Z/H bosons in Higgs-strahlung, compared with the production of pseudoscalar particles and the ZZ background final states; Ref. [46]. Right: The same for the signal plus background in the experimental simulation of Ref. [47].*

The Higgs couplings to massive gauge bosons can be determined from the production cross sections in Higgs-strahlung and WW, ZZ fusion, with the accuracy expected at the per cent level. For heavy enough Higgs bosons the decay width can be exploited to determine the coupling to electroweak gauge bosons. For Higgs couplings to fermions the branching ratios $H \to b\bar{b}, c\bar{c}, \tau^+\tau^-$ can be used in the lower part of the intermediate mass range; these observables allow the direct measurement of the Higgs Yukawa couplings. This is exemplified in Fig. 15 for a Higgs mass of 140 GeV.

A particularly interesting coupling is the Higgs coupling to top quarks. Since the top quark is by far the heaviest fermion in the Standard Model, irregularities in the standard picture of electroweak symmetry breaking through a fundamental Higgs field may become apparent first in this coupling. Thus the *Htt* Yukawa coupling may eventually provide essential clues to the nature of the mechanism breaking the electroweak symmetries.

Top loops mediating the production processes $gg \to H$ and $\gamma\gamma \to H$ (and the corresponding decay channels) give rise to cross sections and partial widths, which are proportional to the square of the Higgs–top Yukawa coupling. This Yukawa coupling can be measured directly, for the lower part of the intermediate mass range, in the bremsstrahlung processes $pp \to t\bar{t}H$ and $e^+e^- \to t\bar{t}H$ [49]. The Higgs boson is radiated, in the first process exclusively, in the second process predominantly, from the heavy top quarks. Even though these experiments are difficult because of the small cross sections [cf. Fig. 16 for e^+e^- collisions] and of the complex topology of the $b\bar{b}b\bar{b}W^+W^-$ final state, this process is an important tool for exploring the mechanism of electroweak symmetry breaking. For large Higgs masses above the $t\bar{t}$ threshold, the decay channel $H \to t\bar{t}$ can be stud-

26

ied; in e^+e^- collisions the cross section of $e^+e^- \to t\bar{t}Z$ increases through the reaction $e^+e^- \to ZH(\to t\bar{t})$ [50]. Higgs exchange between $t\bar{t}$ quarks also affects the excitation curve near the threshold at a level of a few per cent.
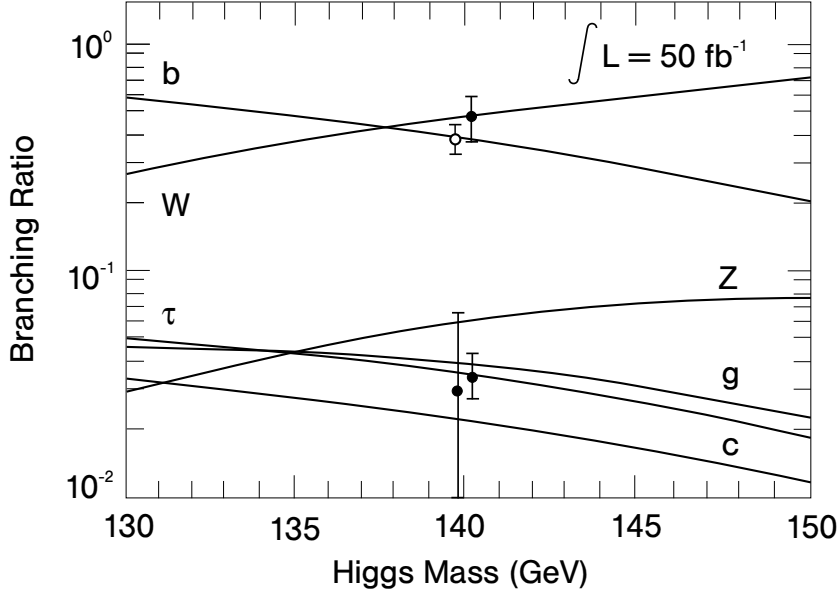

Figure 15: *The measurement of decay branching ratios of the SM Higgs boson for $M_H = 140$ GeV. In the bottom part of the figure the small error bar belongs to the τ branching ratio, the large bar to the average of the charm and gluon branching ratios, which were not separated in the simulation of Ref. [48]. In the upper part of the figure the open circle denotes the b branching ratio, the full circle the W branching ratio.*

(e) Higgs self-couplings

The Higgs mechanism, based on a non-zero value of the Higgs field in the vacuum, must finally be made manifest experimentally by reconstructing the interaction potential that generates the non-zero field in the vacuum. This program can be carried out by measuring the strength of the trilinear and quartic self-couplings of the Higgs particles:

$$g_{H^3} = 3\sqrt{\sqrt{2}G_F}M_H^2 \tag{39}$$

$$g_{H^4} = 3\sqrt{2}G_F M_H^2 \ . \tag{40}$$

This is a difficult task since the processes to be exploited are suppressed by small couplings and phase space. Nevertheless, the problem can be solved at the LHC and in the high-energy phase of the e^+e^- linear colliders for sufficiently high luminosities [51]. The best-suited reaction for the measurement of the trilinear coupling for Higgs masses in the theoretically preferred mass range of $\mathcal{O}(100 \text{ GeV})$, is the WW fusion process
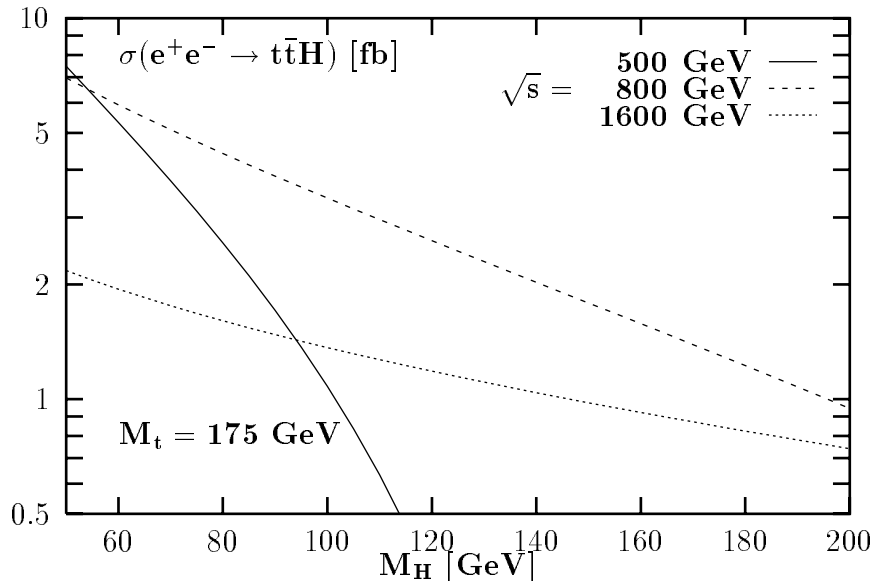
$$pp, e^+e^- \to WW \to HH \tag{41}$$

27

Figure 16: *The cross section for bremsstrahlung of SM Higgs bosons off top quarks in the Yukawa process $e^+e^- \to t\bar{t}H$. [The amplitude for radiation off the intermediate Z-boson line is small.] Ref. [49].*

in which, among other mechanisms, the two-Higgs final state is generated by the s-channel exchange of a virtual Higgs particle so that this process is sensitive to the trilinear HHH coupling in the Higgs potential, Fig. 17. Since the cross section is only a fraction of 1 fb at an energy of ~ 1.6 TeV, an integrated luminosity of $\sim 1ab^{-1}$ is needed to isolate the events at linear colliders. The quartic coupling H^4 seems to be accessible only through loop effects in the foreseeable future.

To sum up, the essential elements of the Higgs mechanism can be established experimentally at the LHC and TeV e^+e^- linear colliders.

3   Higgs Bosons in Supersymmetric Theories

Arguments deeply rooted in the Higg sector play an eminent role in introducing supersymmetry as a fundamental symmetry of nature [14]. This is the only symmetry that correlates bosonic with fermionic degrees of freedom.

(a)   The cancellation between bosonic and fermionic contributions to the radiative corrections of the light Higgs masses in supersymmetric theories provides a solution of the hierarchy problem in the Standard Model. If the Standard Model is embedded in a grand-unified theory, the large gap between the high grand-unification scale and the low scale of electroweak symmetry breaking can be stabilized in a natural way in boson–fermion
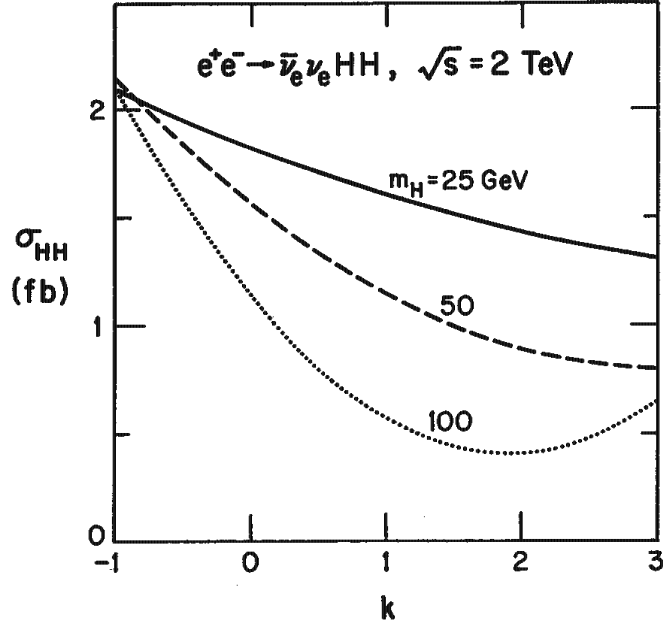
Figure 17: *Dependence of the cross section for Higgs-boson pair production via W fusion on the self-coupling k in units of the Standard Model coupling g_{H^3} at e^+e^- colliders. Ref. [51].*

symmetric theories [15, 52]. Denoting the bare Higgs mass by $M_{H,0}^2$, the radiative corrections due to vector-boson loops in the Standard Model by $\delta M_{H,V}^2$, and the contributions of supersymmetric fermionic gaugino partners by $\delta M_{\tilde{H},\tilde{V}}^2$, the physical Higgs mass is given by the sum $M_H^2 = M_{H,0}^2 + \delta M_{H,V}^2 + \delta M_{\tilde{H},\tilde{V}}^2$. The vector-boson correction is quadratically divergent, $\delta M_{H,V}^2 \sim \alpha[\Lambda^2 - M^2]$, so that for a cut-off scale $\Lambda \sim \Lambda_{GUT}$ extreme fine-tuning between the intrinsic bare mass and the radiative quantum fluctuations would be needed to generate a Higgs mass of order M_W. However, owing to Pauli's principle, the additional fermionic gaugino contributions in supersymmetric theories are just opposite in sign, $\delta M_{\tilde{H},\tilde{V}}^2 \sim -\alpha[\Lambda^2 - \tilde{M}^2]$, so that the divergent terms cancel. Since $\delta M_H^2 \sim \alpha[\tilde{M}^2 - M^2]$, any fine-tuning is avoided for supersymmetric particle masses $\tilde{M} \lesssim \mathcal{O}(1 \text{ TeV})$. Thus, within this symmetry scheme the Higgs sector is stable in the low-energy range $M_H \sim M_W$ even in the context of high-energy GUT scales.

(b) The concept of supersymmetry is strongly supported by the successful prediction of the electroweak mixing angle in the minimal version of this theory [16]. There, the extended particle spectrum drives the evolution of the electroweak mixing angle from the GUT value 3/8 down to $\sin^2 \theta_W = 0.2336 \pm 0.0017$, the error including unknown threshold contributions at the low and the high supersymmetric mass scales. The prediction coincides with the experimentally measured value $\sin^2 \theta_W^{exp} = 0.2317 \pm 0.0003$ within the theoretical uncertainty of less than 2 per mille.

29

(c)   Conceptually very interesting is the interpretation of the Higgs mechanism in supersymmetric theories as a quantum effect [53]. The breaking of the electroweak symmetry $SU(2)_L \times U(1)_Y$ can be induced radiatively while leaving the electromagnetic gauge symmetry $U(1)_{EM}$ and the colour gauge symmetry $SU(3)_C$ unbroken for top-quark masses between 150 and 200 GeV. Starting with a set of universal scalar masses at the high GUT scale, the squared mass parameter of the Higgs sector evolves to negative values at the low electroweak scale, while the squared squark and slepton masses remain positive.

This fundamental mechanism can easily be studied [54] in a simplified model for the two stop fields $\tilde{t}_R$ and $\tilde{t}_L$, and the Higgs field H_2. The Yukawa terms in the renormalization group equations

$$
4\pi^2 \frac{\partial}{\partial \log \mu^2 / M_G^2}
\begin{bmatrix} M_{H_2}^2 \\ M_{\tilde{t}_R}^2 \\ M_{\tilde{t}_L}^2 \end{bmatrix}
= g_t^2 \begin{bmatrix} 3 & 3 & 3 \\ 2 & 2 & 2 \\ 1 & 1 & 1 \end{bmatrix}
\begin{bmatrix} M_{H_2}^2 \\ M_{\tilde{t}_R}^2 \\ M_{\tilde{t}_L}^2 \end{bmatrix}
+ g_t^2 A_t^2 \begin{bmatrix} 3 \\ 2 \\ 1 \end{bmatrix}
- \frac{16}{3} g_s^2 M_3^2 \begin{bmatrix} 0 \\ 1 \\ 1 \end{bmatrix} \quad (42)
$$

drive the masses to smaller values in the evolution from the GUT scale down to the electroweak scale $\mu^2 = M_G^2 \to M_Z^2$. This force is strongest for the Higgs mass and increases with the top Yukawa coupling. It is balanced by the SUSY-QCD contribution for the squark masses, if the top Yukawa coupling is not too large. Solving the renormalization group equations with the initial condition

$$\text{GUT scale:} \qquad M_{H_2}^2 = M_{\tilde{t}_R}^2 = M_{\tilde{t}_L}^2 = M_0^2 > 0 \ , \qquad (43)$$

the masses evolve down to

$$
\begin{aligned}
\text{ELW scale:} \qquad M_{H_2}^2 &= -\frac{1}{2} M_0^2 < 0 \\[2mm]
M_{\tilde{t}_R}^2 &= 0 \\[2mm]
M_{\tilde{t}_L}^2 &= +\frac{1}{2} M_0^2 > 0
\end{aligned}
$$

at low energies in the limit of vanishing gauge and trilinear couplings. Both stop states preserve the normal particle character, while the negative mass squared of the field H_2 generates the Higgs mechanism.

The Higgs sector of supersymmetric theories differs in several aspects from the Standard Model [17]. To preserve supersymmetry and gauge invariance, at least two iso-doublet fields must be introduced, leaving us with a spectrum of five or more physical Higgs particles. In the minimal supersymmetric extension of the Standard Model (MSSM) the Higgs self-interactions are generated by the scalar-gauge action, so that the quartic couplings are related to the gauge couplings in this scenario. This leads to strong bounds

of less than about 130 GeV for the mass of the lightest Higgs boson [18]. If the system is assumed to remain weakly interacting up to scales of the order of the GUT or Planck scale, the mass remains small, for reasons quite analogous to those found in the Standard Model, even in more complex supersymmetric theories involving additional Higgs fields and Yukawa interactions. The masses of the heavy Higgs bosons are expected to be of the scale of electroweak symmetry breaking up to order 1 TeV.

3.1 The Higgs Sector of the MSSM

The particle spectrum of the MSSM [14] consists of leptons, quarks and their scalar supersymmetric partners, and gauge particles, Higgs particles and their spin-1/2 partners. The matter and force fields are coupled in supersymmetric and gauge-invariant actions:

$$S = S_V + S_\phi + S_W : \qquad \begin{aligned} S_V &= \tfrac{1}{4} \int d^6z \, \hat{W}_\alpha \hat{W}_\alpha & \text{gauge action} , \\[2mm] S_\phi &= \int d^8z \, \hat{\phi}^* e^{gV} \hat{\phi} & \text{matter action} , \\[2mm] S_W &= \int d^6z \, W[\hat{\phi}] & \text{superpotential} . \end{aligned} \qquad (44)$$

Decomposing the superfields into fermionic and bosonic components, and carrying out the integration over the Grassmann variables in $z \to x$, the following Lagrangians can be derived, which describe the interactions of the gauge, matter and Higgs fields:

$$\begin{aligned} \mathcal{L}_V &= -\frac{1}{4} F_{\mu\nu} F_{\mu\nu} + \ldots + \frac{1}{2} D^2 , \\[2mm] \mathcal{L}_\phi &= D_\mu \phi^* D_\mu \phi + \ldots + \frac{g}{2} D |\phi|^2 , \\[2mm] \mathcal{L}_W &= -\left| \frac{\partial W}{\partial \phi} \right|^2 . \end{aligned}$$

The D field is an auxiliary field that does not propagate in space-time and can be eliminated by applying the equations of motion: $D = -\frac{g}{2}|\phi|^2$. Reinserted into the Lagrangian, the quartic self-coupling of the scalar Higgs fields is generated:

$$\mathcal{L}[\phi^4] = -\frac{g^2}{8} |\phi^2|^2 . \qquad (45)$$

Thus, the quartic coupling of the Higgs fields is given, in the minimal supersymmetric theory, by the square of the gauge coupling. Unlike the Standard Model case, the quartic coupling is not a free parameter. Moreover, this coupling is weak.

Two independent Higgs doublet fields H_1 and H_2 must be introduced into the superpotential:

$$W = -\mu \epsilon_{ij} \hat{H}_1^i \hat{H}_2^j + \epsilon_{ij} [f_1 \hat{H}_1^i \hat{L}^j \hat{R} + f_2 \hat{H}_1^i \hat{Q}^j \hat{D} + f_2' \hat{H}_2^j \hat{Q}^i \hat{U}] \qquad (46)$$

to provide the down-type particles (H_1) and the up-type particles (H_2) with a mass. Unlike the Standard Model, the second Higgs field cannot be identified with the charge conjugate of the first Higgs field since W must be analytic to preserve supersymmetry. Moreover, the Higgsino fields associated with a single Higgs field would generate triangle anomalies; they cancel if the two conjugate doublets are added up, and the classical gauge invariance of the interactions is not destroyed at the quantum level. Integrating the superpotential over the Grassmann coordinates generates the supersymmetric Higgs self-energy $V_0 = |\mu|^2(|H_1|^2+|H_2|^2)$. The breaking of supersymmetry can be incorporated in the Higgs sector by introducing bilinear mass terms $\mu_{ij}H_iH_j$. Added to the supersymmetric self-energy part H^2 and the quartic part H^4 generated by the gauge action, they lead to the following Higgs potential

$$
\begin{aligned}
V \;\; = \;\; & m_1^2 H_1^{*i}H_1^i + m_2^2 H_2^{*i}H_2^i - m_{12}^2(\epsilon_{ij}H_1^iH_2^j + hc) \\[2mm]
& + \frac{1}{8}(g^2 + g'^2)[H_1^{*i}H_1^i - H_2^{*i}H_2^i]^2 + \frac{1}{2}|H_1^{*i}H_2^{*i}|^2 \; .
\end{aligned}
\tag{47}
$$

The Higgs potential includes three bilinear mass terms, while the strength of the quartic couplings is set by the $SU(2)_L$ and $U(1)_Y$ gauge couplings squared. The three mass terms are free parameters.

The potential develops a stable minimum for $H_1 \to [0,v_1]$ and $H_2 \to [v_2,0]$, if the following conditions are met:

$$
m_1^2 + m_2^2 > 2|m_{12}^2| \quad \text{and} \quad m_1^2 m_2^2 < |m_{12}^2|^2 \; .
\tag{48}
$$

Expanding the fields about the ground-state values v_1 and v_2,

$$
\begin{aligned}
H_1^1 \;\; = & \quad\quad\quad H^+ \cos\beta + G^+ \sin\beta \\[2mm]
H_1^2 \;\; = & \;\; v_1 \;\; + \;\; [H^0 \cos\alpha - h^0 \sin\alpha + iA^0 \sin\beta - iG^0 \cos\beta]/\sqrt{2}
\end{aligned}
\tag{49}
$$

and

$$
\begin{aligned}
H_2^1 \;\; = & \;\; v_2 \;\; + \;\; [H^0 \sin\alpha + h^0 \cos\alpha + iA^0 \cos\beta + iG^0 \sin\beta]/\sqrt{2} \\[2mm]
H_2^2 \;\; = & \quad\quad\quad H^- \sin\beta - G^- \cos\beta \; ,
\end{aligned}
\tag{50}
$$

the mass eigenstates are given by the neutral states h^0, H^0 and A^0, which are even and odd under $\mathcal{CP}$ transformations, and by the charged states $H^\pm$; the G states correspond to the Goldstone modes, which are absorbed by the gauge fields to build up the longitudinal components. After introducing the three parameters

$$
\begin{aligned}
M_Z^2 \;\; = & \;\; \frac{1}{2}(g^2 + g'^2)(v_1^2 + v_2^2) \\[3mm]
M_A^2 \;\; = & \;\; m_{12}^2 \frac{v_1^2 + v_2^2}{v_1 v_2} \\[3mm]
\text{tg}\beta \;\; = & \;\; \frac{v_2}{v_1} \; ,
\end{aligned}
\tag{51}
$$

the mass matrix can be decomposed into three 2×2 blocks, which are easy to diagonalize:

charged matrix: $\qquad M_\pm^2 = \sin 2\beta (M_A^2 + M_W^2) \begin{bmatrix} \text{tg}\beta & 1 \\ 1 & \text{ctg}\beta \end{bmatrix}$

$$\underline{\text{charged mass: }} M_{H^\pm}^2 = M_A^2 + M_W^2$$

pseudoscalar matrix: $\quad M_a^2 = \sin 2\beta M_A^2 \begin{bmatrix} \text{tg}\beta & 1 \\ 1 & \text{ctg}\beta \end{bmatrix}$

$$\underline{\text{pseudoscalar mass: }} M_A^2$$

scalar matrix: $\qquad M_s^2 = \sin 2\beta \left(\frac{M_A^2}{2} \begin{bmatrix} \text{tg}\beta & -1 \\ -1 & \text{ctg}\beta \end{bmatrix} + \frac{M_Z^2}{2} \begin{bmatrix} \text{ctg}\beta & -1 \\ -1 & \text{tg}\beta \end{bmatrix} \right)$

$$\underline{\text{scalar masses:}}$$

$$M_{h,H}^2 = \tfrac{1}{2} \left[M_A^2 + M_Z^2 \mp \sqrt{(M_A^2 + M_Z^2)^2 - 4 M_A^2 M_Z^2 \cos^2 2\beta} \right]$$

$$\text{tg}2\alpha = \text{tg}2\beta \frac{M_A^2 + M_Z^2}{M_A^2 - M_Z^2} \quad \text{with} \quad -\frac{\pi}{2} < \alpha < 0$$

The three zero-mass Goldstone eigenvalues of the charged and pseudoscalar mass matrices are not denoted explicitly.

From the mass formulae, two important inequalities can readily be derived,

$$M_h \leq M_Z, M_A \leq M_H \tag{52}$$

$$M_W \leq M_{H^\pm} \ , \tag{53}$$

which, by construction, are valid in the tree approximation. As a result, the lightest of the scalar Higgs masses is predicted to be bounded by the Z mass, *modulo* radiative corrections. These bounds follow from the fact that the quartic coupling of the Higgs fields is determined in the MSSM by the size of the gauge couplings squared.

SUSY Radiative Corrections

The tree-level relations between the Higgs masses are strongly modified by radiative corrections that involve the supersymmetric particle spectrum of the top sector [55]. These

33

effects are proportional to the fourth power of the top mass and to the logarithm of the stop mass. Their origin are incomplete cancellations between virtual top and stop loops, reflecting the breaking of supersymmetry. Moreover, the mass relations are affected by the potentially large mixing between $\tilde{t}_L$ and $\tilde{t}_R$ due to the top Yukawa coupling.

To leading order in M_t^4 the radiative corrections can be summarized in the parameter

$$\epsilon = \frac{3G_F}{\sqrt{2}\pi^2} \frac{M_t^4}{\sin^2\beta} \log \frac{M_{\tilde{t}_1} M_{\tilde{t}_2}}{M_t^2} \ . \tag{54}$$

In this approximation the light Higgs mass M_h can be expressed by M_A and tgβ in the following compact form:

$$M_h^2 = \frac{1}{2} \Big[M_A^2 + M_Z^2 + \epsilon$$
$$-\sqrt{(M_A^2 + M_Z^2 + \epsilon)^2 - 4M_A^2 M_Z^2 \cos^2 2\beta - 4\epsilon(M_A^2 \sin^2\beta + M_Z^2 \cos^2\beta)} \Big]$$

The heavy Higgs masses M_H and $M_{H\pm}$ follow from the sum rules

$$M_H^2 = M_A^2 + M_Z^2 - M_h^2 + \epsilon$$
$$M_{H\pm}^2 = M_A^2 + M_W^2 \ .$$

Finally, the mixing parameter α, which diagonalizes the $\mathcal{CP}$-even mass matrix, is given by the radiatively improved relation:

$$\mathrm{tg}2\alpha = \mathrm{tg}2\beta \frac{M_A^2 + M_Z^2}{M_A^2 - M_Z^2 + \epsilon/\cos 2\beta} \ . \tag{55}$$

The spectrum of the Higgs masses M_h, M_H and $M_{H\pm}$ is displayed as a function of the pseudoscalar mass M_A in Fig. 18 for two representative values of tg$\beta = 1.5$ and 30. For large A mass, the masses of the heavy Higgs particles coincide approximately, $M_A \simeq M_H \simeq M_{H\pm}$, while the light Higgs mass approaches a small asymptotic value. The spectrum for large values of tgβ is quite regular: for small M_A one finds $\{M_h \simeq M_A; M_H \simeq \mathrm{const}\}$; for large M_A the opposite relationship $\{M_h \simeq \mathrm{const}, M_H \simeq M_{H\pm} \simeq M_A\}$.

While the non-leading effects of mixing on the Higgs mass relations are quite involved, the impact on the upper bound of the light Higgs mass M_h can be summarized in a simple way:

$$M_h^2 \leq M_Z^2 \cos^2 2\beta + \delta M_t^2 + \delta M_X^2 \ . \tag{56}$$

The leading top contribution is related to the parameter ϵ,

$$\delta M_t^2 = \epsilon \sin^2\beta \ . \tag{57}$$

The second contribution

$$\delta M_X^2 = \frac{3G_F}{2\sqrt{2}\pi^2} X_t \left[2h(M_{\tilde{t}_1}^2, M_{\tilde{t}_2}^2) + X_t \ g(M_{\tilde{t}_1}^2, M_{\tilde{t}_2}^2) \right] \tag{58}$$
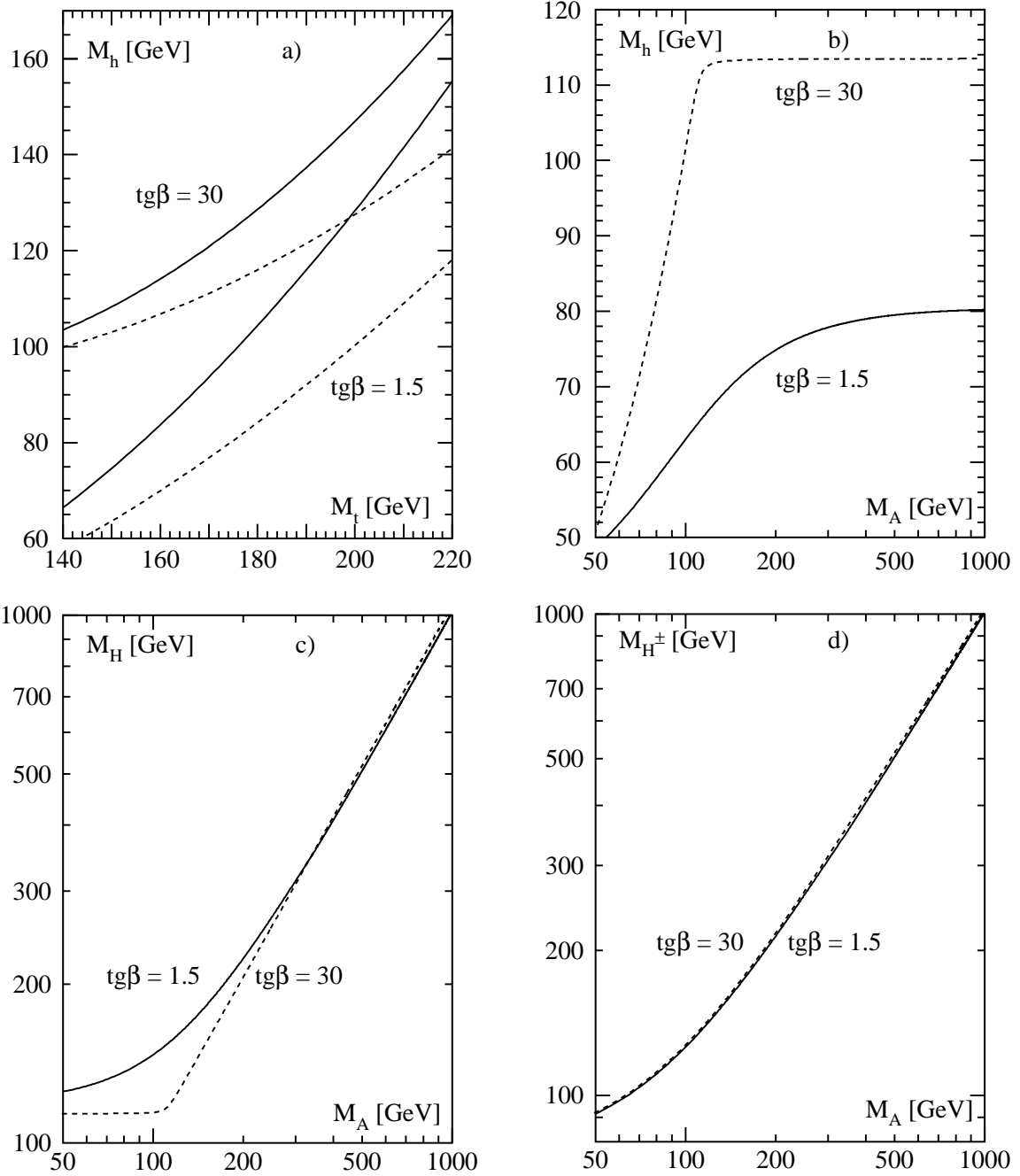
34

Figure 18: *(a) The upper limit on the light scalar Higgs pole mass in the MSSM as a function of the top quark mass for two values of tgβ = 1.5, 30; the common squark mass has been chosen as $M_S = 1$ TeV. The full lines correspond to the case of maximal mixing [$A_t = \sqrt{6}M_S$, $A_b = \mu = 0$] and the dashed lines to vanishing mixing. The pole masses of the other Higgs bosons, $H, A, H^{\pm}$, are shown as a function of the pseudoscalar mass in (b–d) for two values of tgβ = 1.5, 30, vanishing mixing and $M_t = 175$ GeV.*

depends on the mixing parameter

$$M_t X_t = M_t \left[A_t - \mu \, \text{ctg}\beta \right] \; , \tag{59}$$

which couples left- and right-chirality states in the stop mass matrix; h, g are functions of the stop masses:

$$h = \frac{1}{a-b} \log \frac{a}{b} \quad \text{and} \quad g = \frac{1}{(a-b)^2} \left[2 - \frac{a+b}{a-b} \log \frac{a}{b} \right] \; . \tag{60}$$

Subdominant contributions can essentially be reduced to higher-order QCD effects. They can effectively be incorporated by interpreting the top mass parameter $M_t \to M_t(\mu_t)$ as the $\overline{\text{MS}}$ top mass evaluated at the geometric mean between top and stop masses, $\mu_t^2 = M_t M_{\tilde{t}}$.

Upper bounds on the light Higgs mass are shown in Fig. 18a for two representative values of $\text{tg}\beta = 1.5$ and 30. The curves are the results of calculations with and without the mixing effects. It turns out that M_h is bounded by about $M_h \lesssim 100$ GeV for moderate values of $\text{tg}\beta$ while the general upper bound is given by $M_h \lesssim 130$ GeV, including large values of $\text{tg}\beta$. The light Higgs sector can therefore be entirely covered, for small $\text{tg}\beta$, by the LEP2 experiments – a most exciting prospect of the search for this Higgs particle in the next few years.

The two ranges of $\text{tg}\beta$ near $\text{tg}\beta \sim 1.7$ and $\text{tg}\beta \sim M_t/M_b \sim 30$ to 50 are theoretically preferred in the MSSM, if the model is embedded in a grand-unified scenario [57]. Given the experimentally observed top quark mass, universal τ and b masses at the unification scale can be evolved down to the experimental mass values at low energies within these two bands of $\text{tg}\beta$. Qualitative support for small $\text{tg}\beta$ follows from the observation that in this scenario the top mass can be interpreted as a fixed-point of the evolution down from the unification scale [58]. Moreover, the small $\text{tg}\beta$ range is slightly preferred, as radiative corrections that reduce the light Higgs mass extracted from the high-precision electroweak observables, are minimized [59]. By contrast, tuning problems in adjusting the τ/b mass ratio are more severe for the large $\text{tg}\beta$ solution. Nevertheless, this solution is attractive as the $SO(10)$ symmetry relation between $\tau/b/t$ masses can be accommodated in this scenario.

3.2 SUSY Higgs Couplings to SM Particles

The size of MSSM Higgs couplings to quarks, leptons and gauge bosons is similar to the Standard Model, yet modified by the mixing angles α and β. Normalized to the SM values, they are listed in Table 2. The pseudoscalar Higgs boson A does not couple to gauge bosons at the tree level, but the coupling, compatible with $\mathcal{CP}$ symmetry, can be generated by higher-order loops. The charged Higgs bosons couple to up and down fermions with the left- and right-chiral amplitudes $g_\pm = -\frac{1}{\sqrt{2}} [g_t(1 \mp \gamma_5) + g_b(1 \pm \gamma_5)]$, where $g_{t,b} = (\sqrt{2} G_F)^{1/2} m_{t,b}$.

Φ		g_u^Φ	g_d^Φ	g_V^Φ
SM	H	1	1	1
MSSM	h	$\cos\alpha/\sin\beta$	$-\sin\alpha/\cos\beta$	$\sin(\beta-\alpha)$
	H	$\sin\alpha/\sin\beta$	$\cos\alpha/\cos\beta$	$\cos(\beta-\alpha)$
	A	$1/\mathrm{tg}\beta$	$\mathrm{tg}\beta$	0

Table 2: *Higgs couplings in the MSSM to fermions and gauge bosons [V = W, Z] relative to SM couplings.*

The modified couplings incorporate the renormalization due to SUSY radiative corrections, to leading order in M_t, if the mixing angle α is related to β and M_A through the corrected formula Eq. (55). The behaviour of the couplings as a function of mass M_A is exemplified in Fig. 19.

For large M_A, in practice $M_A \gtrsim 200$ GeV, the couplings of the light Higgs boson h to the fermions and gauge bosons approach the SM values asymptotically. This is the essence of the decoupling theorem: Particles with large masses must decouple from the light-particle system as a consequence of the quantum-mechanical uncertainty principle.

3.3   Decays of Higgs Particles

The lightest *neutral Higgs boson* h will decay mainly into fermion pairs since the mass is smaller than ~ 130 GeV, Fig. 20a (cf. [60] for a comprehensive summary). This is, in general, also the dominant decay mode of the pseudoscalar boson A. For values of $\mathrm{tg}\beta$ larger than unity and for masses less than ~ 140 GeV, the main decay modes of the neutral Higgs bosons are decays into $b\bar{b}$ and $\tau^+\tau^-$ pairs; the branching ratios are of order $\sim 90\%$ and 8%, respectively. The decays into $c\bar{c}$ pairs and gluons are suppressed, especially for large $\mathrm{tg}\beta$. For large masses, the top decay channels $H, A \to t\bar{t}$ open up; yet for large $\mathrm{tg}\beta$ this mode remains suppressed and the neutral Higgs bosons decay almost exclusively into $b\bar{b}$ and $\tau^+\tau^-$ pairs. If the mass is large enough, the heavy $\mathcal{CP}$-even Higgs boson H can in principle decay into weak gauge bosons, $H \to WW, ZZ$. Since the partial widths are proportional to $\cos^2(\beta-\alpha)$, they are strongly suppressed in general, and the gold-plated ZZ signal of the heavy Higgs boson in the Standard Model is lost in the supersymmetric extension. As a result, the total widths of the Higgs bosons are much smaller in supersymmetric theories than in the Standard Model.

The heavy neutral Higgs boson H can also decay into two lighter Higgs bosons. Other possible channels are Higgs cascade decays and decays into supersymmetric particles [61–63], Fig. 21. In addition to light sfermions, Higgs boson decays into charginos and neutralinos could eventually be important. These new channels are kinematically accessible,
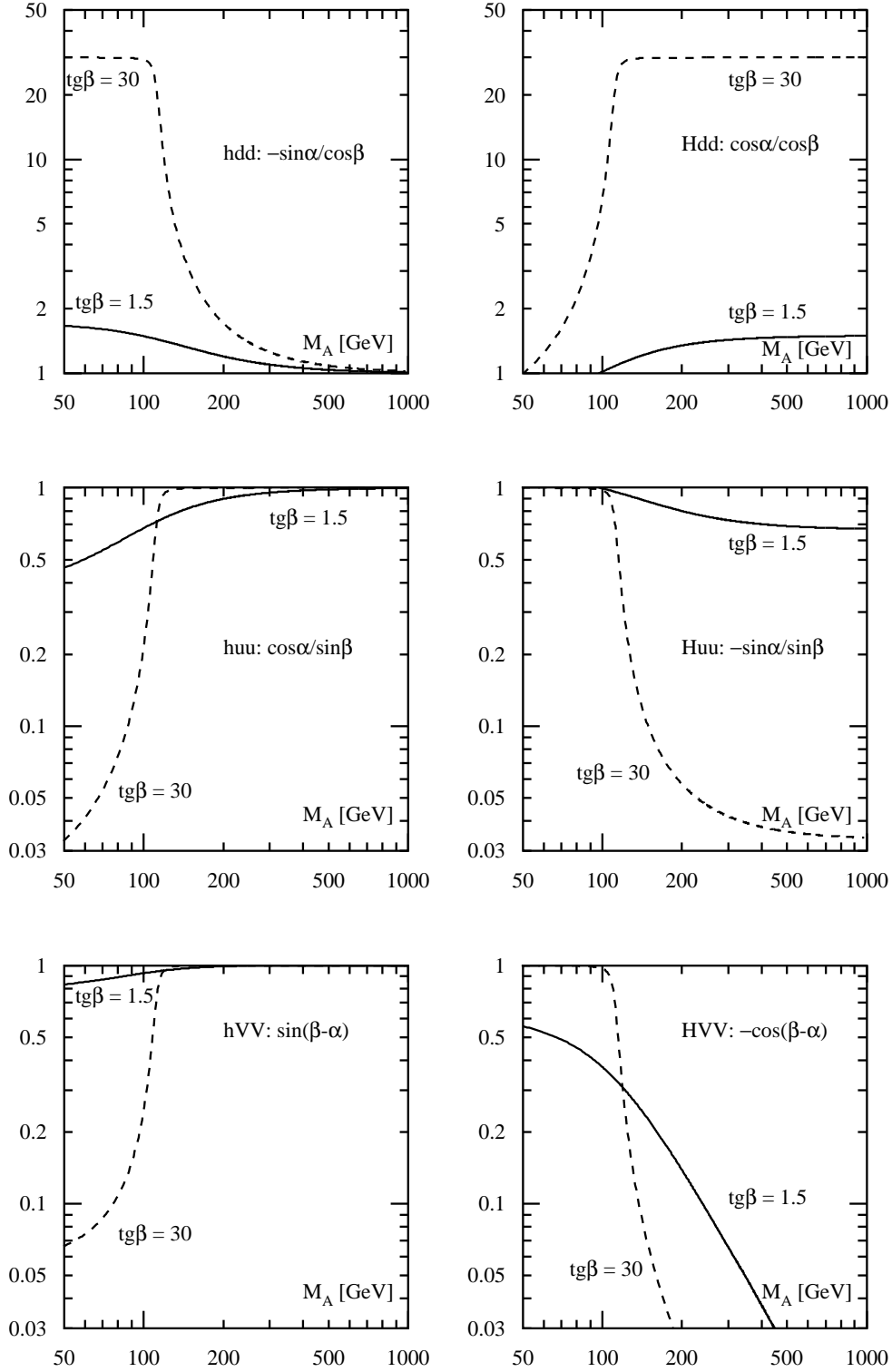
37

Figure 19: *The coupling parameters of the neutral MSSM Higgs bosons as a function of the pseudoscalar mass M_A for two values of $tg\beta = 1.5, 30$ and vanishing mixing. The couplings are defined in Table 2.*
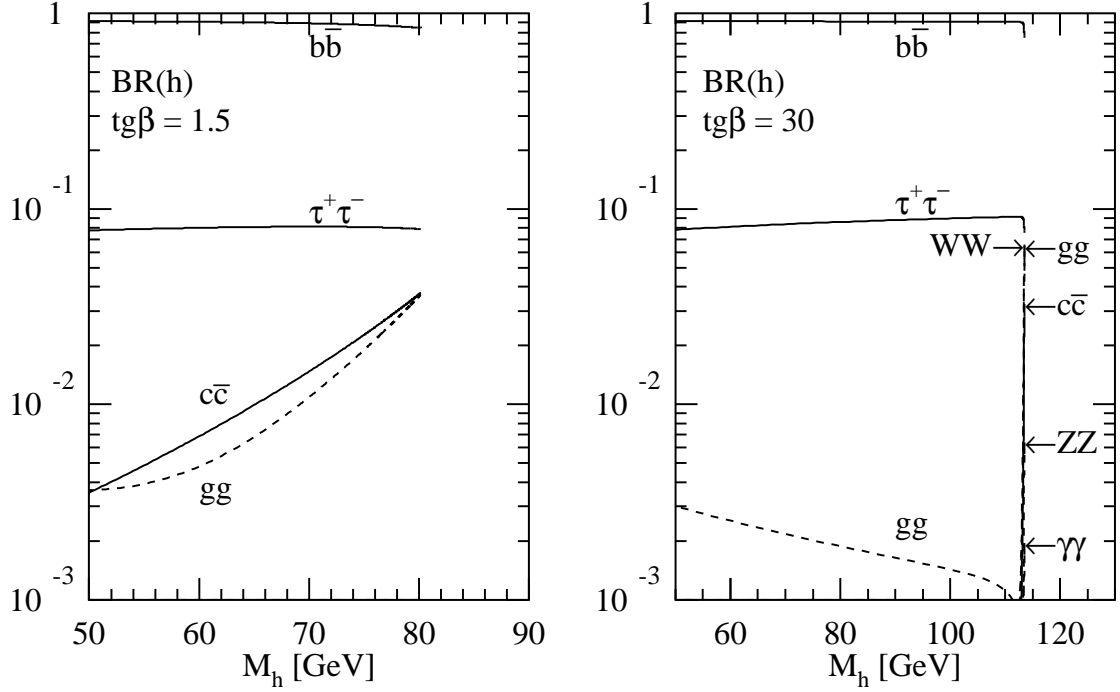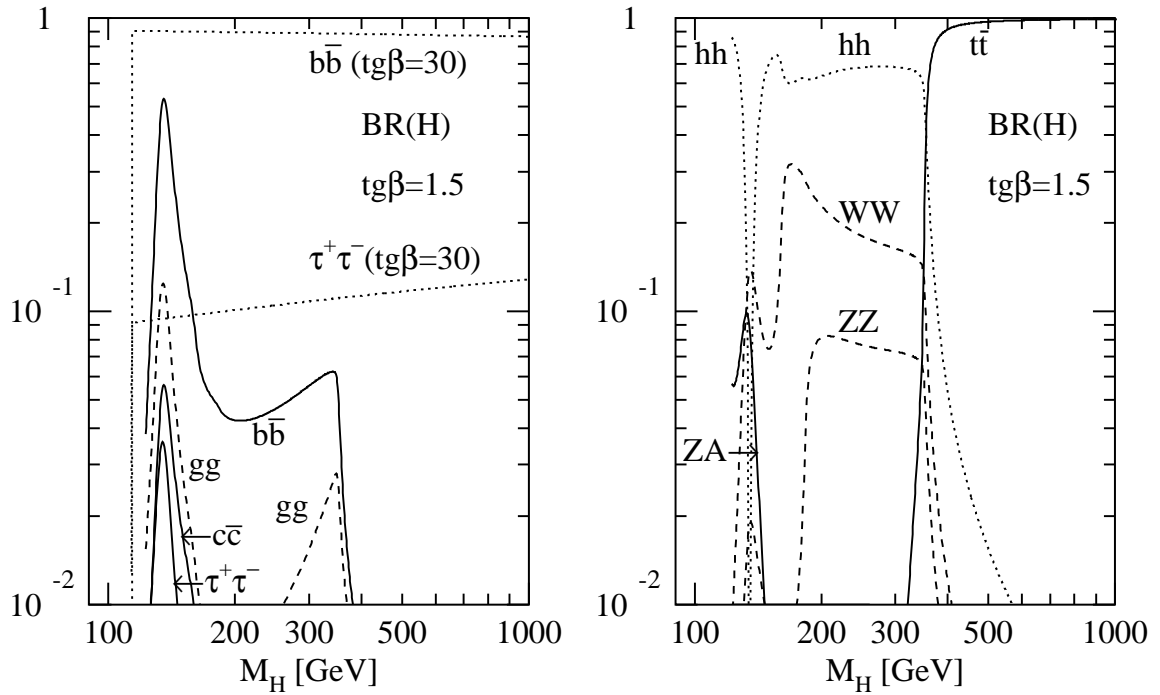
38

Fig. 20a

Fig. 20b

Figure 20: *Branching ratios of the MSSM Higgs bosons* $h, H, A, H^{\pm}$ *for non-SUSY decay modes as a function of the masses for two values of* $tg\beta = 1.5, 30$ *and vanishing mixing. The common squark mass has been chosen as* $M_S = 1$ *TeV.*
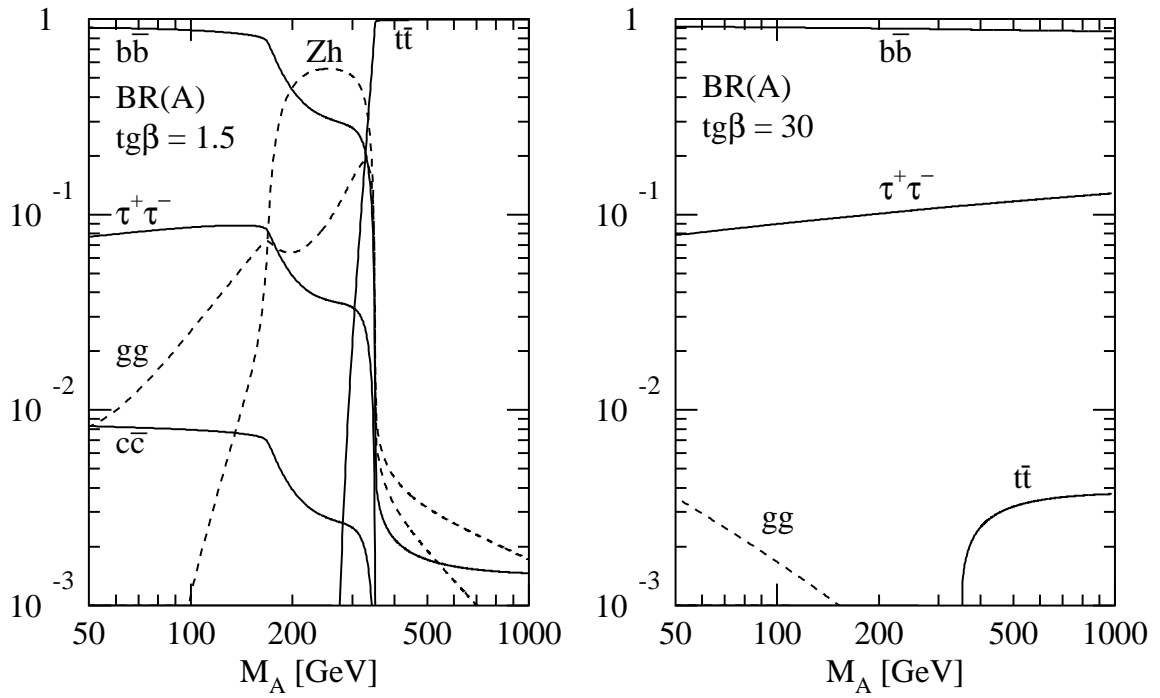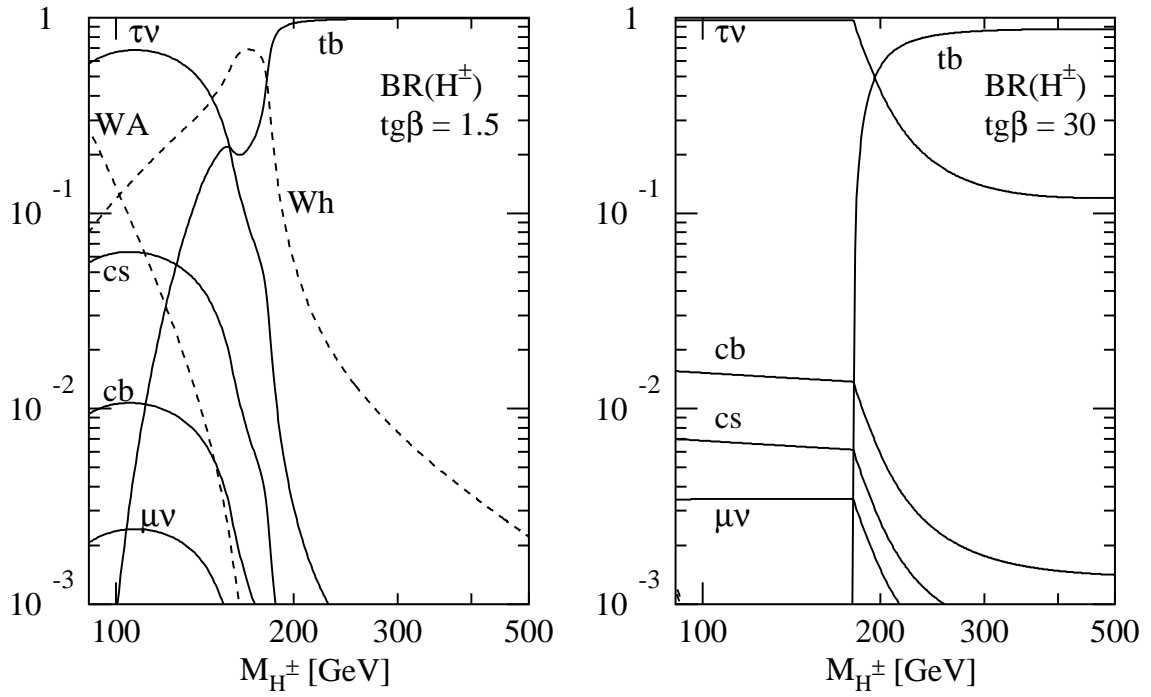
Fig. 20c

Fig. 20d

Figure 20: *Continued.*

at least for the heavy Higgs bosons H, A and $H^{\pm}$; in fact, the branching fractions can be very large and they can even become dominant in some regions of the MSSM parameter space. Decays of h into the lightest neutralinos (LSP) are also important, exceeding 50% in some parts of the parameter space. These decays strongly affect experimental search techniques.
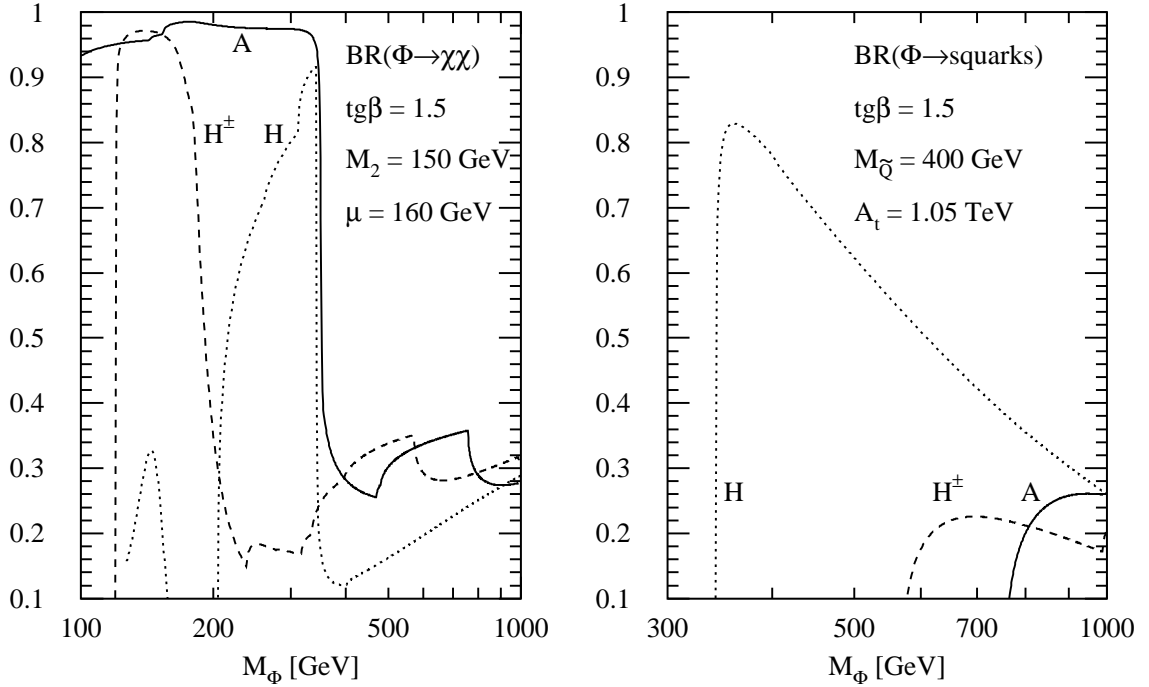

Figure 21: *Branching ratios of the MSSM Higgs boson $H, A, H^{\pm}$ decays into charginos/neutralinos and squarks as a function of their masses for $tg\beta = 1.5$. The mixing parameters have been chosen as $\mu = 160$ GeV, $A_t = 1.05$ TeV, $A_b = 0$ and the squark masses of the first two generations as $M_{\widetilde{Q}} = 400$ GeV. The gaugino mass parameter has been set to $M_2 = 150$ GeV.*

The *charged Higgs particles* decay into fermions, but also, if allowed kinematically, into the lightest neutral Higgs and a W boson. Below the tb and Wh thresholds, the charged Higgs particles will decay mostly into $\tau\nu_\tau$ and cs pairs, the former being dominant for $tg\beta > 1$. For large $M_{H\pm}$ values, the top–bottom decay mode $H^+ \to t\bar{b}$ becomes dominant. In some parts of the SUSY parameter space, decays into supersymmetric particles may exceed 50 %.

Adding up the various decay modes, the width of all five Higgs bosons remains very narrow, being of order 10 GeV even for large masses.

3.4 The Production of SUSY Higgs Particles in e^+e^- Collisions

The search for the neutral SUSY Higgs bosons at e^+e^- linear colliders will be a straight-forward extension of the search now being performed at LEP2, which is expected to cover the mass range up to ~ 100 GeV for neutral Higgs bosons. Higher energies, $\sqrt{s}$ in excess of 250 GeV, are required to sweep the entire parameter space of the MSSM for moderate to large values of tgβ.

The main production mechanisms of *neutral Higgs bosons* at e^+e^- colliders [18, 62, 64] are the Higgs-strahlung process and associated pair production, as well as the fusion processes:

(a) Higgs–strahlung: $\qquad e^+e^- \xrightarrow{Z} Z + h/H$

(b) Pair production : $\qquad e^+e^- \xrightarrow{Z} A + h/H$

(c) Fusion processes : $\qquad e^+e^- \xrightarrow{WW} \overline{\nu_e}\, \nu_e + h/H$

$\qquad\qquad\qquad\qquad\qquad e^+e^- \xrightarrow{ZZ} e^+e^- + h/H$

The $\mathcal{CP}$-odd Higgs boson A cannot be produced in fusion processes to leading order. The cross sections for the four Higgs-strahlung and pair production processes can be expressed as

$$\begin{aligned}
\sigma(e^+e^- \to Z + h/H) &= \sin^2/\cos^2(\beta - \alpha)\, \sigma_{SM} \\
\sigma(e^+e^- \to A + h/H) &= \cos^2/\sin^2(\beta - \alpha)\, \bar{\lambda}\, \sigma_{SM}\ ,
\end{aligned} \qquad (61)$$

where σ_{SM} is the SM cross section for Higgs-strahlung and the coefficient $\bar{\lambda} \sim \lambda_{Aj}^{3/2}/\lambda_{Zj}^{1/2}$ accounts for the suppression of the P-wave Ah/H cross sections near the threshold.

The cross sections for Higgs-strahlung and for pair production, much as those for the production of the light and the heavy neutral Higgs bosons h and H, are complementary, coming either with coefficients $\sin^2(\beta - \alpha)$ or $\cos^2(\beta - \alpha)$. As a result, since σ_{SM} is large, at least the lightest $\mathcal{CP}$-even Higgs boson must be detected in e^+e^- experiments.

Representative examples of the cross sections for the production mechanisms of the neutral Higgs bosons are shown in Fig. 22, as a function of the Higgs masses, for tg$\beta = 1.5$ and 30. The cross section for hZ is large for M_h near the maximum value allowed for tgβ; it is of order 50 fb, corresponding to $\sim 2{,}500$ events for an integrated luminosity of 50 fb^{-1}. By contrast, the cross section for HZ is large if M_h is sufficiently below the maximum value [implying small M_H]. For h and for the light H, the signals consist of a Z boson accompanied by a $b\bar{b}$ or $\tau^+\tau^-$ pair. These signals are easy to separate from the background, which comes mainly from ZZ production if the Higgs mass is close to M_Z. For the associated channels $e^+e^- \to Ah$ and AH, the situation is opposite to the previous case: the cross section for Ah is large for light h, whereas AH pair production is the dominant mechanism in the complementary region for heavy H and A bosons. The sum of the two cross sections decreases from ~ 50 to 10 fb if M_A increases from ~ 50 to 200 GeV at $\sqrt{s} = 500$ GeV. In major parts of the parameter space, the signals consist of
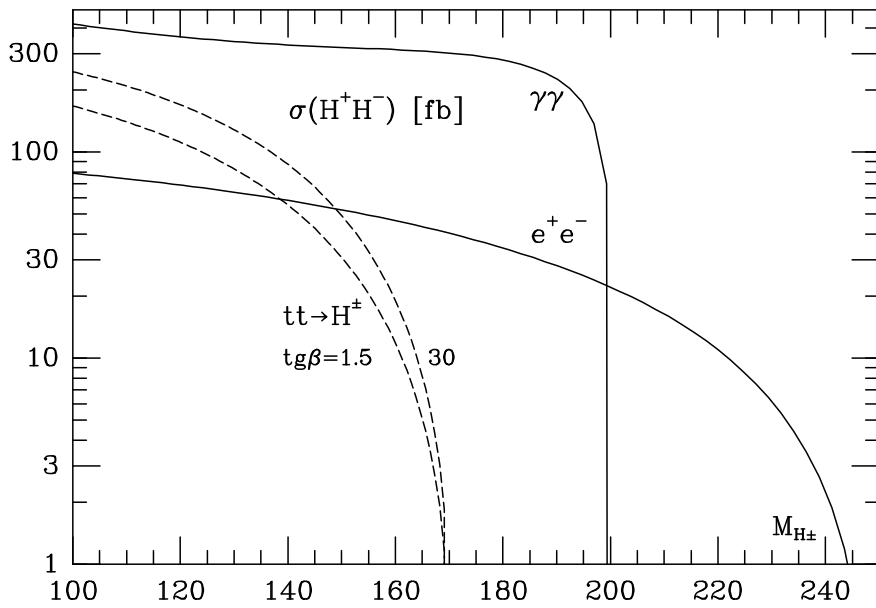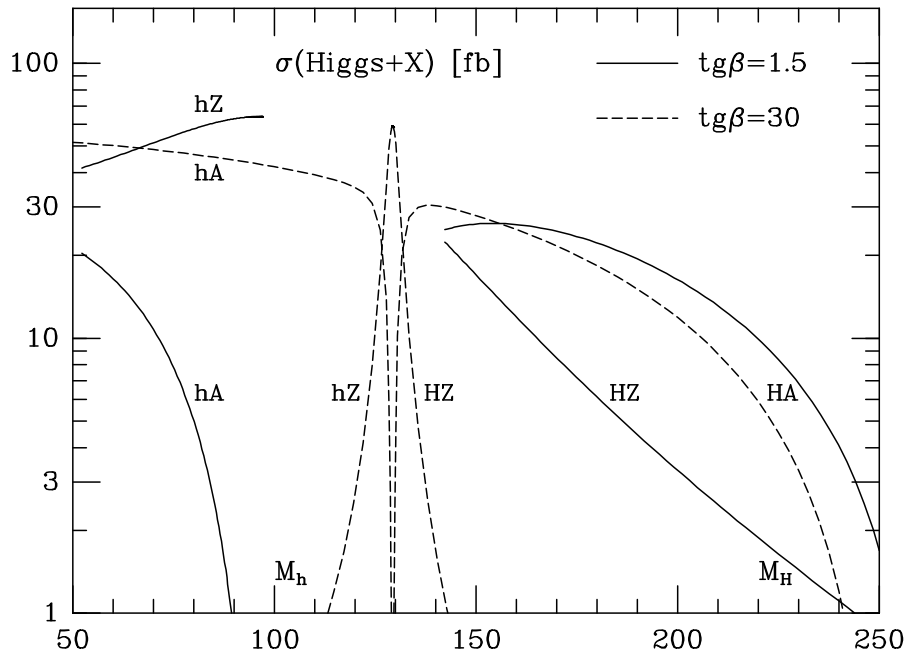
42

Figure 22: *Production cross sections of MSSM Higgs bosons at* $\sqrt{s} = 500$ *GeV: Higgs-strahlung and pair production; upper part: neutral Higgs bosons, lower part: charged Higgs bosons. Ref. [60].*

four b quarks in the final state, requiring provisions for efficient b-quark tagging. Mass constraints will help to eliminate the backgrounds from QCD jets and ZZ final states. For the WW fusion mechanism, the cross sections are larger than for Higgs-strahlung, if the Higgs mass is moderately small – less than 160 GeV at $\sqrt{s} = 500$ GeV. However, since the final state cannot be fully reconstructed, the signal is more difficult to extract. As in the case of the Higgs-strahlung processes, the production of light h and heavy H Higgs bosons complement each other in WW fusion, too.

The _charged Higgs bosons_, if lighter than the top quark, can be produced in top decays, $t \to b + H^+$, with a branching ratio varying between 2% and 20% in the kinematically allowed region. Since the cross section for top-pair production is of order 0.5 pb at $\sqrt{s} = 500$ GeV, this corresponds to 1,000 to 10,000 charged Higgs bosons at a luminosity of 50 fb^{-1}. Since, for tgβ larger than unity, the charged Higgs bosons will decay mainly into $\tau\nu_\tau$, there is a surplus of τ final states over e, μ final states in t decays, an apparent breaking of lepton universality. For large Higgs masses the dominant decay mode is the top decay $H^+ \to t\bar{b}$. In this case the charged Higgs particles must be pair-produced in e^+e^- colliders:

$$e^+e^- \to H^+H^- \ .$$

The cross section depends only on the charged Higgs mass. It is of order 100 fb for small Higgs masses at $\sqrt{s} = 500$ GeV, but it drops very quickly due to the P-wave suppression $\sim \beta^3$ near the threshold. For $M_{H^\pm} = 230$ GeV, the cross section falls to a level of $\simeq 5$ fb, which corresponds, for an integrated luminosity of 50 fb^{-1}, to 250 events. The cross section is considerably larger for $\gamma\gamma$ collisions.

Experimental Search Strategies

Search strategies have been summarized for neutral Higgs bosons in Refs. [65, 66] and for charged Higgs bosons in Ref. [67]. Examples of the results for Higgs-strahlung Zh, ZH and pair production Ah, AH and H^+H^- are given in Fig. 23. Visible as well as invisible decays are under experimental control already for an integrated luminosity of 10 fb^{-1}. The overall experimental situation can be summarized as the following two points:

(i) The lightest $\mathcal{CP}$-even Higgs particle h can be detected in the entire range of the MSSM parameter space, either via Higgs-strahlung $e^+e^- \to hZ$ or via pair production $e^+e^- \to hA$. This conclusion holds true even at a c.m. energy of 250 GeV, independently of the squark mass values; it is also valid if decays to invisible neutralinos and other SUSY particles are realized in the Higgs sector.

(ii) The area in the parameter space where _all SUSY Higgs bosons_ can be discovered at e^+e^- colliders is characterized by $M_H, M_A \lesssim \frac{1}{2}\sqrt{s}$, independently of tg$\beta$. The h, H Higgs bosons can be produced either via Higgs-strahlung or in Ah, AH associated production; charged Higgs bosons will be produced in H^+H^- pairs.

The search for the lightest neutral SUSY Higgs boson h is one of the most important
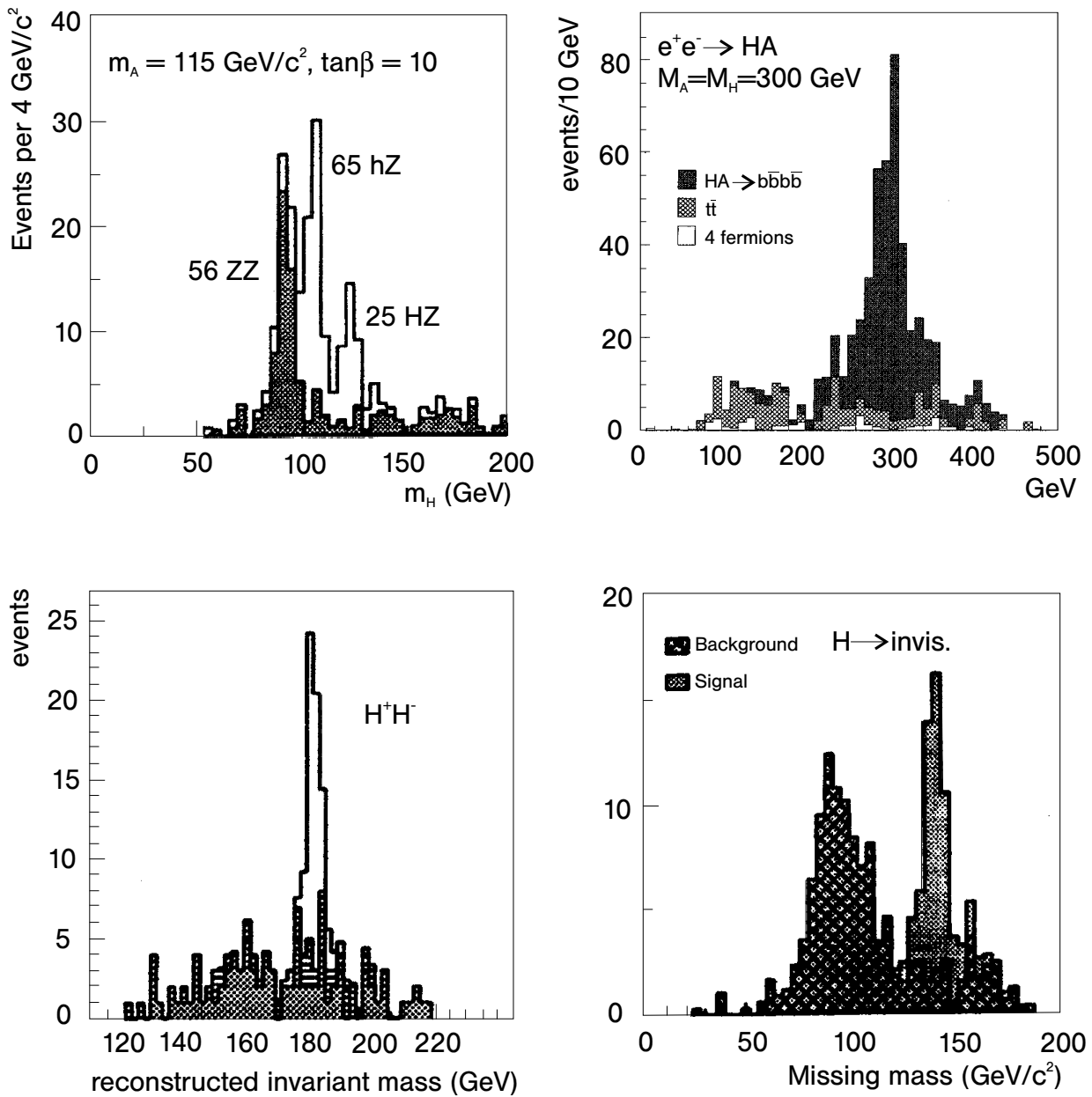
Figure 23: *Experimental simulations of the search for MSSM Higgs bosons in Higgs-strahlung hZ/HZ, heavy-pair production HA, charged-Higgs production H^+H^-, and neutral invisible Higgs decays in Higgs-strahlung. Refs. [65–67].*

experimental tasks at LEP2. Up to the present time, mass values of the pseudoscalar boson A of less than 75 GeV have been excluded, independently of tgβ. In MSSM scenarios without mixing effects, the entire mass range of the lightest Higgs particle h has already been covered for tgβ less than about 1.6; however, this conclusion does not hold true for scenarios with strong mixing effects [9]. With a final energy close to 200 GeV, the Higgs boson h could be discovered within the theoretically allowed mass range if the mixing parameter were realized below tg$\beta \lesssim 2.4$. This range covers one of the two solutions singled out by τ/b mass unification; moreover, it corresponds to the area predicted by the fixed-point solution of the top-quark mass.

3.5 The Production of SUSY Higgs Particles in Hadron Collisions

The basic production processes of SUSY Higgs particles at hadron colliders [68, 34] are essentially the same as in the Standard Model. Important differences are nevertheless generated by the modified couplings, the extended particle spectrum, and the negative parity of the A boson. For large tgβ the coupling $hb\bar{b}$ is enhanced so that the bottom-quark loop becomes competitive to the top-quark loop in the effective hgg coupling. Moreover squark loops will contribute to this coupling [69].

The partonic cross section $\sigma(gg \to \Phi)$ for the gluon fusion of Higgs particles can be expressed by couplings g, in units of the corresponding SM couplings, and form factors A; to lowest order [34, 70]:

$$\hat{\sigma}_{LO}^{\Phi}(gg \to \Phi) = \sigma_0^{\Phi}\delta\left(1 - \frac{M_{\Phi}^2}{\hat{s}}\right) \tag{62}$$

$$\sigma_0^{h/H} = \frac{G_F\alpha_s^2(\mu)}{128\sqrt{2}\pi}\left|\sum_Q g_Q^{h/H}A_Q^{h/H}(\tau_Q) + \sum_{\widetilde{Q}} g_{\widetilde{Q}}^{h/H}A_{\widetilde{Q}}^{h/H}(\tau_{\widetilde{Q}})\right|^2$$

$$\sigma_0^{A} = \frac{G_F\alpha_s^2(\mu)}{128\sqrt{2}\pi}\left|\sum_Q g_Q^{A}A_Q^{A}(\tau_Q)\right|^2$$

While the quark couplings have been defined in Table 2, the couplings of the Higgs particles to squarks are given by

$$g_{\widetilde{Q}_{L,R}}^{h} = \frac{M_Q^2}{M_{\widetilde{Q}}^2}g_Q^{h} \mp \frac{M_Z^2}{M_{\widetilde{Q}}^2}(I_3^Q - e_Q\sin^2\theta_W)\sin(\alpha + \beta)$$

$$g_{\widetilde{Q}_{L,R}}^{H} = \frac{M_Q^2}{M_{\widetilde{Q}}^2}g_Q^{H} \pm \frac{M_Z^2}{M_{\widetilde{Q}}^2}(I_3^Q - e_Q\sin^2\theta_W)\cos(\alpha + \beta) \tag{63}$$

$\mathcal{CP}$ invariance only allows for non-zero squark couplings to the pseudoscalar A boson. The form factors can be expressed in terms of the scaling function $f(\tau_i = 4M_i^2/M_{\Phi}^2)$, cf.

Eq. (27):

$$
\begin{aligned}
A_Q^{h/H}(\tau) &= \tau[1 + (1-\tau)f(\tau)] \\
A_Q^A(\tau) &= \tau f(\tau) \\
A_{\tilde{Q}}^{h/H}(\tau) &= -\frac{1}{2}\tau[1 - \tau f(\tau)] \ .
\end{aligned}
\tag{64}
$$

For small $\text{tg}\beta$ the contribution of the top loop is dominant, while for large $\text{tg}\beta$ the bottom loop is strongly enhanced. The squark loops can be significant for squark masses below ~ 400 GeV [70].

The limits of both large and small loop masses are interesting for SUSY Higgs particles. The contribution of the top loop to the hgg coupling can be calculated approximately in the limit of large loop masses, while the bottom contributions to the Φgg couplings can be calculated in the approximation of small b masses.

The limits of large loop masses for the $\mathcal{CP}$-even h, H Higgs bosons are the same as in the Standard Model,

$$
A_Q^{h/H} \to 2/3
\tag{65}
$$

while the corresponding limit for the $\mathcal{CP}$-odd A Higgs boson reads:

$$
A_Q^A \to 1 \ .
\tag{66}
$$

As a result of the non-renormalization of the axial anomaly, the Agg coupling is not altered by QCD radiative corrections for large loop masses.

In the opposite limit in which the quark-loop mass is much smaller than the Higgs mass, the amplitudes are the same for scalar and pseudoscalar Higgs bosons:

$$
A_Q^\Phi \to -\frac{\tau_Q}{4}\left(\log\frac{\tau_Q}{4} - i\pi\right)^2 \ .
\tag{67}
$$

This result follows from the restoration of chiral symmetry in the limit of vanishing quark masses.

Other production mechanisms for SUSY Higgs bosons, vector boson fusion, Higgs-strahlung off W, Z bosons and Higgs-bremsstrahlung off top and bottom quarks, can be treated in analogy to the corresponding SM processes.

Data from the Tevatron in the channel $p\bar{p} \to b\bar{b}\tau^+\tau^-$ have been exploited [71] to exclude part of the supersymmetric Higgs parameter space in the $[M_A, \text{tg}\beta]$ plane. In the interesting range of $\text{tg}\beta$ between 30 and 50, pseudoscalar masses M_A of up to 150 to 190 GeV appear to be excluded.

The cross sections of the various MSSM Higgs production mechanisms at the LHC are shown in Figs. 24a–d for two representative values of $\text{tg}\beta = 1.5$ and 30, as a function of
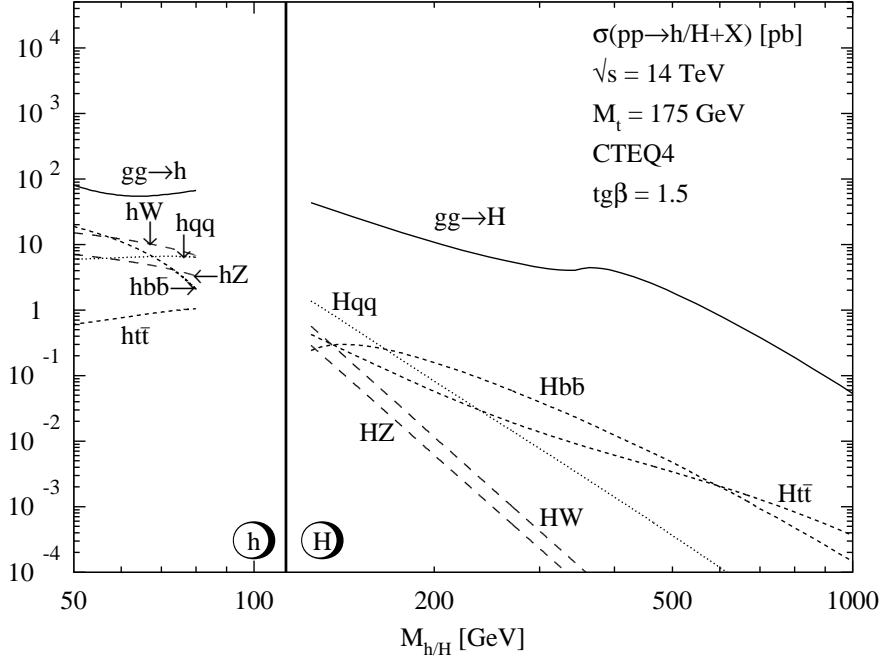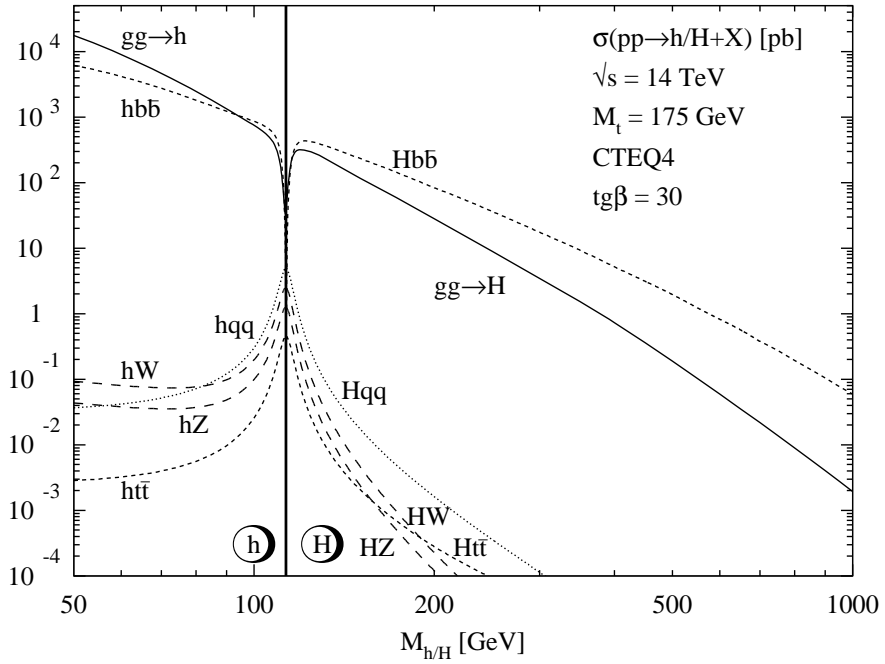
Fig. 24a

Fig. 24b

Figure 24: *Neutral MSSM Higgs production cross sections at the LHC for gluon fusion* $gg \to \Phi$, *vector-boson fusion* $qq \to qqVV \to qqh/qqH$, *vector-boson bremsstrahlung* $q\bar{q} \to V^* \to hV/HV$ *and the associated production* $gg, q\bar{q} \to b\bar{b}\Phi/t\bar{t}\Phi$, *including all known QCD corrections. (a)* h, H *production for* $tg\beta = 1.5$, *(b)* h, H *production for* $tg\beta = 30$, *(c)* A *production for* $tg\beta = 1.5$, *(d)* A *production for* $tg\beta = 30$.
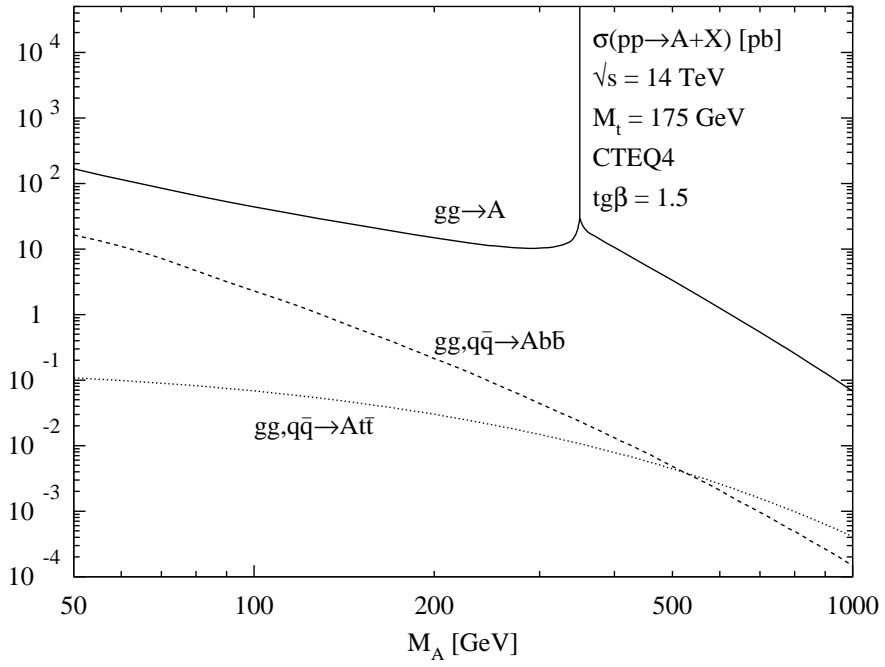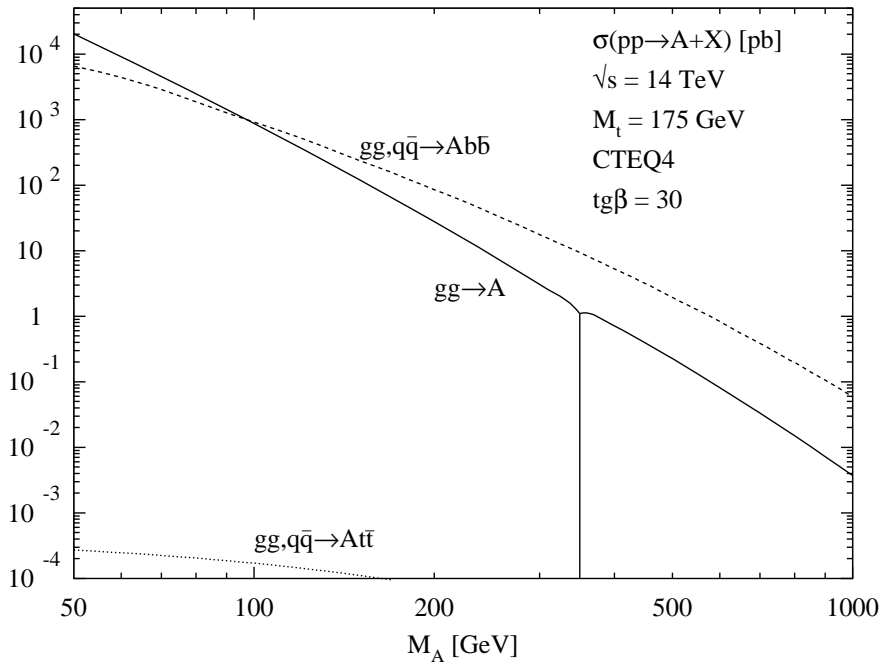
48

Fig. 24c

Fig. 24d

Figure 24: *Continued.*

the corresponding Higgs mass. The CTEQ4M parton densities have been adopted with $\alpha_s(M_Z) = 0.116$; the top and bottom masses have been set to $M_t = 175$ GeV and $M_b = 5$ GeV. For the Higgs bremsstrahlung off t, b quarks, $pp \to Q\bar{Q}\Phi + X$, the leading-order CTEQ4L parton densities have been used. For small and moderate values of tg$\beta \lesssim 10$ the gluon-fusion cross section provides the dominant production cross section for the entire Higgs mass region up to $M_\Phi \sim 1$ TeV. However, for large tgβ, Higgs bremsstrahlung off bottom quarks, $pp \to b\bar{b}\Phi + X$, dominates over the gluon-fusion mechanism since the bottom Yukawa couplings are strongly enhanced in this case.

The MSSM Higgs search at the LHC will be more involved than the SM Higgs search. The basic features can be summarized as follows.

(i) For large pseudoscalar Higgs masses, $M_A \gtrsim 200$ GeV, the light scalar Higgs boson h can only be found in the photonic decay mode $h \to \gamma\gamma$. In a significant part of this MSSM parameter region, especially for moderate values of tgβ, no other MSSM Higgs particle can be discovered. Because of the decoupling limit for large M_A, the MSSM cannot be distinguished from the SM in this mass range.

(ii) For small values of tg$\beta \lesssim 3$ and pseudoscalar Higgs masses between about 200 and 350 GeV, the heavy scalar Higgs boson can be searched for in the 'gold-plated' channel $H \to ZZ \to 4l^\pm$. Otherwise this 'gold-plated' signal does not play any role in the MSSM. However, the MSSM parameter region covered in this scenario hardly exceeds the anticipated exclusion limits of the LEP2 experiments.

(iii) For large and moderate values of tgβ ($\gtrsim 3$), the decays $H, A \to \tau^+\tau^-$ become visible at the LHC. Thus this decay mode plays a significant role for the MSSM in contrast to the SM. Moreover, this mode can also be detected for small values of tgβ ($\gtrsim 1$–2) and M_A ($\lesssim 200$ GeV).

(iv) For tg$\beta \lesssim 4$ and 150 GeV $\lesssim M_A \lesssim 400$ GeV, the heavy scalar Higgs particle can be detected in the decay mode $H \to hh \to b\bar{b}\gamma\gamma$. However, the MSSM parameter range for this signature is very limited.

(v) For tg$\beta \lesssim 3$–5 and 50 GeV $\lesssim M_A \lesssim 350$ GeV, the pseudoscalar decay mode $A \to Zh \to l^+l^-b\bar{b}$ will be visible, but hardly exceeds the exclusion limits from LEP2.

(vi) For pseudoscalar Higgs masses $M_A \lesssim 100$ GeV, charged Higgs bosons, produced from top quark decays $t \to H^+b$, can be discovered in the decay mode $H^+ \to \tau^+\bar{\nu}_\tau$. The search for charged Higgs bosons is quite difficult in general if the mass exceeds the top-quark mass and $t \to b + H^+$ decays are forbidden kinematically. Since $H^\pm$ bosons cannot be radiated off Z or W bosons, they must be produced in pairs in the Drell–Yan process [72] or in gg collisions [73]. In the second process, and equivalently in $W^\pm H^\mp$ final states, the effective couplings are built up by loops of heavy quarks.

50

The final summary, Fig. 25, exhibits a difficult region for the MSSM Higgs search at the LHC. For tg$\beta \sim 5$ and $M_A \sim 150$ GeV, the full luminosity and the full data sample of both the ATLAS and CMS experiments at the LHC are needed to cover the problematic parameter region [74]. On the other hand, if no excess of Higgs events above the SM background processes beyond 2 standard deviations will be found, the MSSM Higgs bosons can be excluded at 95% C.L.

The overall picture reveals several difficulties, as evident from Fig. 25. Even though the entire supersymmetric Higgs parameter space may finally be covered by the LHC experiments, the entire ensemble of individual Higgs bosons is accessible only in part of the parameter space. Moreover, the search for heavy H, A Higgs particles is very difficult, because of the $t\bar{t}$ continuum background for masses $\gtrsim 500$ GeV.

3.6 Measuring the Parity of Higgs Bosons

Once the Higgs bosons are discovered, the properties of the particles must be established. Besides the reconstruction of the supersymmetric Higgs potential [75], which will be a very demanding effort, the external quantum numbers must be established, in particular the parity of the heavy scalar and pseudoscalar Higgs particles H and A [76].

For large H, A masses the decays $H, A \to t\bar{t}$ to top final states can be used to discriminate between the different parity assignments [76]. For example, the W^+ and W^- bosons in the t and $\bar{t}$ decays tend to be emitted antiparallel and parallel in the plane perpendicular to the $t\bar{t}$ axis:

$$\frac{d\Gamma^\pm}{d\phi_*} \propto 1 \mp \left(\frac{\pi}{4}\right)^2 \cos \phi_* \tag{68}$$

for H and A decays, respectively.

For light H, A masses, $\gamma\gamma$ collisions appear to provide a viable solution [76]. The fusion of Higgs particles in linearly polarized photon beams depends on the angle between the polarization vectors. For scalar 0^+ particles the production amplitude is non-zero for parallel polarization vectors, while pseudoscalar 0^- particles require perpendicular polarization vectors:

$$\mathcal{M}(H)^+ \sim \vec{\epsilon}_1 \cdot \vec{\epsilon}_2 \quad \text{and} \quad \mathcal{M}(A)^- \sim \vec{\epsilon}_1 \times \vec{\epsilon}_2 \ . \tag{69}$$

The experimental set-up for Compton back-scattering of laser light can be tuned in such a way that the linear polarization of the hard-photon beams approaches values close to 100%. Depending on the $\pm$ parity of the resonance produced, the measured asymmetry for photons of parallel and perpendicular polarization,

$$\mathcal{A} = \frac{\sigma_\parallel - \sigma_\perp}{\sigma_\parallel + \sigma_\perp} \ , \tag{70}$$
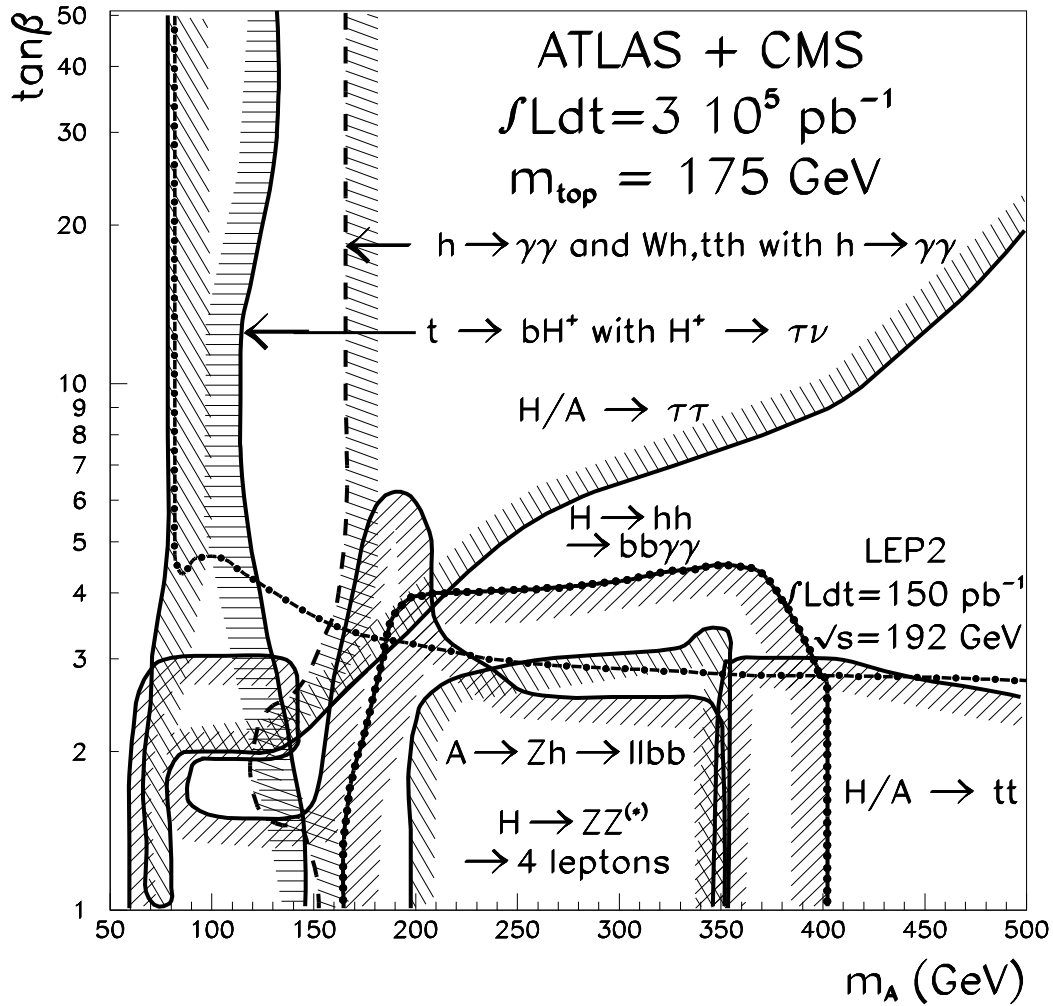
is either positive or negative.

Figure 25: *MSSM parameter space including the contours of the various Higgs decay modes, which will be visible at the LHC after reaching the anticipated integrated luminosity $\int \mathcal{L} = 0.3\ ab^{-1}$ and combining the experimental data of both LHC experiments, ATLAS and CMS [taken from Ref. [74]].*

3.7 Non-minimal Supersymmetric Extensions

The minimal supersymmetric extension of the Standard Model may appear very restrictive for supersymmetric theories in general, in particular in the Higgs sector where the quartic couplings are identified with the gauge couplings. However, it turns out that the mass pattern of the MSSM is quite typical if the theory is assumed to be valid up to the GUT scale – the motivation for supersymmetry *sui generis*. This general pattern has been studied thoroughly within the next-to-minimal extension: the MSSM, incorporating two Higgs isodoublets, is extended by introducing an additional isosinglet field N. This extension leads to a model [77–79] that is generally referred to as the (M+1)SSM.

The additional Higgs singlet can solve the so-called μ-problem [i.e. $\mu \sim$ order M_W] by eliminating the μ higgsino parameter from the potential and by replacing this parameter by the vacuum expectation value of the N field, which can naturally be related to the usual vacuum expectation values of the Higgs isodoublet fields. In this scenario the super-potential involves the two trilinear couplings $H_1 H_2 N$ and N^3. The consequences of this extended Higgs sector will be outlined in the context of (s)grand unification, including the universal soft breaking terms of the supersymmetry [78].

The Higgs spectrum of the (M+1)SSM includes, besides the minimal set of Higgs particles, one additional scalar and pseudoscalar Higgs particle. The neutral Higgs particles are in general mixtures of iso scalar doublets, which couple to W, Z bosons and fermions, and the iso scalar singlet, decoupled from the non-Higgs sector. The trilinear self-interactions contribute to the masses of the Higgs particles; for the lightest Higgs boson of each species:

$$
\begin{aligned}
M^2(h_1) &\leq M_Z^2 \cos^2 2\beta + \lambda^2 v^2 \sin^2 2\beta \\
M^2(A_1) &\leq M^2(A) \\
M^2(H^\pm) &\leq M^2(W) + M^2(A) - \lambda^2 v^2
\end{aligned}
\tag{71}
$$

In contrast with the minimal model, the mass of the charged Higgs particle could be smaller than the W mass. Since the trilinear couplings increase with energy, upper bounds on the mass of the lightest neutral Higgs boson h_1^0 can be derived, in analogy to the Standard Model, from the assumption that the theory be valid up to the GUT scale: $m(h_1^0) \lesssim 140$ GeV. Thus, despite the additional interactions, the distinct pattern of the minimal extension remains valid also in more complex supersymmetric scenarios . In fact, the mass bound of 140 GeV for the lightest Higgs particle is realized in almost all supersymmetric theories [80]. If h_1^0 is (nearly) pure iso scalar, it decouples from the gauge boson and fermion system and its role is taken by the next Higgs particle with a large isodoublet component, implying the validity of the mass bound again.

The couplings R_i of the $\mathcal{CP}$-even neutral Higgs particles h_i^0 to the Z boson, ZZh_i^0, are defined relative to the usual SM coupling. If the Higgs particle h_1^0 is primarily isosinglet, the coupling R_1 is small and the particle cannot be produced by Higgs-strahlung.

However, in this case h_2^0 is generally light and couples with sufficient strength to the Z boson; if not, h_3^0 plays this role. This scenario is quantified in Fig. 26, where the couplings R_1 and R_2 are shown for the ensemble of allowed Higgs masses $m(h_1^0)$ and $m(h_2^0)$
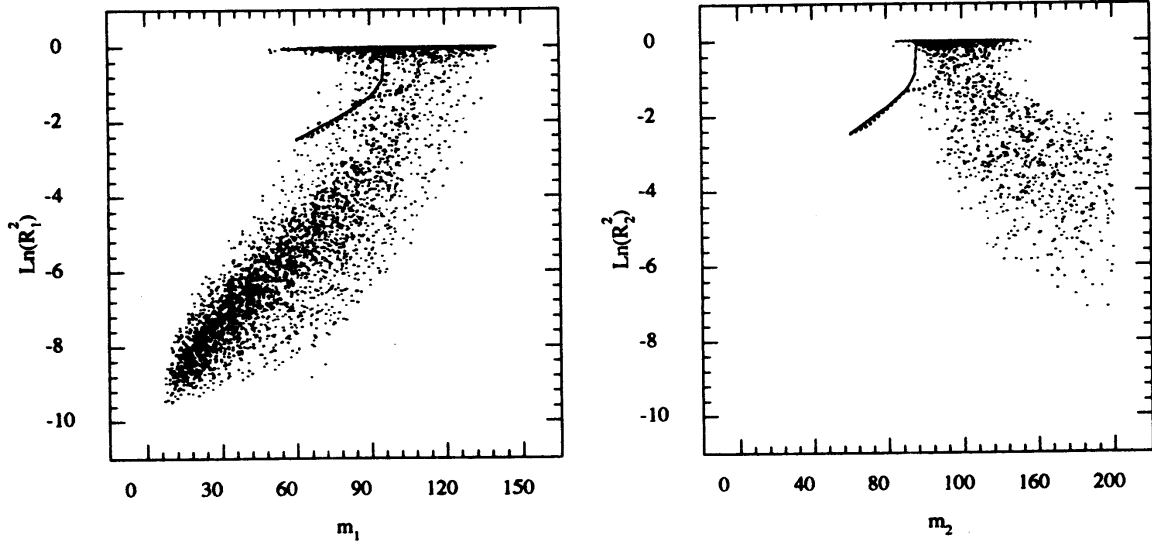

Figure 26: *The couplings ZZh_1 and ZZh_2 of the two lightest $\mathcal{CP}$-even Higgs bosons in the next-to-minimal supersymmetric extension of the Standard Model, $(M+1)SSM$. The solid lines indicate the accessible range at LEP2 for an energy of 192 GeV, the dotted lines for 205 GeV. The scatter plots are solutions for an ensemble of possible SUSY parameters defined at the scale of grand unification. Ref. [78].*

[adopted from Ref. [10]; see also Refs. [78, 81]]. Two different regions exist within the GUT (M+1)SSM: a densely populated region with $R_1 \sim 1$ and $m_1 > 50$ GeV, and a tail with $R_1 < 1$ to $\ll 1$ and small m_1. Within this tail, the lightest Higgs boson is essentially a gauge-singlet state so that it can escape detection at LEP [full/solid lines]. If the lightest Higgs boson is essentially a gauge singlet, the second lightest Higgs particle cannot be heavy. In the tail of diagram 26a the mass of the second Higgs boson h_2^0 varies between 80 GeV and, essentially, the general upper limit of ~ 140 GeV; h_2^0 couples with full strength to Z bosons, $R_2 \sim 1$. If this coupling becomes weak in the tail of diagram 26b, the third Higgs boson will finally take the role of the leading light particle.

In summa. Experiments at e^+e^- colliders are in a 'no-lose' situation [81] for detecting the Higgs particles in general supersymmetric theories, even for c.m. energies as low as $\sqrt{s} \sim 300$ GeV.

4 Strongly Interacting W Bosons

The Higgs mechanism is based on the theoretical concept of spontaneous symmetry breaking [1]. In the canonical formulation, adopted in the Standard Model, a four-component *fundamental* scalar field is introduced, which is endowed with a self-interation such that the field acquires a non-zero value in the ground state. The specific direction in iso space, which is singled out by the ground-state solution, breaks the isospin invariance of the interaction spontaneously. The interaction of the gauge fields with the scalar field in the ground state generates the masses of these fields. The longitudinal degrees of freedom of the gauge fields are built up by absorption of the Goldstone modes, which are associated with the spontaneous breaking of the electroweak symmetries in the scalar field sector. Fermions acquire masses through Yukawa interactions with the ground-state field. While three scalar components are absorbed by the gauge fields, one degree of freedom manifests itself as a physical particle, the Higgs boson. The exchange of this particle in scattering amplitudes, including longitudinal gauge fields and massive fermion fields, guarantees the unitarity of the theory up to asymptotic energies.

In the alternative to this scenario based on a fundamental Higgs field, the spontaneous symmetry breaking is generated *dynamically* [2]. A system of novel fermions is introduced, which interact strongly at a scale of order 1 TeV. In the ground state of such a system a scalar condensate of fermion–antifermion pairs may form. Such a process is generally expected to be realized in any non-Abelian gauge theory of the novel strong interactions [and realized in QCD, for instance]. Since the scalar condensate breaks the chiral symmetry of the fermion system, Goldstone fields will form, and these can be absorbed by the electroweak gauge fields to build up the longitudinal components and the masses of the gauge fields. Novel gauge interactions must be introduced, which couple the leptons and quarks of the Standard Model to the new fermions in order to generate lepton and quark masses through interactions with the ground-state fermion–antifermion condensate. In the low-energy sector of the electroweak theory, the fundamental Higgs-field approach and the dynamical alternative are equivalent. However, the two theories are fundamentally different at high energies. While the unitarity of the electroweak gauge theory is guaranteed by the exchange of the scalar Higgs particle in scattering processes, unitarity is restored in the dynamical theory at high energies through the non-perturbative strong interactions between the particles. Since the longitudinal gauge field components are equivalent to the Goldstone fields associated with the microscopic theory, their strong interactions at high energies are transferred to the electroweak gauge bosons. Since, by unitarity, the S-wave scattering amplitude of longitudinally polarized W, Z bosons in the isoscalar channel $(2W^+W^- + ZZ)/\sqrt{3}$, $a_0^0 = \sqrt{2}G_F s/16\pi$, is bounded by $1/2$, the characteristic scale of the new strong interactions must be close to 1.2 TeV. Thus near the critial energy of 1 TeV the W, Z bosons interact strongly with each other. Technicolour theories provide an elaborate form of such scenarios.

4.1 Dynamical Symmetry Breaking

Physical scenarios of dynamical symmetry breaking may be based on new strong interaction theories, which extend the spectrum of matter particles and of the interactions beyond the degrees of freedom realized in the Standard Model. If the new strong interactions are invariant under transformations of a chiral $SU(2) \times SU(2)$ group, the chiral invariance is generally broken spontaneously down to the diagonal custodial isospin group $SU(2)$. This process is associated with the formation of a chiral condensate in the ground state and the existence of three massless Goldstone bosons.

Figure 27: *Generating gauge-boson masses (V) through the interaction with the Goldstone bosons (G).*

The Goldstone bosons can be absorbed by the gauge fields, generating longitudinal states and non-zero masses of the gauge bosons, as shown in Fig. 27. Summing up the geometric series of vector-boson–Goldstone-boson transitions in the propagator leads to in a shift of the mass pole:

$$\frac{1}{q^2} \quad \rightarrow \quad \frac{1}{q^2} + \frac{1}{q^2} q_\mu \frac{g^2 F^2/2}{q^2} q_\mu \frac{1}{q^2} + \frac{1}{q^2} \left[\frac{g^2 F^2}{2} \frac{1}{q^2} \right]^2 + \cdots$$
$$\rightarrow \quad \frac{1}{q^2 - M^2} \tag{72}$$

The coupling between gauge fields and Goldstone bosons has been defined as $igF/\sqrt{2}q_\mu$. The mass generated for the gauge field is related to this coupling by

$$M^2 = \frac{1}{2} g^2 F^2 \ . \tag{73}$$

The numerical value of the coupling F must coincide with $v = 246$ GeV.

The remaining custodial $SU(2)$ symmetry guarantees that the ρ parameter, the relative strength between NC and CC couplings, is one. Denoting the W/B mass matrix elements by

$$\langle W^i | \mathcal{M}^2 | W^j \rangle = \frac{1}{2} g^2 F^2 \delta_{ij} \qquad \langle W^3 | \mathcal{M}^2 | B \rangle = \langle B | \mathcal{M}^2 | W^3 \rangle$$
$$\langle B | \mathcal{M}^2 | B \rangle = \frac{1}{2} g'^2 F^2 \qquad\qquad = \frac{1}{2} g g' F^2 \tag{74}$$

the universality of the coupling F leads to the ratio $M_W^2/M_Z^2 = g^2/(g^2 + g'^2) = \cos^2 \theta_W$ of the mass eigenvalues, equivalent to $\rho = 1$.

Since the wave functions of longitudinally polarized vector bosons grow with the energy, the longitudinal field components are the dominant degrees of freedom at high energies. These states can, however, for asymptotic energies be identified with the absorbed Goldstone bosons. This equivalence [82] is apparent in the 't Hooft–Feynman gauge where, for asymptotic energies,

$$\epsilon_\mu^L W_\mu \to k_\mu W_\mu \sim M^2 \Phi \ . \tag{75}$$

The dynamics of gauge bosons can therefore be identified at high energies with the dynamics of scalar Goldstone fields. An elegant representation of the Goldstone fields $\vec{G}$ in this context is provided by the exponentiated form

$$U = \exp[-i\vec{G}\vec{\tau}/v] \ , \tag{76}$$

which corresponds to an $SU(2)$ matrix field.

The Lagrangian of a system of strongly interacting bosons consists in such a scenario of the Yang–Mills part $\mathcal{L}_{YM}$ and the interactions $\mathcal{L}_G$ of the Goldstone fields,

$$\mathcal{L} = \mathcal{L}_{YM} + \mathcal{L}_G \ . \tag{77}$$

The Yang–Mills part is written in the usual form $\mathcal{L}_{YM} = -\frac{1}{4}\text{Tr}[W_{\mu\nu}W_{\mu\nu} + B_{\mu\nu}B_{\mu\nu}]$. The interaction of the Goldstone fields can be systematically expanded in chiral theories in the derivatives of the fields, corresponding to expansions in powers of the energy for scattering amplitudes [83]:

$$\mathcal{L}_G = \mathcal{L}_0 + \sum_{dim=4} \mathcal{L}_i + \cdots \tag{78}$$

Denoting the SM covariant derivative of the Goldstone fields by

$$D_\mu U = \partial_\mu U - ig W_\mu U + ig' B_\mu U \ , \tag{79}$$

the leading term $\mathcal{L}_0$, which is of dimension $= 2$, is given by

$$\mathcal{L}_0 = \frac{v^2}{4}\text{Tr}[D_\mu U^+ D_\mu U] \ . \tag{80}$$

This term generates the masses of the W, Z gauge bosons: $M_W^2 = \frac{1}{4}g^2 v^2$ and $M_Z^2 = \frac{1}{4}(g^2 + g'^2)v^2$. The only parameter in this part of the interaction is v, which however is fixed uniquely by the experimental value of the W mass; thus the amplitudes predicted by the leading term in the chiral expansion can effectively be considered as parameter-free.

The next-to-leading component in the expansion with dimension $= 4$ consists of ten individual terms. If the custodial $SU(2)$ symmetry is imposed, only two terms are left, which do not affect propagators and 3-boson vertices but only 4-boson vertices. Introducing the vector field V_μ by

$$V_\mu = U^+ D_\mu U \tag{81}$$

these two terms are given by the interaction densities

$$\mathcal{L}_4 = \alpha_4 \left[Tr V_\mu V_\nu \right]^2 \quad \text{and} \quad \mathcal{L}_5 = \alpha_5 \left[Tr V_\mu V_\mu \right]^2 \tag{82}$$

The two coefficients α_4, α_5 are free parameters that must be adjusted experimentally from WW scattering data.

Higher orders in the chiral expansion give rise to an energy expansion of the scattering amplitudes of the form $\mathcal{A} = \sum c_n (s/v^2)^n$. This series will diverge at energies for which the resonances of the new strong interaction theory can be formed in WW collisions: 0^+ 'Higgs-like', 1^- 'ρ-like' resonances, etc. The masses of these resonance states are expected in the range $M_R \sim 4\pi v$ where chiral loop expansions diverge, i.e. between about 1 and 3 TeV.

4.2 WW Scattering at High-Energy Colliders

The (quasi-)elastic 2–2 WW scattering amplitudes can be expressed at high energies by a master amplitude $A(s,t,u)$, which depends on the three Mandelstam variables of the scattering processes:

$$
\begin{aligned}
A(W^+W^- \to ZZ) &= A(s,t,u) \\
A(W^+W^- \to W^+W^-) &= A(s,t,u) + A(t,s,u) \\
A(ZZ \to ZZ) &= A(s,t,u) + A(t,s,u) + A(u,s,t) \\
A(W^-W^- \to W^-W^-) &= A(t,s,u) + A(u,s,t) \ .
\end{aligned}
\tag{83}
$$

To lowest order in the chiral expansion, $\mathcal{L} \to \mathcal{L}_{YM} + \mathcal{L}_0$, the master amplitude is given, in a parameter-free form, by the energy squared s:

$$A(s,t,u) \to \frac{s}{v^2} \ . \tag{84}$$

This representation is valid for energies $s \gg M_W^2$ but below the new resonance region, i.e. in practice at energies $\sqrt{s} = \mathcal{O}(1 \text{ TeV})$. Denoting the scattering length for the channel carrying isospin I and angular momentum J by a_{IJ}, the only non-zero scattering channels predicted by the leading term of the chiral expansion correspond to

$$
\begin{aligned}
a_{00} &= +\frac{s}{16\pi v^2} \tag{85} \\
a_{11} &= +\frac{s}{96\pi v^2} \\
a_{20} &= -\frac{s}{32\pi v^2} \ . \tag{86}
\end{aligned}
$$

While the exotic $I = 2$ channel is repulsive, the $I = J = 0$ and $I = J = 1$ channels are attractive, indicating the formation of non-fundamental Higgs-type and ρ-type resonances.

58

Taking into account the next-to-leading terms in the chiral expansion, the master amplitude turns out to be [23]

$$A(s,t,u) = \frac{s}{v^2} + \alpha_4 \frac{4(t^2 + u^2)}{v^4} + \alpha_5 \frac{8s^2}{v^4} + \cdots , \qquad (87)$$

including the two parameters α_4 and α_5.

Increasing the energy, the amplitudes will approach the resonance area. There, the chiral character of the theory does not provide any more guiding principle for constructing the scattering amplitudes. Instead, *ad-hoc* hypotheses must be introduced to define the nature of the resonances; see e.g. Ref. [24]. A sample of resonances is provided by the following models:

(a) SM heavy Higgs boson:

$$A = -\frac{M_H^2}{v^2} \left[1 + \frac{M_H^2}{s - M_H^2 + iM_H\Gamma_H} \right] \qquad (88)$$
$$\text{with} \quad \Gamma_H = \frac{3M_H^3}{32\pi v^2}$$

(b) Chirally coupled scalar resonance:

$$A = \frac{s}{v^2} - \frac{g_s^2 s^2}{v^2} \frac{1}{s - M_S^2 - iM_S\Gamma_S} \qquad (89)$$
$$\text{with} \quad \Gamma_S = \frac{3g_s^2 M_S^3}{32\pi v^2}$$

(c) Chirally coupled vector resonance:

$$A = \frac{s}{v^2} \left[1 - \frac{3a}{4} \right] + \frac{aM_V^2}{4v^2} \left[\frac{u - s}{t - M_V^2 + iM_V\Gamma_V} + (u \leftrightarrow t) \right] \qquad (90)$$
$$\text{with} \quad \Gamma_V = \frac{aM_V^3}{192\pi v^2}$$

For small energies, the scattering amplitudes reduce to the leading chiral form s/v^2. In the resonance region they are described by two parameters, the mass and the width of the resonance. The amplitudes interpolate between the two regions in a simplified smooth way.

WW scattering can be studied at the LHC and at TeV e^+e^- linear colliders. At high energies, equivalent W beams accompany the quark and electron/positron beams (Fig. 28) in the fragmentation processes $pp \to qq \to qqWW$ and $ee \to \nu\nu WW$; the spectra of the longitudinally polarized W bosons have been given in Eq. (33). In the hadronic LHC environment the final-state W bosons can only be observed in leptonic decays. Resonance reconstruction is thus not possible for charged W final states. However, the clean
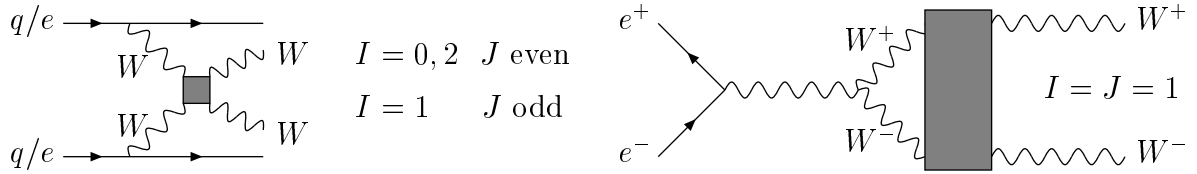
Figure 28: *WW scattering and rescattering at high energies at the LHC and TeV e^+e^- linear colliders.*

environment of e^+e^- colliders will allow the reconstruction of resonances from W decays to jet pairs. The results of three experimental simulations are displayed in Fig. 29. In Fig. 29a the sensitivity to the parameters α_4, α_5 of the chiral expansion is shown for WW scattering in e^+e^- colliders [23]. The results of this analysis can be reinterpreted as sensitivity to the parameter-free prediction of the chiral expansion, corresponding to an error of about 10% in the first term of the master amplitude s/v^2. These experiments test the basic concept of dynamical symmetry breaking through spontaneous symmetry breaking. The production of a vector-boson resonance of mass $M_V = 1$ TeV is exemplified in Fig. 29b [24]. Expectations for leptonic invariant energies of WW scattering final states at the LHC are compared in the vector model with the background in Fig. 30 [22].

A second powerful method measures the elastic $W^+W^- \to W^+W^-$ scattering in the $I = 1, J = 1$ channel. The rescattering of W^+W^- bosons produced in e^+e^- annihilation, cf. Fig. 28, depends at high energies on the WW scattering phase δ_{11} [84]. The production amplitude $F = F_{LO} \times R$ is the product of the lowest-order perturbative diagram with the Mushkelishvili–Omnès rescattering amplitude $\mathcal{R}_{11}$,

$$\mathcal{R}_{11} = \exp \frac{s}{\pi} \int \frac{ds'}{s'} \frac{\delta_{11}(s')}{s' - s - i\epsilon} \,, \tag{91}$$

which is determined by the $I = J = 1$ WW phase shift δ_{11}. The power of this method derives from the fact that the entire e^+e^- collider energy is transferred to the WW system [while a major fraction of the energy is lost in the fragmentation of $e \to \nu W$ if the WW scattering is studied in the process $ee \to \nu\nu WW$]. Detailed simulations [85] have shown that this process is sensitive to vector-boson masses up to about $M_V \lesssim 6$ TeV in technicolor-type theories. More elaborate scenarios [86] have been analysed in Ref. [87].
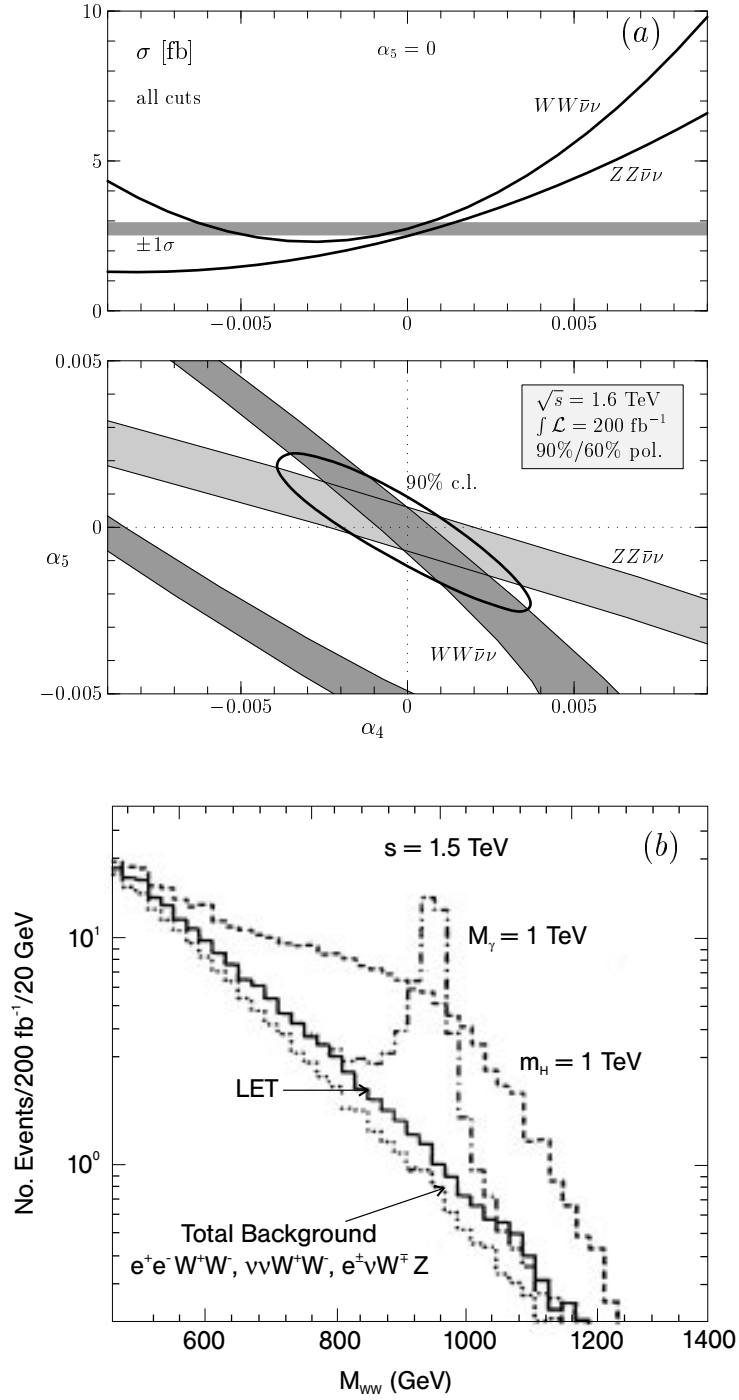
Figure 29: *Upper part: Sensitivity to the expansion parameters in chiral electroweak models of $WW \to WW$ and $WW \to ZZ$ scattering at the strong-interaction threshold; Ref. [23]. Lower part: The distribution of the WW invariant energy in $e^+e^- \to \overline{\nu}\nu WW$ for scalar and vector resonance models $[M_H, M_V = 1\ TeV]$; Ref. [24].*

61
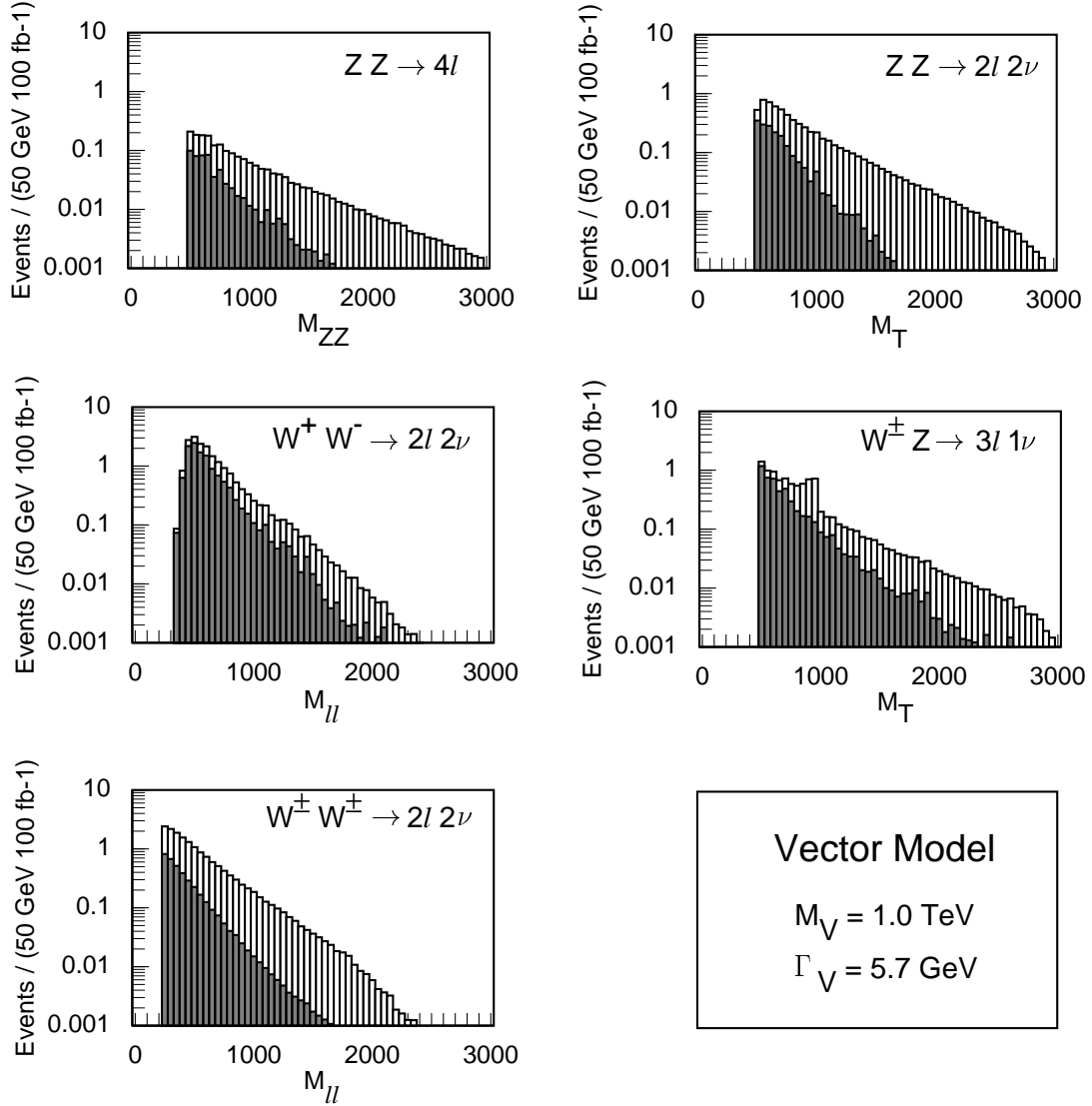
Figure 30: *Invariant mass distributions for the gold-plated purely leptonic final states that arise from the processes* $pp \to ZZX \to 4\ell X, pp \to ZZX \to 2\ell 2\nu X, pp \to W^+W^-X, pp \to W^{\pm}ZX$ *and* $pp \to W^{\pm}W^{\pm}X$, *for the LHC (mass in GeV). The signal is plotted above the summed background. Distributions are shown for a chirally coupled vector with* $M_V = 1$ *TeV,* $\Gamma_V = 5.7$ *GeV; Ref. [22].*

5 Summary

The mechanism of electroweak symmetry breaking can be established in the present or the next generation of e^+e^- and $p\bar{p}/pp$ colliders:

⋆ Whether there exists a light fundamental Higgs boson;

⋆ The profile of the Higgs particle can be reconstructed, which reveals the physical nature of the underlying mechanism of electroweak symmetry breaking;

⋆ Analyses of strong WW scattering can be performed if the symmetry breaking is of a dynamical nature and generated in a novel strong interaction theory.

Moreover, depending on the experimental answer to these questions, the electroweak sector will provide the platform for extrapolations into physical areas beyond the Standard Model: either to the low-energy supersymmetry sector or, alternatively, to a new strong interaction theory at a characteristic scale of order 1 TeV.

References

[1] P. W. Higgs, Phys. Rev. Lett. **12** (1964) 132 and Phys. Rev. **145** (1966) 1156; F. Englert and R. Brout, Phys. Rev. Lett. **13** (1964) 321; G. S. Guralnik, C. R. Hagen and T. W. Kibble, Phys. Rev. Lett. **13** (1964) 585.

[2] S. Weinberg, Phys. Rev. **D13** (1979) 974, *ibid.* **D19** (1979) 1277; L. Susskind, Phys. Rev. **D20** (1979) 2619.

[3] S.L. Glashow, Nucl. Phys. **20** (1961) 579; S. Weinberg, Phys. Rev. Lett. **19** (1967) 1264; A. Salam, in Elementary Particle Theory, ed. N. Svartholm (Almqvist and Wiksells, Stockholm, 1968).

[4] N. Cabibbo, L. Maiani, G. Parisi and R. Petronzio, Nucl. Phys. **B158** (1979) 295; R.A. Flores and M. Sher, Phys. Rev. **D27** (1983) 1679; M. Lindner, Z. Phys. **C31** (1986) 295; M. Sher, Phys. Rep. **179** (1989) 273; J. Casas, J. Espinosa and M. Quiros, Phys. Lett. **B342** (1995) 171.

[5] G. Altarelli and G. Isidori, Phys. Lett. **B337** (1994) 141; J. Espinosa and M. Quiros, Phys. Lett. **B353** (1995) 257.

[6] A. Hasenfratz, K. Jansen, C. Lang, T. Neuhaus and H. Yoneyama, Phys. Lett. **B199** (1987) 531; J. Kuti, L. Liu and Y. Shen, Phys. Rev. Lett. **61** (1988) 678; M. Lüscher and P. Weisz, Nucl. Phys. **B318** (1989) 705.

[7] M. Veltman, Acta Phys. Polon. **B8** (1977) 475.

[8] LEP Electroweak Working Group, Report CERN–PPE/97–154.

[9] Experimental reports to the LEPC meeting, CERN November 1997.

[10] M. Carena, P.M. Zerwas (conv.) et al., *Higgs Physics at LEP2*, CERN Report 96–01 [hep-ph/9602250], G. Altarelli, T. Sjöstrand and F. Zwirner (eds.).

[11] *Future Electroweak Physics at the Fermilab Tevatron*, FERMI LAB–PUB–96/082 [hep-ph/9602250], D. Amidei and R. Brock (eds.).

[12] ATLAS Collaboration, Technical Proposal, Report CERN–LHCC 94–43; CMS Collaboration, Technical Proposal, Report CERN–LHCC 94–38.

[13] E. Accomando et al., Report DESY 97-100 [hep-ph/9705442] and Phys. Rep. in press.

[14] P. Fayet and S. Ferrara, Phys. Rep. **32** (1977) 249; H.P. Nilles, Phys. Rep. **110** (1984) 1; H. Haber and G. Kane, Phys. Rep. **117** (1985) 75; R. Barbieri, Riv. Nuovo Cimento **11** (1988) 1.

[15] E. Witten, Phys. Lett. **B105** (1981) 267.

[16] L.E. Ibañez and G.G. Ross, Phys. Lett. **B105** (1981) 439; S. Dimopoulos, S. Raby and F. Wilczek, Phys. Rev. **D24** (1981) 1681; J. Ellis, S. Kelley and D.V. Nanopoulos, Phys. Lett. **B249** (1990) 441; P. Langacker and M. Luo, Phys. Rev. **D44** (1991) 817; U. Amaldi, W. de Boer and H. Fürstenau, Phys. Lett. **B260** (1991) 447.

[17] K. Inonue, A. Kakuto, H. Komatsu and S. Takeshita, Prog. Theor. Phys. **67** (1982) 1889; R. Flores and M. Sher, Ann. Phys. **148** (1983) 95; H.P. Nilles and M. Nusbaumer, Phys. Lett. **B145** (1984) 73; P. Majumdar and P. Roy, Phys. Rev. **D30** (1984) 2432.

[18] J.F. Gunion and H.E. Haber, Nucl. Phys. **B272** (1986) 1 and **B278** (1986) 449.

[19] S. Dawson, Nucl. Phys. **B249** (1985) 42; M. Chanowitz and M.K. Gaillard, Phys. Lett. **B142** (1984) 85; G. Kane, W. Repko and W. Rolnick, Phys. Lett. **B148** (1984) 367.

[20] R.N. Cahn and S. Dawson, Phys. Lett. **B136** (1984) 196; K. Hikasa, Phys. Lett. **B164** (1985) 341; G. Altarelli, B. Mele and F. Pitolli, Nucl. Phys. **B287** (1987) 205; T. Han, G. Valencia and S. Willenbrock, Phys. Rev. Lett. **69** (1992) 3274.

[21] A. Dobado, M.J. Herrero, J.R. Pelaez, E. Ruiz Morales and M.T. Urdiales, Phys. Lett. **B352** (1995) 400; A. Dobado and M.T. Urdiales, Z. Phys. **C71** (1996) 659.

[22] J. Bagger, V. Barger, K. Cheung, J. Gunion, T. Ham, G.A. Ladinksy, R. Rosenfeld, and C.-P. Yuan, Phys. Rev. **D52** (1995) 3878.

[23] E. Boos, H.-J. He, W. Kilian, A. Pukhov, C.-P. Yuan and P.M. Zerwas, Phys. Rev. **D57** (1998) 1553.

[24] V. Barger, K. Cheung, T. Han and R.J.N. Phillips, Phys. Rev. **D52** (1995) 3815.

[25] J.F. Gunion, H.E. Haber, G. Kane and S. Dawson, *The Higgs Hunter's Guide*, (Addison–Wesley, 1990).

[26] A. Djouadi, Int. J. Mod. Phys. **A10** (1995) 1; M. Spira, Report CERN-TH/97-68 [hep-ph/9705337], Fort. Phys. in press; S. Dawson, BNL-HET-SD-97-004 [hep-ph/9703387]; D. Dominici, Report Firenze, hep-ph/9711385.

[27] B.W. Lee, C. Quigg and H.B. Thacker, Phys. Rev. Lett. **38** (1977) 883.

[28] E. Braaten and J.P. Léveille, Phys. Rev. **D22** (1980) 715; N. Sakai, Phys. Rev. **D22** (1980) 2220; T. Inami and T. Kubota, Nucl. Phys. **B179** (1981) 171; S.G. Gorishny, A.L. Kataev and S.A. Larin, Sov. J. Nucl. Phys. **40** (1984) 329; M. Drees and K. Hikasa, Phys. Rev. **D41** (1990) 1547; Phys. Lett. **B240** (1990) 455 and (E) **B262** (1991) 497; K.G. Chetyrkin, Phys. Lett. **B390** (1997) 309.

[29] B.A. Kniehl, Nucl. Phys. **B352** (1991) 1 and **B357** (1991) 357; D.Yu. Bardin, B.M. Vilenskiĭ and P.Kh. Khristova, Report JINR-P2-91-140.

[30] T.G. Rizzo, Phys. Rev. **D22** (1980) 389; W.-Y. Keung and W.J. Marciano, Phys. Rev. **D30** (1984) 248.

[31] A. Djouadi, M. Spira and P.M. Zerwas, Phys. Lett. **B264** (1991) 440.

[32] J. Ellis, M.K. Gaillard and D.V. Nanopoulos, Nucl. Phys. **B106** (1976) 292.

[33] B.A. Kniehl and M. Spira, Z. Phys. **C69** (1995) 77.

[34] M. Spira, A. Djouadi, D. Graudenz and P.M. Zerwas, Nucl. Phys. **B453** (1995) 17.

[35] V. Barger, M.S. Berger, J.F. Gunion and T. Han, Report UCD-96-6 [hep-ph/ 9602415].

[36] B.L. Ioffe and V.A. Khoze, Sov. J. Part. Nucl. **9** (1978) 50; J.D. Bjorken, Proc. Summer Institute on Particle Physics, Report SLAC-198 (1976).

[37] B.W. Lee, C. Quigg and H.B. Thacker, Phys. Rev. **D16** (1977) 1519.

[38] R.N. Cahn and S. Dawson, Phys. Lett. **B136** (1984) 96; G.L. Kane, W.W. Repko and W.B. Rolnick, Phys. Lett. **B148** (1984) 367; G. Altarelli, B. Mele and F. Pitolli, Nucl. Phys. **B287** (1987) 205; W. Kilian, M. Krämer and P.M. Zerwas, Phys. Lett. **B373** (1996) 135.

[39] H.J Schreiber et al., in: DESY–ECFA Conceptual LC Design Report (1997).

[40] D.L. Borden, D.A. Bauer, and D.O. Caldwell, Phys. Rev. **D48** (1993) 4018.

[41] I.F. Ginzburg, G.L. Kotkin, S.L. Panfil, V.G. Serbo and V.I. Telnov, Nucl. Instr. Meth. **219** (1984) 5.

[42] G. Jikia, Nucl. Phys. **B405** (1993) 24.

[43] For general reviews see M. Spira, in Ref. [26]; Z. Kunszt, S. Moretti and W.J. Stirling, Z. Phys. **C74** (1997) 479.

[44] H. Georgi, S.L. Glashow, M. Machacek and D. Nanopoulos, Phys. Rev. Lett. **40** (1978) 692.

[45] S. Dawson, Nucl. Phys. **B359** (1991) 283.

[46] V. Barger, K. Cheung, A. Djouadi, B.A. Kniehl and P. Zerwas, Phys. Rev. **D49** (1994) 79.

[47] P. Janot, Proceedings *Physics and Experiments with e^+e^- Linear Colliders*, Waikoloa/Hawaii 1993, eds. F. Harris, S. Olsen, S. Pakvasa and X. Tata (World Scientific, Singapore, 1993).

[48] M. Hildreth, T. Barklow and D. Burke, Phys. Rev. **D49** (1994) 3441; M. Battaglia et al., in: DESY–ECFA Conceptual LC Design Report (1997).

[49] A. Djouadi, J. Kalinowski and P.M. Zerwas, Mod. Phys. Lett. **A7** (1992) 1765 and Z. Phys. **C54** (1992) 255.

[50] K. Hagiwara, H. Murayama and I. Watanabe, Nucl. Phys. **B367** (1991) 257.

[51] V. Barger and T. Han, Mod. Phys. Lett. **A5** (1990) 667.

[52] J. Polchinski and L. Susskind, Phys. Rev. **D26** (1982) 3661; S. Dimopoulos and H. Georgi, Nucl. Phys. **B193** (1981) 150; N. Sakai, Z. Phys. **C11** (1981) 153.

[53] L.E. Ibañez and G.G. Ross, Phys. Lett. **B110** (1982) 215.

[54] D.J. Castano, E.J. Piard and P. Ramond, Phys. Rev. **D49** (1994) 4882.

[55] Y. Okada, M. Yamaguchi and T. Yanagida, Progr. Theor. Phys. **85** (1991) 1; H. Haber and R. Hempfling, Phys. Lett. **66** (1991) 1815; J. Ellis, G. Ridolfi and F. Zwirner, Phys. Lett. **257B** (1991) 83; M. Carena, J.R. Espinosa, M. Quiros and C.E.M. Wagner, Phys. Lett. **B335** (1995) 209.

[56] H.E. Haber, R. Hempfling and A.H. Hoang, Z. Phys. **C75** (1997) 539.

[57] M. Carena, S. Pokorski and C. Wagner, Nucl. Phys. **B406** (1993) 59; V. Barger, M.S. Berger and P. Ohmann, Phys. Rev. **D47** (1993) 1093.

[58] M. Carena and C. Wagner, Nucl. Phys. **B452** (1995) 45; see also B. Schrempp and M. Wimmer, Report DESY 96-109.

[59] G. Altarelli, R. Barbieri and F. Caravaglios, Preprint CERN-TH 97/290.

[60] A. Djouadi, J. Kalinowski and P.M. Zerwas, Z. Phys. **C70** (1996) 435.

[61] A. Djouadi, P. Janot, J. Kalinowski and P.M. Zerwas, Phys. Lett. **B376** (1996) 220.

[62] A. Djouadi, J. Kalinowski, P. Ohmann and P.M. Zerwas, Z. Phys. **C74** (1997) 93.

[63] A. Bartl, H. Eberl, K. Hidaka, T. Kon, W. Majerotto and Y. Yamada, Phys. Lett. **B389** (1996) 538.

[64] A. Djouadi, J. Kalinowski and P.M. Zerwas, Z. Phys. **C57** (1993) 569.

[65] P. Janot, Proceedings, Physics and Experiments with e^+e^- Linear Colliders, Waikoloa/Hawaii 1993, eds. F. Harris, S. Olsen, S. Pakvasa and X. Tata (World Scientific, Singapore, 1993).

[66] A. Andreazza and C. Troncon, in: DESY–ECFA Conceptual LC Design Report (1997).

[67] A. Sopczak, Z. Phys. **C65** (1995) 449.

[68] Z. Kunszt and F. Zwirner, Nucl. Phys. **B385** (1992) 3.

[69] G. Kane, G. Kribs, S. Martin and J. Wells, Phys. Rev. **D53** (1996) 213; B. Kileng, P. Osland and P. Pandita, Proceedings 10th International Workshop on High Energy Physics and Quantum Field Theory, Zvenigorod, Russia, September 1995, hep-ph/9601284.

[70] S. Dawson, A. Djouadi and M. Spira, Phys. Rev. Lett. **77** (1996) 16.

[71] J.M. Drees, M. Guchait and P. Roy, APCTP Report 97-21.

[72] E. Eichten, I. Hinchliffe, K. Lane and C. Quigg, Rev. Mod. Phys. **56** (1984) 579.

[73] A. Krause, T. Plehn, M. Spira and P.M. Zerwas, CERN-TH/97-137 [hep-ph/9707430] and Nucl. Phys. **B** in press.

[74] E. Richter-Was, D. Froidevaux, F. Gianotti, L. Poggioli, D. Cavalli and S. Resconi, Preprint CERN-TH/96-111.

[75] A. Djouadi, H.E. Haber and P.M. Zerwas, Phys. Lett. **B375** (1996) 203; T. Plehn, M. Spira and P.M. Zerwas, Nucl. Phys. **B479** (1996) 46.

[76] M. Krämer, J. Kühn, M.L. Stong and P.M. Zerwas, Z. Phys. **C64** (1994) 21.

[77] P. Fayet, Nucl. Phys. **B90** (1975) 104; H.-P. Nilles, M. Srednicki and D. Wyler, Phys. Lett. **B120** (1983) 346; J.-P. Derendinger and C.A. Savoy, Nucl. Phys. **B237** (1984) 307; J.F. Gunion and H.E. Haber, Nucl. Phys. **B272** (1986) 1; J. Ellis, J.F. Gunion, H.E. Haber, L. Roszkowski and F. Zwirner, Phys. Rev. **D39** (1989) 844.

[78] U. Ellwanger, M. Rausch de Traubenberg and C.A. Savoy, Z. Phys. **C67** (1995) 665; S.F. King and P.L. White, Phys. Rev. **D52** (1995) 4183; H. Asatrian and K. Eguin, Mod. Phys. Lett. **A10** (1995) 2943.

[79] S.W. Ham, H. Genten, B.R. Kim and S.K. Oh, Phys. Lett. **B383** (1996) 179 and Z. Phys. **C76** (1997) 117.

[80] J.R. Espinosa and M. Quiros, Phys. Lett. **B279** (1992) 92; G.L. Kane, C. Kolda and J.D. Wells, Phys. Rev. Lett. **70** (1993) 2686.

[81] J. Kamoshita, Y. Okada and M. Tanaka, Phys. Lett. **B328** (1994) 67.

[82] J.M. Cornwall, D.N. Levin and G. Tiktopoulos, Phys. Rev. **D10** (1974) 1145; B. Lee, C. Quigg and H. Thacker, Phys. Rev. **D16** (1977) 1519; M. Chanowitz and M.K. Gaillard, Nucl. Phys. **B261** (1985) 379; G.J. Gounaris, R. Kogerler and H. Neufeld, Phys. Rev. **D34** (1986) 3257; Y.P. Yao and C.P. Yuan, Phys. Rev. **D38** (1988) 2237; H.-J. He, Y.-P. Kuang, and X.-Y. Li, Phys. Rev. Lett. **69** (1992) 2619.

[83] T. Appelquist and C. Bernard, Phys. Rev. **D22** (1980) 200; A. Longhitano, Phys. Rev. **D22** (1980) 1166, Nucl. Phys. **B188** (1981) 118; T. Appelquist and G.-H. Wu, Phys. Rev. **D48** (1993) 3235.

[84] M.E. Peskin, Proceedings, *Physics and Experiments with Linear Colliders*, Saariselkä (1991).

[85] T.L. Barklow, DPF Conference, Albuquerque (1994).

[86] R. Casalbuoni, S. DeCurtis, D. Dominici and R. Gatto, Phys. Lett. **B155** (1985) 95.

[87] D. Dominici in Ref. [26], including earlier references; see also Ref. [13].